CLIMATE-INDUCED CHANGES IN ECOLOGICAL DYNAMICS OF THE ALASKAN BOREAL FOREST: A STUDY OF FIRE-PERMAFROST INTERACTIONS

By

Dana Rachel Nossov Brown, M.S., B.A.

A Dissertation submitted in Partial Fulfillment of the Requirements

for the Degree of

Doctor of Philosophy

in

Biological Sciences

University of Alaska Fairbanks

August 2016

APPROVED:

Knut Kielland, Committee Chair
M. Torre Jorgenson, Committee Co-Chair
Eugénie S. Euskirchen, Committee Member
Vladimir E. Romanovsky, Committee Member
Roger R. Ruess, Committee Member
David L. Verbyla, Committee Member
Diane Wagner, Chair
Department of Biology and Wildlife
Paul W. Layer, Dean
College of Natural Science and Mathematics
Michael Castellini, *Dean of the Graduate School*

Abstract

A warming climate is expected to cause widespread thawing of discontinuous permafrost, and the co-occurrence of wildfire may function to exacerbate this process. Here, I examined the vulnerability of permafrost to degradation from fire disturbance as it varies across different landscapes of the interior Alaskan boreal forest using a combination of observational, modeling, and remote sensing approaches. Across all landscapes, the severity of burning strongly influenced both post-fire vegetation and permafrost degradation. The thickness of the remaining surface organic layer was a key control on permafrost degradation because its low thermal conductivity limits ground heat flux. Thus, variation in burn severity controlled the local distribution of near-surface permafrost. Mineral soil texture and permafrost ice content interacted with climate to influence the response of permafrost to fire. Permafrost was vulnerable to deep thawing after fire in coarse-textured or rocky soils throughout the region; low ice content likely enabled this rapid thawing. After thawing, increased drainage in coarse-textured soils caused reductions in surface soil moisture, which contributed to warmer soil temperatures. By contrast, permafrost in fine-textured soils was resilient to fire disturbance in the silty uplands of the Yukon Flats ecoregion, but was highly vulnerable to thawing in the silty lowlands of the Tanana Flats. The resilience of silty upland permafrost was attributed to higher water content of the active layer and the associated high latent heat content of the ice-rich permafrost, coupled with a relatively cold continental climate and sloping topography that removes surface water. In the Tanana Flats, permafrost in silty lowlands thawed after fire despite high water and ice content of soils. This thawing was associated with significant ground surface subsidence, which resulted in water impoundment on the flat terrain, generating a positive feedback to permafrost degradation and wetland expansion. The response of permafrost to fire, and its ecological effects, thus varied spatially due to complex interactions between climate, topography, vegetation, burn severity, soil properties, and hydrology. The sensitivity of permafrost to fire disturbance has also changed over time due to variation in weather at multi-year to multi-decadal time scales. Simulations of soil thermal dynamics showed that increased air temperature, increased snow accumulation, and their interactive effects, have since the 1970s caused permafrost to become more vulnerable to talik formation and deep thawing from fire disturbance. Wildfire coupled with climate change has become an important driver of permafrost loss and ecological change in the northern boreal forest. With continued climate warming, we expect fire disturbance to accelerate permafrost thawing and reduce the likelihood of permafrost recovery. This regime shift is likely to have strong effects on a suite of ecological characteristics of the boreal forest, including surface energy balance, soil moisture, nutrient cycling, vegetation composition, and ecosystem productivity.

Table of Contents

List of Figures

Page

Page

List of Tables

Page

Chapter 1

Chapter 2

Chapter 3

Preface

I have many people to thank for their contributions to this dissertation and for their support throughout my doctoral program. Much of the research presented here grew from seeds that were planted by Torre Jorgenson, co-chair of my advisory committee. He was actively involved in all aspects of this research, and was a close mentor from beginning to end. Knut Kielland, faculty chair of my advisory committee, served as a continuous source of guidance, support, and encouragement. I am grateful for the time and contributions of each of my committee members. I thank Vladimir Romanovsky for sharing his expertise in permafrost thermal dynamics and modeling; David Verbyla for his mentoring in geospatial analysis; Roger Ruess for his enthusiasm for this work and long term mentoring; Eugénie Euskirchen for her support and constructive input on this research. I also thank collaborators Thomas Douglas, Anupma Prakash, Mikhail Kanevskiy, Christopher Hiemstra, and Joshua Koch, co-authors on the manuscripts from the dissertation. I am indebted to Amy Marsh and Katie Nicolato for all of their help with fieldwork and data collection. Many other individuals have contributed to this work, and are acknowledged within each research chapter. Finally, I thank my family with all of my heart for their love and support, especially my husband Steve Brown, my sweet little baby Nathan Brown, and my mother Wanda Nossov.

This research was funded by the United States Geological Survey through the Changing Arctic Ecosystems Initiative, the Yukon River Basin studies, and the Land Carbon Program, the Department of Defense's Strategic Environmental Research and Development Program (Project RC-2110), the Bonanza Creek Long Term Ecological Research Program, funded jointly by the National Science Foundation (DEB-0423442) and the United States Forest Service, Pacific Northwest Research Station (PNW-01-JV-11261952-231), and by an award from Alaska's Experimental Program to Stimulate Competitive Research. The Alaska Cooperative Fish and Wildlife Research Unit, the Institute of Arctic Biology, and the Department of Biology and Wildlife at the University of Alaska Fairbanks provided support this research.

The three research chapters which comprise this dissertation have been submitted to or published in peer-reviewed journals as follows:

- Chapter 1: Brown, D. R. N., M. T. Jorgenson, T. A. Douglas, V. E. Romanovsky, K. Kielland, C. Hiemstra, E. S. Euskirchen, and R.W. Ruess (2015), Interactive effects of wildfire and climate on permafrost degradation in Alaskan lowland forests, *J. Geophys. Res. Biogeosci.,120*, doi:10.1002/2015JG003033.
- Chapter 2: Nossov, D. R., M. T. Jorgenson, K. Kielland, and M. Kanevskiy (2013) Edaphic and microclimatic controls over permafrost response to fire in interior Alaska *Environ. Res. Lett.,* 8 035013 doi:10.1088/1748-9326/8/3/035013

- Chapter 3: Brown, D. R. N, M. T. Jorgenson, K. Kielland, D. L. Verbyla, A. Prakash, and J. C. Koch (Submitted) Landscape effects of wildfire on permafrost distribution in interior Alaska derived from remote sensing. *Remote Sensing.*

Introduction

Background and overview

Because permafrost is ultimately a thermal condition of soil, it is influenced by climate and sensitive to climate change, especially in areas where its temperature is close to the melting point of ice. Discontinuous permafrost is typically within just a few degrees of thawing, and is therefore of particular concern [*Osterkamp and Romanovsky*, 1999]. The degradation of discontinuous permafrost has begun in some areas, and widespread thawing is predicted in future climate scenarios [*Jafarov et al.*, 2012]. However, the relationship between permafrost and climate is complex. Permafrost is separated from the atmosphere by snow, vegetation, and the active layer of soil, the thermal properties of which impact the vulnerability of permafrost to thawing. In cold regions, slow decomposition rates promote the accumulation of thick layers of insulating organic material, which reduce summer heat flux into soils, thereby buffering permafrost from increasing air temperatures [*Jorgenson et al.*, 2010]. The accumulation of thick organic layers over time is therefore a strong negative feedback to permafrost degradation. Conversely, a major positive feedback to permafrost degradation is the loss of this protective organic layer through wildfire, a widespread disturbance of boreal forest ecosystems [*Yoshikawa et al.*, 2003]. The characteristics of the fire regime have recently changed as a result of climate warming, with a shift towards increased fire severity, frequency, and extent in the northern boreal forest [*Calef et al.*, 2015; *Kasischke et al.*, 2010]. The intensification of the fire regime amidst a warming climate stands to further exacerbate permafrost degradation.

Permafrost strongly influences ecosystem processes, vegetation, and hydrology, and plays a significant role in the global climate system through the sequestration of carbon in frozen soils [*Grosse et al.*, 2011; *Jorgenson et al.*, 2010, 2013; *Schuur et al.*, 2015]. The degradation of permafrost therefore has important implications from local to, potentially, global scales. The vulnerability of permafrost to long-term thawing, and the ecological consequences thereof, are influenced by many factors and may vary widely within a region. For my dissertation research, I examined the vulnerability of permafrost to degradation after fire across the heterogeneous landscapes of interior Alaska through observational, modeling, and remote sensing approaches. In Chapter 1, I examine the effects of fire on permafrost within ice-rich lowlands vulnerable to thermokarst. Chapter 2 addresses the variability in the response of permafrost to recent fires across different soil landscapes (rocky uplands, silty uplands, and sandy lowlands). Chapter 3 describes a study on using remote sensing data to map permafrost distribution and associated drainage conditions after fire in a rocky upland landscape. My final dissertation section synthesizes the conclusions from the three research chapters.

Vulnerability of ice-rich lowlands to permafrost degradation from wildfire

Chapter 1 examines fire effects on permafrost within a silty lowland landscape in the Tanana Flats, where the consequences of permafrost thaw may be particularly severe due to the coupling of high permafrost ice content with flat topography. The melting of ice can result in the subsidence of the ground surface. After this thaw settlement, the surface then becomes susceptible to water impoundment and further thawing. This hydrologic shift can foster sustained permafrost degradation and dramatic changes in vegetation composition and ecosystem function as forests become wetland or aquatic systems. Collapse-scar bogs, evidence of previous thaw settlement and water impoundment, are abundant throughout this landscape.

To examine the vulnerability of lowland permafrost to degradation and collapse as a result of wildfire we used a chronosequence approach to field-sampling, comparing vegetation and soils across five fire scars dating from the 1930s to 2010. We utilized cryostratigraphy to infer the history of permafrost dynamics and ecological succession. We assessed the current state of permafrost through monitoring soil thermal regimes and depth to the permafrost table, and at the most recent fires, we documented thaw settlement and water impoundment of burned forests. Finally, we investigated the effects of burn severity and historic climate variation on permafrost dynamics using numerical soil thermal model simulations.

Variation in permafrost response to fire across soil landscapes

Variations in microclimate, vegetation, and soils create a wide range of thermal conditions that can influence the permafrost response to fire across the discontinuous permafrost zone. The effect of air temperature on soil temperature is buffered by insulating layers of snow in winter and the surface organic layer in the summer. In boreal evergreen forests, thick layers of moss accumulate over time and reduce heat flux into soils. The water content of the active layer of soil strongly influences soil thermal regimes in cold climates because of the nearly 4-fold higher thermal conductivity of ice compared to liquid water. Therefore, active layer soils with high water content tend to lose more heat in the winter than they gain in the summer, resulting in colder soil conditions. The presence of an impermeable permafrost table further increases the moisture content of active layer soils. The ice content of permafrost may also influence its susceptibility to thawing due to the large heat requirements for phase change. Many of these soil properties that influence thermal regimes are influenced by mineral soil texture. Fine-grained soils with higher water holding capacities are typically colder and have higher permafrost ice content than coarse-grained soils, which likely impacts their vulnerability to thawing. The variation in water holding capacities between these soil textures should also impact the effects of permafrost thawing on soil

moisture. Through interactions with climate and soil properties, topography further influences soil thermal regimes.

Chapter 2 examines how these edaphic and microclimatic factors influence the vulnerability of permafrost to degradation after fire through comparisons of recently burned and unburned evergreen stands across rocky upland, silty upland, and sandy lowland landscapes in the Yukon Flats and Yukon-Tanana Uplands ecoregions of interior Alaska. We assessed how the effects of fire on permafrost were influenced by vegetation, soil characteristics, and climate. We hypothesized that the reduction of organic layer thickness by fire would initiate permafrost degradation, but soil texture would modify the effects on permafrost by influencing soil moisture regimes after fire.

Mapping post-fire permafrost distribution in rocky uplands

Chapter 3 builds upon the findings of Chapter 2, which demonstrated that coarse-textured or rocky soils in interior Alaska were vulnerable to thawing of permafrost and drying of surface soils after reduction of surface organic layer thickness through moderate to high severity burns. This chapter focuses on characterizing the spatial heterogeneity of the impact of fire on permafrost and soil moisture within a rocky upland landscape. We analyzed relationships between soil properties, vegetation, and remote sensing data from topographic, optical, and synthetic aperture datasets. We examined the remote sensing indices most closely related to field data and used these empirical relationships to map permafrost distribution and drainage classes. We assessed the landscape patterns of permafrost degradation and described the influence of topography, vegetation, and burn severity.

References

Calef, M. P., A. Varvak, A. D. McGuire, F. S. Chapin, and K. B. Reinhold (2015), Recent changes in annual area burned in interior Alaska: the impact of fire management, *Earth Interactions*, *19*(5), 1-17.

Grosse, G., et al. (2011), Vulnerability of high-latitude soil organic carbon in North America to disturbance, *Journal of Geophysical Research*, *116*, G00K06.

Jafarov, E. E., S. S. Marchenko, and V. E. Romanovsky (2012), Numerical modeling of permafrost dynamics in Alaska using a high spatial resolution dataset, *The Cryosphere*, *6*(3), 613-624.

Jorgenson, M. T., V. Romanovsky, J. Harden, Y. Shur, J. O'Donnell, E. A. G. Schuur, M. Kanevskiy, and S. Marchenko (2010), Resilience and vulnerability of permafrost to climate change, *Canadian Journal of Forest Research*, *40*(7), 1219-1236.

Jorgenson, M. T., et al. (2013), Reorganization of vegetation, hydrology and soil carbon after permafrost degradation across heterogeneous boreal landscapes, *Environmental Research Letters*, *8*(3), 035017.

Kasischke, E. S., et al. (2010), Alaska's changing fire regime — implications for the vulnerability of its boreal forests, *Canadian Journal of Forest Research*, *40*(7), 1313-1324.

Osterkamp, T. E., and V. E. Romanovsky (1999), Evidence for warming and thawing of discontinuous permafrost in Alaska, *Permafrost and Periglacial Processes*, *10*, 17-37.

Schuur, E. A., et al. (2015), Climate change and the permafrost carbon feedback, *Nature*, *520*(7546), 171-179.

Yoshikawa, K., W. R. Bolton, V. E. Romanovsky, M. Fukuda, and L. D. Hinzman (2003), Impacts of wildfire on the permafrost in the boreal forests of Interior Alaska, *Journal of Geophysical Research*, *108*(D1), 8148.

Chapter 1: Interactive effects of wildfire and climate on permafrost degradation in Alaskan lowland forests[1]

Abstract

We examined the effects of fire disturbance on permafrost degradation and thaw settlement across a series of wildfires (from ~1930 to 2010) in the forested areas of collapse-scar bog complexes in the Tanana Flats lowland of interior Alaska. Field measurements were combined with numerical modeling of soil thermal dynamics to assess the roles of fire severity and climate history in postfire permafrost dynamics. Field-based calculations of potential thaw settlement following the loss of remaining ice-rich permafrost averaged 0.6 m. This subsidence would cause the surface elevations of forests to drop on average 0.1 m below the surface water level of adjacent collapse-scar features. Up to 0.5 m of thaw settlement was documented after recent fires, causing water impoundment and further thawing along forest margins. Substantial heterogeneity in soil properties (organic layer thickness, texture, moisture, and ice content) was attributed to differing site histories, which resulted in distinct soil thermal regimes by soil type. Model simulations showed increasing vulnerability of permafrost to deep thawing and thaw settlement with increased fire severity (i.e., reduced organic layer thickness). However, the thresholds of fire severity that triggered permafrost destabilization varied temporally in response to climate. Simulated permafrost dynamics underscore the importance of multiyear to multidecadal fluctuations in air temperature and snow depth in mediating the effects of fire on permafrost. Our results suggest that permafrost is becoming increasingly vulnerable to substantial thaw and collapse after moderate to high-severity fire, and the ability of permafrost to recover is diminishing as the climate continues to warm.

Introduction

Permafrost degradation is expected to become more widespread in response to changes in climate [*Jafarov et al.*, 2012] because of the directional changes in air temperature and snow cover, which are the principal climatic controls over soil thermal regimes [*Osterkamp and Romanovsky*, 1999; *Zhang*, 2005]. When ice volume exceeds the pore space of permafrost soils, thawing will result in the vertical subsidence of the ground surface. In flat lowland areas, the resulting thermokarst features usually impound water unless water can drain through coarse subsurface materials. The presence of surface water can substantially increase surface energy gains [*Eugster et al.*, 2000], raise the temperature of the

[1] Brown, D. R. N., M. T. Jorgenson, T. A. Douglas, V. E. Romanovsky, K. Kielland, C. Hiemstra, E. S. Euskirchen, and R.W. Ruess (2015), Interactive effects of wildfire and climate on permafrost degradation in Alaskan lowland forests, *J. Geophys. Res. Biogeosci.,120*, doi:10.1002/2015JG003033.

underlying soil, and accelerate permafrost thaw [*Jorgenson et al.*, 2010]. Lowland forests on ice-rich soils may thus become wetland or aquatic systems as a result of thaw settlement, with associated changes in vegetation, productivity, and carbon and nutrient cycling [*Camill et al.*, 2001; *Johnston et al.*, 2014; *Jorgenson et al.*, 2001, 2013; *Myers-Smith et al.*, 2008; *O'Donnell et al.*, 2012; *Olefeldt et al.*, 2013; *Turetsky et al.*, 2007].

The expansion of wetland ecosystems through thermokarst has been attributed to interactions of climate and hydrology, as well as to wildfire [*Camill and Clark*, 2000; *Jorgenson et al.*, 2001; *Kuhry*, 1994; *Myers-Smith et al.*, 2008; *Thie*, 1974; *Vitt et al.*, 1994; *Zoltai*, 1993]. Wildfire is a widespread disturbance influencing boreal forest ecosystems, and the severity, frequency, and spatial extent of fire may be increasing with climate warming [*Gillett et al.*, 2004; *Kasischke et al.*, 2010; *Turetsky et al.*, 2011]. Here we consider fire severity to be analogous to the reduction in surface organic layer thickness [*Barrett et al.*, 2010; *Genet et al.*, 2013] and the thickness of the residual surface organic layer after combustion [*Yoshikawa et al.*, 2003]. The removal of insulating surface organics increases soil heat flux and causes permafrost degradation after severe fire [*Burn,* 1998; *Mackay*,1995; *Nossov et al.*, 2013; *Viereck et al.*, 2008; *Yoshikawa et al.*, 2003]. Deep and sustained permafrost degradation is associated with the development of a talik, a portion of the soil bordered by permafrost that remains unfrozen year-round. The talik buffers underlying permafrost from freezing winter air temperatures and may facilitate continued degradation [*Osterkamp and Burn,* 2003].

After fire, reaccumulation of the surface organic layer may initiate permafrost recovery [*Jafarov et al.*, 2013; *Jorgenson et al.*, 2010; *Shur and Jorgenson*, 2007; *Viereck et al.*, 2008]; or changes in climatic conditions, hydrology, or plant successional trajectories may cause further degradation [*Genet et al.*, 2013; *Jafarov et al.*, 2013; *Johnstone et al.*, 2010; *Jorgenson et al.*, 2010; *Shur and Jorgenson*, 2007; *Viereck et al.*, 2008]. In addition to the temporal controls over permafrost dynamics, the spatial variations in microclimate, snow depth, vegetation, topography, soil texture, and soil moisture contribute to the heterogeneity of the permafrost response to fire [*Genet et al.*, 2013; *Harden et al.*, 2006; *Johnson et al.*, 2013; *Jorgenson et al.*,2013; *Nossov et al.*, 2013; *Pastick et al.*, 2014].

The enhanced climate warming at northern latitudes, the high frequency and spatial extent of wildfires in boreal regions, and the potential for major ecosystem shifts with permafrost thaw necessitate a better understanding of the vulnerability of lowland permafrost to degradation and collapse as a result of wildfire disturbance, and how this vulnerability may be changing over time. Here we focused on the effects of fire on permafrost within the Tanana Flats lowland of interior Alaska, a landscape characterized by organic-rich, fine-grained soils associated with flat, abandoned floodplain deposits. We employed a chronosequence study design with fire scars ranging from ~1930 to 2010 to infer the history of permafrost dynamics after fire and in relation to ecological succession over time. We recognize in our interpretation

of results, however, that factors other than time contributed to the variability among fire scars. Through the field study, we compared vegetation and soil characteristics and assessed the magnitude of permafrost degradation, thaw settlement, and water impoundment across fire scars. Finally, we utilized a numerical soil thermal model to evaluate the influence of fire severity and historic climate variation on permafrost dynamics.

Methods

Study area and design

Our study area was within the Tanana Flats of interior Alaska, which extends north from the foothills of the Alaska Range to the Tanana River, encompassing an area of approximately 6000 km^2 (Figure 1.1). The area is characterized by a gentle elevation gradient of approximately 1 m/km that declines from the southeast to the northwest, with surface and subsurface water flowing in this direction [*Racine and Walters*, 1991]. The Tanana Flats is situated in a large alluvial fan and abandoned floodplain complex, formed by the deposition of fluvial and glaciofluvial sediments from the Alaska Range, up to hundreds of meters thick [*Péwé,* 1975]. The history of channel migration, deposition, and permafrost dynamics creates a fine topographic relief within this landscape that is associated with differences in vegetation, permafrost, and hydrology [*Jorgenson et al.*, 1999, 2001]. Forested areas typically occur on ice-rich permafrost plateaus elevated above bogs and fens that occur in thermokarst depressions. These relative elevations can shift with the formation or thawing of ice-rich permafrost. The climate of this region is continental, with low precipitation and a wide variation in seasonal air temperatures. From 1971 to 2000, mean annual air temperature was -3.7°C and mean annual precipitation was 323 mm in interior Alaska [*Alaska Climate Research Center,* 2013].

Study sites were established in the forested portions of collapse-scar bog complexes in five fire scars (~1930s, 1975, 1988, 2001, and 2010; Figure 1.1). The fire years were ascertained using a combination of fire perimeter maps [*Alaska Interagency Coordination Center*, 2011], tree ring dating, and interpretation of air photos and satellite imagery, since some of the fires have not been mapped or were mapped imprecisely. The 1988 fire scar had also previously burned in the 1950s, likely in the 1950 Salchaket Slough Fire (Figure 1.1).

Field sampling was conducted from May 2011 to October 2014. Within each fire scar, a 200–300 m linear transect was established that was oriented to cross both burned forest patches and old thermokarst bogs. One exception was the 1975 fire transect, which did not cross a thermokarst feature. Along each transect, three permanent intensive plots (5 × 10m) were established in separate patches of burned forest (separated by thermokarst bogs) for monitoring vegetation and soils. For vegetation, two additional extensive plots were established along each transect to increase sample size.

Vegetation

Percent cover of each plant species was estimated in each plot using a point-sampling technique employing a 100-point grid [*Kent*, 2012]. At each point, the first occurrence of each species encountered was recorded. Litter, charred organic soil, or mineral soil was recorded when no live plants were present. The plots were examined for additional species and a cover of 0.1% was assigned to all species that were present but not captured in the point sampling. Plant community composition was analyzed with nonmetric multidimensional scaling (NMDS), a multivariate ordination technique, using PC-ORD 6.0 (MjM Software, Gleneden Beach, OR) [*McCune and Grace*, 2002; *McCune and Mefford*, 2011]. The ordination axes represent the dominant patterns of species composition. Correlation analyses of the ordination axes scores with species and environmental data were conducted. Species and environmental data were assessed for normality and transformed prior to analysis as needed.

Soil physical characteristics

Soils were sampled at each permanent plot (3 plots per fire scar). For unfrozen surface soils, a soil plug (~40 cm diameter) was extracted with a shovel and a cross-section was cut with a knife. Frozen soils were cored to 3–4 m depths using a 7.5-cm-diameter SIPRE (Snow, Ice, and Permafrost Research Establishment) corer. Soil stratigraphy was described according to Natural Resources Conservation Service methods. Coarse-fragment (>2 mm) percentage was visually estimated. Cryostructures were described using the system by French and Shur [2010]. Total carbon content was determined at the Colorado State University Soil, Water, and Plant Testing Lab using a LECO TruSpec CN combustion furnace (St. Joseph, MI) following methods of Nelson and Sommers [1996]. For samples with pH < 6.5, it was assumed that total carbon content was equivalent to total organic carbon (OC) content. For samples with pH ≥ 6.5, CO_3-C was subtracted from total carbon to derive OC content. OC stocks (kg/m^2) were calculated by multiplying OC concentration by bulk density and by the thickness of the stratigraphic layer. Several samples were also taken at distinctive breaks in peat stratigraphy for radiocarbon dating at the National Ocean Sciences Accelerator Mass Spectrometry Facility (Woods Hole, MA) and Geochron Laboratories (Chelmsford, MA).

Volumetric soil samples were obtained every ~20 cm vertically. For the unfrozen soil plugs, either a serrated knife was used to cut blocks of organic material or a volumetric ring was used for less compressible soils. The SIPRE cores were used for the frozen soil samples. The samples were weighed before and after oven-drying at 60 °C for determination of moisture/ice content and bulk density. Volumetric soil moisture was calculated for each unfrozen stratigraphic layer, and was weighted by the thickness of each layer to calculate the weighted mean volumetric water contents of the active layer in

late summer. Volumetric ice content of the permafrost to 3 m depth was calculated using the same methods, and water-equivalent depth of moisture in permafrost was determined.

Thaw depths, thaw settlement, and water impoundment

Thaw depth, ground-surface elevation, and water-surface elevation were measured at 1-m intervals along each transect. Thaw depth was measured near the time of maximum seasonal thaw in late August-September using a metal probe. The elevation of the permafrost table was calculated by subtracting thaw depth from the ground surface elevation. Elevations of the ground surface and of the water level of adjacent bogs were determined using high resolution differential GPS (dGPS) and differential leveling. Thaw settlement was measured at the 2010 fire by comparing ground-based surface elevations over multiple years (2011 – 2014), and by comparing dGPS elevations (August 2012) with airborne LiDAR-derived elevations (May 2014). A companion study utilized electrical resistivity tomography (ERT) to characterize permafrost distribution along these transects to depths up to 30 m (T. A. Douglas *et al.*, Degrading permafrost mapped with electrical resistivity tomography, airborne imagery and LiDAR, and seasonal thaw measurements, *Geophysics*, in review, 2015).

The horizontal and vertical precision of ground-based dGPS measurements averaged 1.9 cm and 2.9 cm respectively. Airborne LiDAR imagery were collected by Quantum Spatial Incorporated (Anchorage, Alaska) using a Leica (Wetzlar, Germany) ALS70 system (1064 nm) mounted in a Partenavia aircraft with an average pulse density of $\geq$25 pulses/m^2 at an altitude of 1,000 m. The measurement accuracy yielded a root mean square error (RMS) of $\leq$9.2 cm and a spatial resolution of 0.25 m.

Potential thaw settlement at each plot was calculated from thaw strain estimates for each layer of permafrost in the upper 3 m of soil, and represents the predicted vertical surface settlement following the thawing of existing permafrost to this depth [*Crory*, 1973; *Pullman et al.*, 2007]. Thaw strain of each permafrost layer (T_l) was calculated:

$$T_l = (D_u - D_f)/ D_u \qquad (1)$$

where D_u is the estimated dry density of the unfrozen soil (estimated using the average dry density of unfrozen samples of similar horizons and soil textures as the permafrost soil), D_f is the measured dry density of permafrost soil. Potential thaw settlement of each permafrost layer (P_l) was then calculated:

$$P_l = T_l \times t_l \qquad (2)$$

where T_l is thaw strain of the layer and t_l is the thickness of the soil layer. The total potential thaw settlement is the sum of the potential thaw settlement for each layer in the upper 3 m of the soil column.

Potential thaw settlement was subtracted from current surface elevations at the soil sampling sites to derive post-thaw surface elevations. The current and post-thaw elevations of the ground surface relative to the bog water level were calculated to infer the potential for water impoundment.

Soil thermal regimes

At each of the 15 intensive plots (3 per fire scar) soil temperatures were recorded at two-hour intervals using two-channel dataloggers (HoboProV2, Onset Corp.) with a thermistor probe installed at 5 cm and 100 cm depths. One datalogger at the 2001 burn malfunctioned; therefore, data from a total of 14 plots (n = 2 or 3 per fire scar) were used in statistical analyses comparing thermal metrics and related soil characteristics among the 5 fire scars. Mean annual surface temperatures (MAST), mean annual deep temperatures (MADT), thawing degree-day sums (TDD), and freezing degree-day sums (FDD) were calculated based on hydrological year, named by the calendar year of the end date. After assessing variables for normality and homoscedasticity, comparisons between fire scars were conducted with one-way analysis of variance (ANOVA; JMP 10.0.0, SAS 2012, Cary, NC). Least square mean differences were calculated with Tukey's Honest Significant Difference (HSD) post hoc tests. Statistical significance was considered with $p < 0.05$.

Thermal modeling simulations

The Geophysical Institute Permafrost Laboratory (GIPL) thermal model was used to compare the sensitivity of permafrost to variations in surface organic layer thickness (OLT), a proxy for fire severity, and in relation to meteorological variables [*Nicolsky et al.*, 2007; *Romanovsky and Osterkamp*, 2000; *Sergueev et al.*, 2003]. The GIPL numerical transient model uses daily air temperature and snow depth forcing data and subsurface soil properties to simulate ground temperatures by solving nonlinear heat diffusion equations, taking into account the effects of unfrozen water during freezing and thawing to accurately represent phase change. Climate data for the Fairbanks International Airport from 1930 –2013 were used in the simulations [*Alaska Climate Research Center*, 2014] (Figure 1.2). The airport is located on lowlands north of the Tanana River at a similar elevation and within 30 km of our field sites. The model was parameterized to reflect the observed soil stratigraphy and moisture profile at one of our field sites (TF01-075) with silt loam-dominated soils (Table 1.1). It was assumed that the deepest observed soil type extended to 100 m depth. The model was calibrated using the measured soil temperature record from 5/21/2011–9/24/2013. Volumetric water content, thermal conductivity (frozen and unfrozen), heat capacity (frozen and unfrozen), and unfrozen water content curves for each soil layer were adjusted through the calibration process, and were within the range of expected values by soil type [*Farouki*, 1981; *Jafarov et al.*, 2013; *O'Donnell et al.*, 2009; *Romanovsky and Osterkamp*, 2000]. Modeled thaw depths

were within 10 cm of measured thaw depths, and modeled mean annual temperatures were within 0.2°C of the measured values.

The levels of OLT that were tested were 30 cm (unburned), 15 cm (low-severity fire), 7 cm (moderate-severity fire), and 0 cm (high-severity fire). The same thermal and moisture properties as in the model calibration were assumed (Table 1.1). The surface organic layer thickness and soil moisture were assumed to be constant. Simulations were run with a spin-up, in which climate forcing data from 1930 were repeated for 30 years to allow the soil temperatures to stabilize prior to time zero. We report the results of the simulations from 1930 to 2013, summarizing soil temperature data to depict the boundaries of the permafrost tables and taliks in the upper 10 m of soil.

The GIPL model output was used in conjunction with the mean thaw strain estimates by soil horizon from borehole sampling to simulate annual thaw settlement. Mean thaw strain values of 0.42 and 0.05 were used for the silt loam and sandy soil horizons, respectively. Annual simulated thaw depths were adjusted to reflect the relative changes in the position of the soil surface as a direct result of reductions in organic layer depth. The simulated thaw depth (0.6 m) for the year 1930 of the unburned scenario was considered the baseline permafrost condition. The thickness of each layer of thawed permafrost, by soil type, was then multiplied by the thaw strain and summed for the 10-m vertical soil profile to calculate thaw settlement. Thaw settlement was subtracted from the baseline surface elevation of 0 m to represent the surface elevation changes resulting from thaw settlement. There are several assumptions and limitations to this approach, however. First, the effects of thaw settlement, water impoundment, and accompanying positive feedbacks were not considered in the GIPL model simulations. Second, the effects of refreezing thawed permafrost on surface elevation are not realistic, as the newly formed permafrost would not have the same ice content as the older permafrost it replaced because ice aggrades slowly in permafrost over the course of many years [*Nossov et al.*, 2013; *Shur et al.*, 2005] and the thermal effects of ice migrating to the freezing front were not incorporated. Third, we assumed sandy soils extended to 10 m depth, although gravel is likely present. Even with these limitations the simulations were useful to couple the thermal and physical soil characteristics and to assess the relationships among climate, burn severity, and permafrost dynamics on surface topography. In our interpretation of these results we emphasize potential thaw settlement rather than the effects of refreezing.

The GIPL model has previously been used to explore the effects of fire on permafrost [*Jafarov et al.*, 2013; *O'Donnell et al.*, 2011; *Yoshikawa et al.*, 2003]. Yoshikawa *et al.* [2003] utilized the GIPL model to reconstruct site-based permafrost history after a 1983 fire. O'Donnell *et al.* [2011] and Jafarov *et al.* [2013] used the model to simulate permafrost response to fires of different severities under theoretical future climate scenarios. Our approach is unique in that we test the effects of fire severity on permafrost dynamics using historic climate data to drive the simulations. Our use of measured climate data enables

us to assess how short to long-term variations in air temperature and snow depth have influenced the sensitivity of permafrost to fire throughout the last century.

Results

Vegetation

Complete species cover data at our vegetation plots were averaged by fire scar and detailed in Table 1.2. The dominant vegetation cover differed across the fire scars. In the oldest fire scar (~1930), the canopy was dominated by *Picea mariana* (black spruce), with understory ericaceous shrubs (*Ledum groenlandicum*, *Vaccinium uliginosum*, *Vaccinium vitis-idaea*), herbs (*Equisetum sylvaticum*, *Geocaulon lividum*) and groundcover consisting primarily of feathermosses (*Hylocomnium splendens*, *Pleurozium schreberi*). The vegetation canopy of the 1975 burn was a mixture of evergreen and deciduous trees, including black spruce, *Betula neoalaskana* (birch), *Populus tremuloides* (aspen), and *Picea glauca* (white spruce). The dominant shrubs were *Salix* spp., *Rosa acicularis*, *Shepherdia canadensis,* and *Linnaea borealis*, and dominant herbs were *Equisetum pratense* and *Chamerion angustifolium*. Leaf litter and feathermosses were the predominant ground cover. The 1988 burn was a closed birch forest, with ericaceous shrubs, *Spirea beauverdiana,* and *Betula glandulosa*, abundant grasses (*Calamagrostis canadensis*), and leaf litter groundcover. The 2001 fire, a burned black spruce stand, lacked mature trees but had black spruce, birch, aspen, and *Populus balsamifera* (balsam poplar) seedlings. Shrub cover was predominantly ericaceous with *Betula* spp, *Salix* spp, and *Chamaedaphne calyculata*. Graminoid cover consisted primarily of sedges (*Eriophorum vaginatum* tussocks, *Carex* spp) and grasses. The moss layer included colonizing mosses *Ceratodon purpureus* and *Polytrichum juniperinum*. In the 2010 burn, vegetation varied across the transect. The primary pre-fire vegetation from ~0–80 m was a closed black spruce forest with a feathermoss groundcover, whereas vegetation from ~160–200 m was an open black spruce forest with dense sedge tussocks (*Eriophorum vaginatum*). The post-fire vegetation of the closed forest was characterized as a forb meadow, with recruitment of birch, poplar, and black spruce seedlings, high *Chamerion angustifolium* and *Equisetum* spp. cover, abundant *Marchantia polymorpha* and *Ceratodon purpureus*, and exposed mineral and charred organic soils. The post-fire vegetation of the open forest was dominated by recovering tussocks, low shrubs (*Betula glandulosa*, ericaceous shrubs), and grasses, with some recruitment of birch and black spruce seedlings.

The clustering of plots by fire year in the NMDS ordination showed that vegetation composition was more similar within burn scars than among burn scars (Figure 1.3). Axis 1 represented 47% of the variation in plant community structure and Axis 2 accounted for 19%. Axis 1 was negatively correlated with black spruce cover ($r = -0.86$), and Axis 2 was negatively correlated with birch cover ($r = -0.90$). Axis 1 was correlated with stand age ($r = -0.79$), indicating vegetation succession was an important factor

influencing the ordination of communities. However, the plant species composition itself suggests that the burn scars did not all represent different stages of the same successional sequence. The strong linear relationship between Axis 1 and soil moisture ($r = 0.79$) indicates that plant community composition is most reflective of this soil parameter. Although surface OLT and thaw depth were not correlated with either ordination axis, there were similarities in these variables within fire scars. The 1975 fire scar had relatively dry sandy soils and deep thaw; the ~1930 and 1988 fire scars had thick surface organics and shallow thaw depths; and the 2001 and 2010 fire scars had saturated silty soils and thawing permafrost.

Soil physical characteristics

Surface OLT was highly variable across all sites, ranging from 0 to 260 cm. The soils at the 1930 and 1988 fires were similar in that they typically had thick peat layers greater than 1 m, with mean surface OLT of 89 cm and 176 cm, respectively (Figures 1.4 and 1.5a). Mean organic carbon (OC) stocks in the upper 3 m of the soil profile were likewise greatest in the 1930 and 1988 fire scars (141 kg/m^2 and 125 kg/m^2, respectively) (Figure 1.5b). In contrast, the soils in the 1975, 2001, and 2010 burns had thinner organic layers (7 cm, 14 cm, and 2 cm, respectively) and less organic carbon in the upper 3 m (18 kg/m^2, 52 kg/m^2, 55 kg/m^2, respectively) (Figures 1.4 and 1.5b).

Soil texture of the underlying mineral soil varied across fire scars (Figure 1.4). The upper mineral soils of the 2001 and 2010 fire scars were fine textured silt loams approximately 2 m thick, whereas the near-surface soils of the 1975 fire scar were typically sandy loams, sands, or thin layers of silt loams underlain by sandy soils, with gravels occurring at depths less than 1 m.

Mean soil volumetric moisture content of the active layer varied five-fold across fire scars (Figure 1.5c). Mean soil moisture in the 1975 fire scar with sandy soils (13%) was significantly lower than in the 2001 and 2010 fire scars with silty soils (56% and 65%, respectively), and the 1930 and 1988 sites with thick peat had intermediate soil moisture (37% and 43%, respectively). We attribute the higher active layer moisture in the recent fire scars to the surface being nearer to the water table and to moisture released from the thawing permafrost.

Soil stratigraphy descriptions revealed complex sediment deposition, organic matter accumulation, and permafrost histories that contributed to the large differences among sites. The 2001 and 2010 sites were similar in that they had a moderately thick eolian silt cap over fluvial interbedded silts, sands, and gravels. They had relatively thin surface organics with no evidence of herbaceous peat associated with previous thermokarst. The thick silt caps contributed to the prevalence of braided and layered ice morphologies within high ice contents in the frozen soils. In contrast, the 1930 and 1988 sites had thick peat with buried layers of herbaceous peat (*Menyanthes trifoliata*) indicative of past thermokarst fens. At the 1988 fire scar, the ice-poor lenticular ice morphology at 1.1 to 2.8 m depth suggests that soils

had previously thawed to 2.8 m (from the current surface) and have subsequently refrozen. The previous thawing of ice-rich permafrost presumably contributed to the thermokarst microtopography prevalent within the birch forest at this site. At the 1930 site, the basal hemic peat (116 cm depth) had an age of 3,040 ± 25 B.P., and the fibric and hemic peat transition (48 cm depth) was dated at 920 ± 20 B.P. In the 1988 burn, the base of the fibric peat layer (48 cm depth) was aged at 1,550 ± 25 B.P. Large portions of these peat layers comprised the permafrost layer. Dates from the interbedded silt and sandy and gravelly sand layers (6,390 ± 40 and 9,820 ± 35 B.P.) indicate fluvial activity on the flats ended in early to mid-Holocene. The 1975 site was an outlier with eolian sand over fluvial sandy gravel. Overall, the stratigraphy shows that abandoned floodplains have complex histories involving disparate fluvial environments ending at differing times, sand deposits developing near channels, eolian silt being deposited over wide areas after the end of fluvial activity, and complex histories of organic accumulation related to patchy thermokarst.

Thaw depths, thaw settlement, and water impoundment

Thaw depths in late summer of 2012 were compared across all soil intensive plots. Mean thaw depths were relatively shallow in the 1930 (57 cm) and 1988 (52 cm) fire scars compared to the 2001 (119 cm) and 2010 fire scars (119 cm), and in the 1975 fire scar with sandy soils, no permafrost was found in the upper 2.5 m or 3 m of soil (Figures 1.4 and 1.6a). Permafrost was absent within the ~2.5 m depth of probing within the collapse-scar bogs (Figures 1.7a and 1.8).

Ice content is critical in determining potential thaw settlement. Mean ice content of permafrost within the upper 3 m of soil ranged from 55 to 79 vol %. (Figure 1.6b). The equivalent depths of water contained in the ice at the 1930 and 1988 sites were nearly double those of the 2001 and 2010 fire scars, in part due to the shallower permafrost table (Figure 1.6c). For both the 1930 and 1988 fire scars, calculated potential thaw settlement from thawing the remaining permafrost in the upper 3 m was 0.9 m, two to four times greater than the potential thaw settlement at the 2001 and 2010 burns (0.4 m and 0.3 m, respectively) (Figure 1.6d). Some of the reduced potential thaw settlement in the recent burns can be attributed to the deeper thaw already having removed some of the excess ice. The measured surface elevations at the 1930 and 1988 boreholes (+0.7 m and +0.8 m, respectively) were about twice as high above the water level of adjacent bogs than those of the 2001 and 2010 fires (+0.3 m and +0.4 m, respectively) (Figure 1.6e). On average, predicted post-thaw elevations were below or equal to water level at the 1930, 1988, and 2001 burns, and were 0.1 m above water level at the 2010 burn (Figure 1.6e), although thaw settlement and water impoundment were observed in the recent burns (Figures 1.7a and 1.7b). Overall, these results suggest that permafrost thaw can lower the ground surface to approximately

water level over most areas, with 77% of our 13 plots with permafrost predicted to collapse to water level or below with thawing.

The elevation profile of the burned closed black spruce forest portion of the 2010 fire transect (Figure 1.7a) shows the lowering of the permafrost table from 2011–2014 (mean = 1.04 m, max > 1.57 m), the thaw settlement of the ground surface (mean = 0.27 m, max = 0.54 m), and the water inundation of the forest margins from adjacent collapse-scar features (at transect locations ~0–10 m and ~70–80 m). An independent comparison between ground-based dGPS measurements from August 2012 and airborne LiDAR-derived elevations from May 2014 showed similar spatial patterns of thaw settlement, with maximum subsidence found near 0–15 m and 30–50 m of the transect (Figure 1.7b). These datasets also extended into the burned open black spruce forest/tussock portion of the transect (~165–200 m), which did not experience significant thaw settlement between fall 2012 and spring 2014 (Figure 1.7b).

The cross-section of the 2001 transect showed that the permafrost table in most portions of the burned black spruce forest (~0–190 m) declined substantially between 2011 and 2014, with the greatest changes (> 1 m) occurring along the edges of the large bog (Figure 1.8). The large increases in thaw depth between 2012 and 2013 could be due either to the abrupt thawing of the original pre-fire permafrost, or to the thawing of a thin frozen layer which remained or reformed after fire. With only one year of surface elevation measurements at this transect, we were unable to assess the magnitude of thaw settlement from 2011–2014, though previous thaw settlement was evident by burned and submerged black spruce along the bog margins. As of 2012, the elevations of the burned forest with thawing permafrost were similar to bog surface elevations. In fall 2014, almost the entire low-lying burned forest area from ~0–190 m was flooded (mean water depth = 24 cm). In 2014, a total of 241 mm of precipitation fell during the wettest June and second wettest July on record since 1930, and prolonged flooding was subsequently observed at several of our sites [*Alaska Climate Research Center*, 2014].

Observed soil thermal regimes

Mean annual surface temperatures (MAST, 5-cm depth) were 2–3 °C higher in the most recent burns (Figure 1.9a). In particular, the 2010 burn had the highest MAST (2.6 °C), whereas, the 1975 burn had the lowest MAST (-0.6 °C). Mean annual deep temperatures (MADT, 1-m depth) were also higher in the most recent burns, though only the 2010 burn had MADT (0.6 °C) significantly warmer than the coldest sites, the 1930 and 1988 burns (-0.7 °C, for each) (Figure 1.9b). MADT was inversely correlated with OLT (n = 14, r = -0.73, $p = 0.003$), but was not well correlated with active layer soil moisture (n = 14, r = 0.41, $p = 0.151$).

Surface thawing-degree days (TDD) were similar among fire scars (Figure 1.9c). Surface freezing degree days (FDD) were lowest (coldest) in the oldest stands (1930 and 1975), and highest (warmest) in

the youngest stands (2001 and 2010) (Figure 1.9d). The 1930 and 1988 burns were frozen at 1-m depth and had TDD equal to 0 (Figure 1.9e). Mean deep TDD sums were highest in the 2010 and 1975 burns (Figure 1.9e). At 1-m depth, mean FDD sums were generally higher in the two youngest stands (Figure 1.9f). The 1975 burn was unique in that it had both relatively high deep TDD and low deep FDD (Figures 1.9e and 1.9f).

The 1930 and 1988 sites showed soil thermal patterns similar to each other, with soils remaining at or below 0 °C year-round and maximum permafrost temperatures from -0.3 to 0 °C (Figures 1.10a and 1.10c). Seasonal soil temperature dynamics at 1-m depth were distinct at the 1975 burn, which exhibited the greatest seasonal fluctuation of soil temperature (Figure 1.10b). These soils were the first to freeze in the winter and thawed rapidly in the summer. The 2001 and 2010 sites had similar thermal regimes (Figures 1.10d and 1.10e). Within the 2001 fire scar, one plot (OLT = 6 cm) showed the progressive thawing and warming of soil from 2011–2013, with winter soil temperatures constrained at 0 °C. This observed warming trend was consistent with the thaw depth monitoring at this plot, which showed increases in thaw depth from 99 cm to 179 cm between 2011 and 2013. At the other plot in the 2001 fire scar (OLT = 13 cm), warm permafrost remained at 1-m depth, and thaw depths likewise were similar over the three years, remaining between 59–64 cm. In the 2010 fire scar, all three plots lacked permafrost at 1-m depth, and all exhibited increasing summer temperatures over the 2–3 year record (Figure 1.10e). Winter soil temperatures at two of the three plots in the 2010 burn (in the closed burned black spruce forest) did not fall below 0 °C. The coldest of the three plots was in the open burned black spruce forest with a tussock understory.

Thermal model simulations

The impacts of fire severity (OLT) and climate history (air temperature and snow depth) on permafrost dynamics were evaluated using the GIPL thermal model calibrated using soil properties of a silt loam-dominated plot (Table 1.1, Figures 1.11a-d). The GIPL model did not account for thaw settlement; however, the simulated thaw depths were combined with thaw strain calculations from borehole measurements to estimate changes in surface elevation as a result of thaw settlement (Figure 1.12).

The reduction of OLT between simulated unburned conditions (OLT = 30 cm), low-severity fire (OLT = 15 cm), moderate-severity fire (OLT = 7 cm), and high-severity fire (OLT = 0 cm) caused increases in permafrost table depth (Figures 1.11a-d) and surface subsidence (Figure 1.12). In the unburned and low-severity fire simulations, permafrost remained relatively stable from1930–2013 (Figures 1.11a and 1.11b). However, in the low-severity fire simulation, a temporary increase in thaw depths from 1990–1995 (Figure 1.11b) was associated with additional thaw settlement up to 0.7 m

(Figure 1.12). In the moderate-severity fire simulation (Figure 1.11c), permafrost was stable from the 1930s to the 1960s, but began to thaw rapidly beginning in the 1970s. In the 1980s, a talik formed and increased the rate of permafrost thawing. The original permafrost table dropped to about 7.6 m, and stabilized at that depth. In the early 2000s, new permafrost began to aggrade with the refreezing of the uppermost portions of the talik. In the 2010s, this new permafrost reverted back to a talik. The thawing from the 1970s to the early 1980s in the moderate-severity fire was associated with a rapid decline in surface elevation up to 1.0 m (Figure 1.12). Despite the rapid thawing from the early 1980s to the mid-1990s (Figure 1.11c), the rate of thaw settlement slowed (Figure 1.12) as thaw depth reached beyond the ice-rich silt loam layer at about 3-m depth into the ice-poor sandy layer (Figure 1.4). The final surface elevation at the end of the moderate-severity fire simulation was 1.3 m lower than in the unburned simulation (Figure 1.12). In the high-severity fire simulation, the permafrost table was below 10-m depth for the entire simulation period, except for a thin layer of near-surface permafrost that formed in the mid-1950s and disappeared in the early 1970s (Figure 1.11d). The deep thawing in the high-severity fire simulation resulted in 1.4 m of thaw settlement (Figure 1.12), equivalent to the maximum difference of 1.39 m in surface elevations we observed between burned forest soon after fire and the adjacent collapse-scar bogs (Figure 1.7a). Overall, the reduction of OLT consistently caused increased permafrost thawing; however, the sensitivity of permafrost to OLT thresholds, the magnitude of change, and the vulnerability to talik development and thaw settlement varied over time and in relation to climate.

When comparing climatic periods, simulated thaw depths and thaw settlement were generally deeper in the 1976–2013 period overall compared with the 1930–1975 period (Figures 1.11a-d and 1.12). Mean annual air temperature was significantly higher in the 1976–2013 period (-2.3 °C) relative to the previous 46 years (-3.4 °C) (t-ratio = 5.14, df = 82, p <0.0001), whereas mean annual snow depths were similar (t-ratio = 0.05, df = 82, p = 0.96) (Figure 1.2). The permafrost dynamics in the simulation of a moderately severe fire in particular appeared to be closely related to short-term to multi-decadal weather patterns (Figures 1.11c and 1.13). Increased thaw depth and initial talik development began during 1976–1989, a period with relatively high air temperatures and average snow depths. Extensive talik development and rapid declines in the permafrost table occurred from 1990–1995, coincident with generally above average snow accumulation and relatively high air temperatures. Despite relatively high air temperature during 1996–2010, thaw depths decreased and the partial refreezing of taliks occurred in conjunction with low snow depths. From 2011–2013, the thawing of the upper newly-aggraded permafrost above taliks corresponded with increased snow accumulation, despite relatively low air temperatures. These observations suggest that permafrost stability can be significantly impacted by either increases in air temperature or snow accumulation, but especially by their interaction.

Discussion

Heterogeneity of soils and vegetation

Our field monitoring of the response of permafrost to fire across a series of fire scars found that the 2001 and 2010 fires caused substantial permafrost thaw, whereas the 1930 and 1988 fires had relatively stable permafrost. Assessing the response to fire, however, was complicated by heterogeneous soil conditions, which limited the utility of the chronosequence study design. The soil thermal patterns observed among burn ages appeared to be more closely related to variations in organic layer thickness, soil moisture, and mineral soil texture than time since fire. Overall, the observed soil physical and thermal patterns could be broadly grouped by the dominant soil characteristics: the peaty sites (1930 and 1988 fires), the silty sites (2001 and 2010 fires), and the sandy site (1975 fire).

The peaty sites were characterized by organic layers typically over 1 m thick. Radiocarbon dating indicated that the peat had accumulated over the course of at least 2,000-3,000 years, though some peat was lost through previous wildfires. Thaw depths were shallow in these sites due to the insulating upper organic layers, and thus, much of the organic material is frozen as permafrost and protected from combustion. The soil thermal regimes of the peaty sites were all similar, with currently stable but warm (-1.0 – -0.4 °C) permafrost. The ice-poor cryostructures found in the 1988 peaty sites suggest that permafrost thawed after either the 1950 or 1988 fire to at least 2.8 m depth (not accounting for thaw settlement), creating thermokarst microtopography, and subsequently recovered. This progression of permafrost degradation and recovery after fire in lowland peatlands is consistent with the theoretical results of Jafarov *et al.* [2013]. The younger silty sites had thinner post-fire (and presumably pre-fire) organic layers (0–15 cm) underlain by thick layers of moist to saturated silt loams. The relatively thin organic layers corresponded to relatively thick active layers in these soils, which are still changing in response to the recent fires. Several of the plots showed potential talik development, with minimum soil temperatures constrained at 0 °C, suggesting the presence of an unfrozen layer year-round. Such talik development buffers the underlying soils from freezing air temperatures and can cause a positive feedback to permafrost thawing [*Osterkamp and Burn*, 2003]. The 1975 burn scar was distinct due to the presence of sandy loams or sands near the surface and low soil moisture content. Consequently, the dry soils with thin organic layers exhibited large thermal amplitude, with early and deep thawing, and rapid freezing.

Plant community composition among the burn scars indicated that the sites did not all represent stages of the same post-fire successional sequence, and soil stratigraphy revealed that pre-fire environmental and successional histories also were quite different. The present vegetation composition was most closely related to soil moisture, which is associated with soil texture. The mixed forest (1975)

with dry sandy soils, a thin organic layer, and deep thaw had unique soil thermal regimes. The birch forest (1988) and black spruce forest (~1930) alike were underlain by thick peats and thin active layers. The most recently burned black spruce stands (2001 and 2010) had early successional vegetation and thawing permafrost in most cases. Within the 2010 fire scar, a greater impact of fire on permafrost was observed in the closed black spruce forest-feathermoss vegetation type versus the open black spruce forest-tussock vegetation type, despite similar fire severity and organic layer thickness. We hypothesize that the tussock growth form has a cooling effect on subsurface soils and contributes to the resilience of permafrost.

The heterogeneity in soil and vegetation within the Tanana Flats reflects the legacy of complex ecological histories. The temporal variation in historic floodplain abandonment has left a legacy of fluvial and eolian sediment deposition that is manifested in spatial heterogeneity of mineral soil stratigraphy and subsequent soil development. Vegetation establishment promotes accumulation of soil organic material, which reduces soil heat flux. In fine-grained soils with high soil moisture, this cooling results in the aggradation of ice-rich permafrost and the uplift of peat plateaus, upon which forested ecosystems continue to develop. In our peaty sites, historic permafrost degradation and thaw settlement led to the conversion of forests to aquatic systems. Subsequent peat accumulation and aggradation of ice-rich permafrost reformed peat plateaus, which returned to a forested state. The long-term history of sediment deposition, permafrost aggradation and degradation, hydrology, organic accumulation, and vegetation succession thus created heterogeneous soil environments within current forests in the Tanana Flats. Other lowland areas exhibit similar inherent patchiness resulting from these dynamic processes, complicating generalizations and predictions across these landscapes [*Jorgenson et al.*, 2013; *Kanevskiy et al.*, 2014].

Thaw settlement, feedbacks, and wetland expansion

Minor differences in elevation are related to major differences in hydrology, permafrost, vegetation, and ecosystem properties in the lowlands [*Jorgenson et al.*, 2001]. The Tanana Flats landscape is a mosaic of forest, scrub, and meadow ecosystems interrupted by numerous collapse-scar bogs and fens. Moderate changes in microtopography due to the thawing of ice-rich permafrost in forests and subsequent collapse of the soil surface can result in significant changes in hydrology. Water impoundment greatly alters the surface energy balance, and can cause a strong positive feedback to permafrost degradation, in addition to altering vegetation composition and ecosystem function [*Camill et al.*, 2001; *Hayashi et al.*, 2011; *Jorgenson et al.*, 2001, 2010; *Myers-Smith et al.*, 2008; *O'Donnell et al.*, 2012; *Turetsky et al.*, 2007].

We found that the upper permafrost (within 3 m of soil surface) within our study area was generally ice-rich (55–79 vol %), and that the thawing of the remaining upper permafrost could cause up to 0.9 m of thaw settlement, resulting in the soil surface collapsing on average to 0.1 m below the water

level of the adjacent collapse-scar bogs. This minimization of relative elevations between forest and bog suggests the potential for water impoundment through collapse-scar expansion or the creation of new thermokarst depressions at many of our sites. Thaw settlement and lateral collapse-scar bog expansion were observed after the 2010 and 2001 fires. The effects of the 2010 fire were particularly notable for the rapid collapse of some of the ground surface in the burned forest to below the water level, with up to 0.5 m of subsidence recorded between 2011 and 2014. The magnitude of permafrost thawing was typically greatest along the forest-bog interface, suggesting the importance of hydrologic feedbacks to fire-initiated permafrost thaw. In the absence of fire, collapse-scar bogs in this region have expanded at rates of 0.1–0.5 m/year [*Jorgenson et al.*, 2001], whereas lateral expansion averaged 2 m/year in the first 3 years after the 2001 fire [*Myers-Smith et al.*, 2008].

In addition to these observations, our simulations of thaw settlement at a silt-dominated site showed substantial surface subsidence of up to 1.3 m or 1.4 m after moderate-severity (OLT = 7 cm) and high-severity fires (OLT = 0 cm), respectively. Our simulations also suggest that significant thaw settlement may even result from low-severity fires (OLT = 15 cm) when air temperatures and snow accumulation are relatively high. The magnitude of thaw settlement was greatest from the thawing of the upper 3 m of soil, which was characterized by ice-rich silt loam. Our observations and modeling results suggest that the interaction between climate, fire, ground ice, surface topography, and hydrology is a significant mechanism accelerating the decline in forested ecosystems and the expansion of collapse-scar bogs across this landscape.

The thawing of permafrost and subsequent ecosystem shifts have important implications for carbon cycling. Permafrost stores large stocks of organic carbon which can become remobilized upon thawing and released into the atmosphere [*Schuur et al.*, 2015]. The inundation of forests following collapse leads to a shift from predominantly aerobic to anaerobic pathways of respiration, increasing the release of methane, a potent greenhouse gas [*Frolking et al.*, 2011; *Johnston et al.*, 2014; *Olefeldt et al.*, 2013; *Turetsky et al.*, 2007; *Wickland et al.*, 2006]. The increased radiative forcing resulting from these carbon losses, however, may be offset by enhanced organic matter accumulation over time following thaw in collapse-scar bogs [*Camill et al.*, 2001; *Turetsky et al.*, 2007], though some studies report a net reduction in carbon storage [*O'Donnell et al.*, 2012].

Permafrost dynamics after fire and relationship to climate

We assessed the influence of fire severity (through related changes in OLT) and climate history (1930–2013) on permafrost dynamics by conducting several simulations using the GIPL soil thermal model and thaw strain estimates. The simulations showed the increased vulnerability of permafrost to talik formation, deep thawing, and thaw settlement with increased fire severity (i.e., reduced OLT). The

simulations suggest that there are thresholds of OLT below which permafrost will destabilize, but the thresholds vary over time in response to climate. With a low-severity fire (OLT = 15 cm), thaw depth increased slightly, but underlying permafrost remained stable in the absence of talik development. With a high-severity fire (OLT = 0 cm), permafrost could not be sustained within the upper 10 m of soil. With a moderate-severity fire (OLT = 7 cm), the permafrost dynamics were more complex and dependent on climatic variations. In this simulation, permafrost remained stable from the 1930s through the 1960s, until rapid thawing beginning in the 1970s led to the development of a deep talik, the upper portion of which temporarily refroze, developing a thin layer of short-lived permafrost. The original permafrost table eventually stabilized beneath the talik at 7.6 m depth.

The complex permafrost dynamics under the simulated moderate-severity fire underscore the importance of short-term to multi-decadal fluctuations in weather in influencing the impact of fire on permafrost. The vulnerability of permafrost to degradation after moderate-severity fire increased sharply in the 1970s, coincident with multi-decadal increases in air temperatures after a major shift in the Pacific Decadal Oscillation in 1976 [*Hartmann and Wendler*, 2005]. Since the 1970s, permafrost appeared to be sensitive to short-term variations in snow accumulation. The pronounced thawing of permafrost during 1990–1995 and 2011–2013 was associated with periods of high snow accumulation, whereas a period of permafrost recovery during 1996–2010 occurred during a period of low snow accumulation, despite relatively high air temperatures. Increased air temperatures, increased snow accumulation, and their interactive effects contribute to the instability of permafrost after moderate-severity fire. The warming effect of increased snow depth during 2011–2013 may have also contributed to the rapid increase in thaw depths and soil temperatures that we observed at the 2001 and 2010 fire scars in these years. Though a significant impact of fire on permafrost often occurs within just a few years of disturbance, these findings suggest the full impact of OLT reduction on permafrost may not be realized for many years until climatic conditions are conducive to thawing, unless sufficient organic layer recovery inhibits thaw.

Permafrost monitoring after a 1983 fire in the nearby lowlands at the Bonanza Creek Long Term Ecological Research site documented a progression of deep permafrost thawing, talik formation, stabilization of the original permafrost table at depth, refreezing of the upper talik, and recent degradation of the new permafrost, similar to our simulation results for the moderate-severity fire [*Romanovsky*, 2014; *Viereck et al.*, 2014]. In the 36 years after a 1971 fire in the Yukon-Tanana Uplands of interior Alaska, the degradation of permafrost, development of a talik, and recovery of permafrost was observed [*Viereck et al.*, 2008]. The initial permafrost recovery was attributed to low snowfall combined with cold temperatures in the winter of 1995-1996, which led to persistence of frost and the eventual freezing of the entire talik. These short to long-term climatic controls interact with fire severity, plant succession, organic layer recovery, and hydrologic changes to create complex temporal dynamics of permafrost change,

which also vary across the landscape in response to local controls. Under future climate scenarios with projected increases in air temperatures and snowfall [*Romero-Lankao et al.*, 2014], the thresholds of OLT needed to protect permafrost would increase (i.e., less severe fires will have greater impacts on permafrost in a warmer climate with increased snowfall), and the likelihood of permafrost recovery will be reduced.

Conclusions

Fire can increase soil heat flux and trigger permafrost thaw in boreal lowland forests, but the magnitude of this response is dependent on interactions between fire severity, soil properties, and climatic conditions. These controls vary spatially and temporally, contributing to the complexity of post-fire permafrost dynamics. We found that substantial permafrost thaw, surface collapse, and water impoundment has occurred on the more recent burns with silty soils, whereas the burns with peaty soils had relatively stable or recovered permafrost. Variations in long-term environmental and successional history gave rise to substantial heterogeneity in soil properties and vegetation within the lowland forests. Given this spatial heterogeneity and temporal variation in air temperature and snow conditions, we used thermal modeling to better evaluate the effects of fire severity and climate history on permafrost. Simulated moderate to high-severity fires led to talik formation, deep permafrost thawing, and thaw settlement in silty soils. Permafrost dynamics in moderate-severity fires were controlled by climatic fluctuations, with taliks forming during periods of warmer air temperatures and/or deeper snow and permafrost aggrading under colder and/or lower-snow conditions. Together, the field observations and soil thermal modeling indicate that ice-rich lowland forested ecosystems in interior Alaska may be reaching a climatic tipping point where they are increasingly vulnerable to deep permafrost thawing and severe collapse after fire, with the potential for permafrost recovery diminishing as the climate continues to warm.

Acknowledgements

Data used in this article are available upon request to the corresponding author. This research was funded by the Department of Defense's Strategic Environmental Research and Development Program (Project RC-2110), the Changing Arctic Ecosystems Initiative of the US Geological Survey's Ecosystem Mission Area, and the Bonanza Creek Long Term Ecological Research Program, funded jointly by the National Science Foundation (DEB-0423442) and the United States Forest Service, Pacific Northwest Research Station (PNW-01-JV-11261952-231). The Alaska Cooperative Fish and Wildlife Research Unit and the Institute of Arctic Biology at the University of Alaska Fairbanks provided support. We thank Amanda Barker, Maria Berkeland, Kevin Bjella, Seth Campbell, Tiffany Gatesman, Art Gelvin, Hélène

Genet, Sarah Hayes, Karen Jorgenson, Mark Lara, Anna Liljedahl, Heikki Lotvonen, Katie Nicolato, Stephanie Saari, and Anna Wagner for all of their help with this project.

Figures

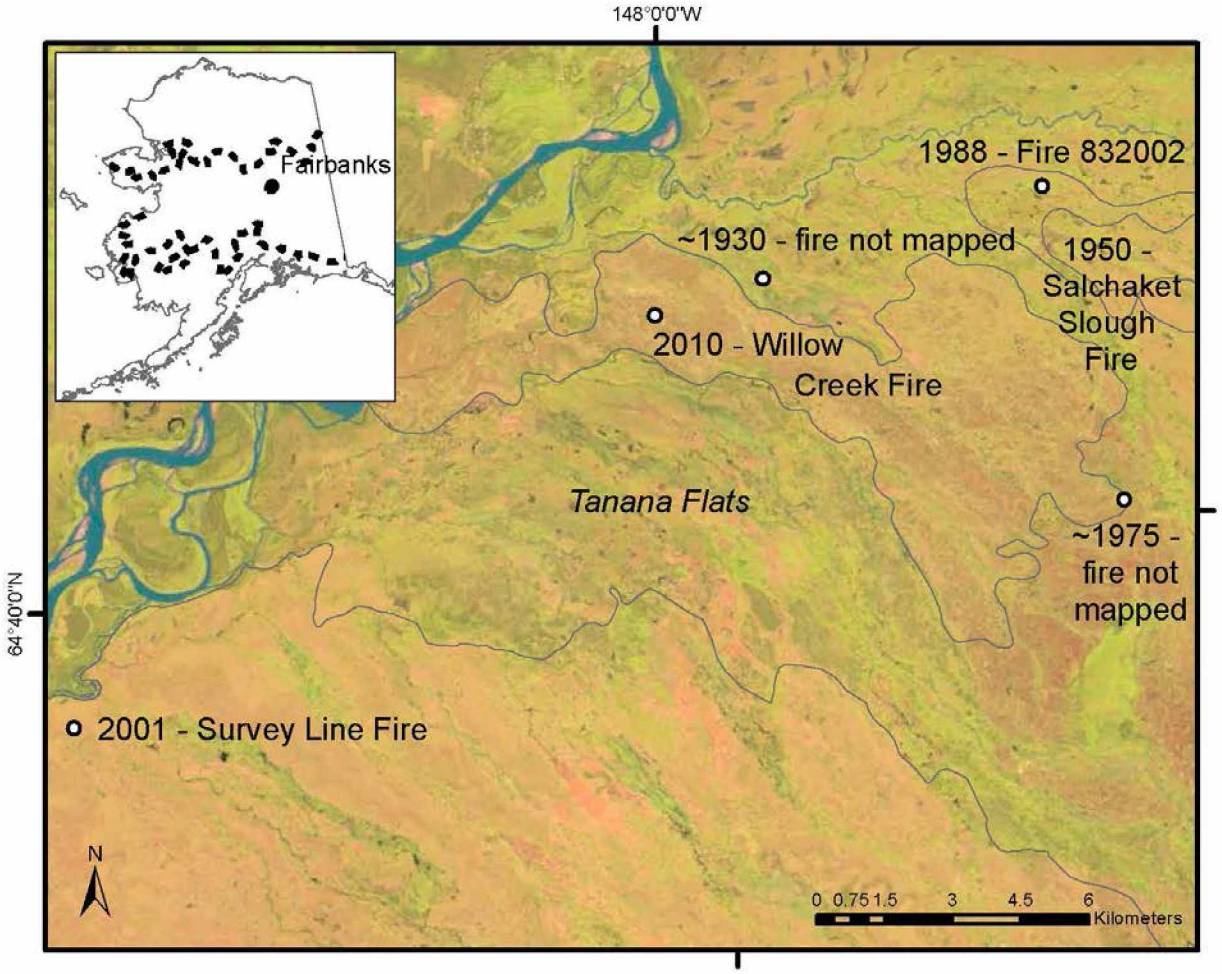

Figure 1.1. Map of study area. Study sites (open circles) are identified by fire year and name, and perimeters of associated fires from the Alaska Interagency Coordination Center [2011], when available, are overlain on satellite image. The Landsat 8 OLI image (acquired 18 June 2013) is displayed as a color composite of bands 6 (SWIR), 5 (NIR), and 4 (red). Inset shows location of the Tanana Flats study area, just south of Fairbanks, within the discontinuous permafrost zone of Alaska [*Jorgenson et al.*, 2008].

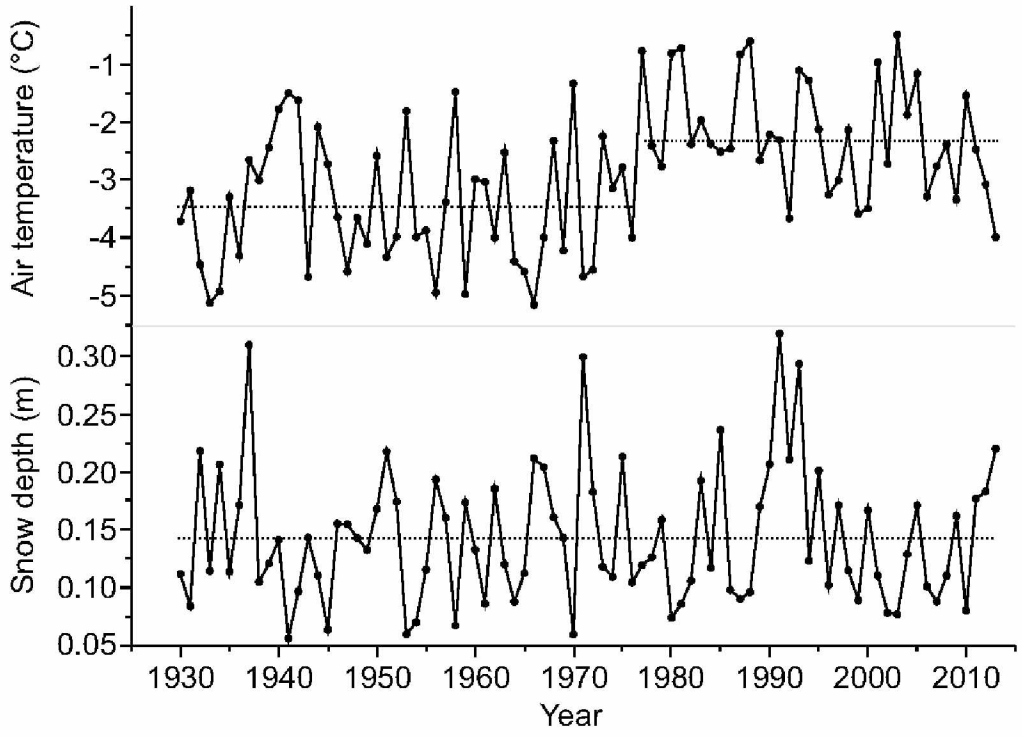

Figure 1.2. Mean annual air temperatures and snow depths. Data were from the Fairbanks International Airport and computed by hydrological year (1 October to 30 September) from 1930 to 2013 [*Alaska Climate Research Center*, 2014]. Dotted lines indicate mean values over the specified time period.

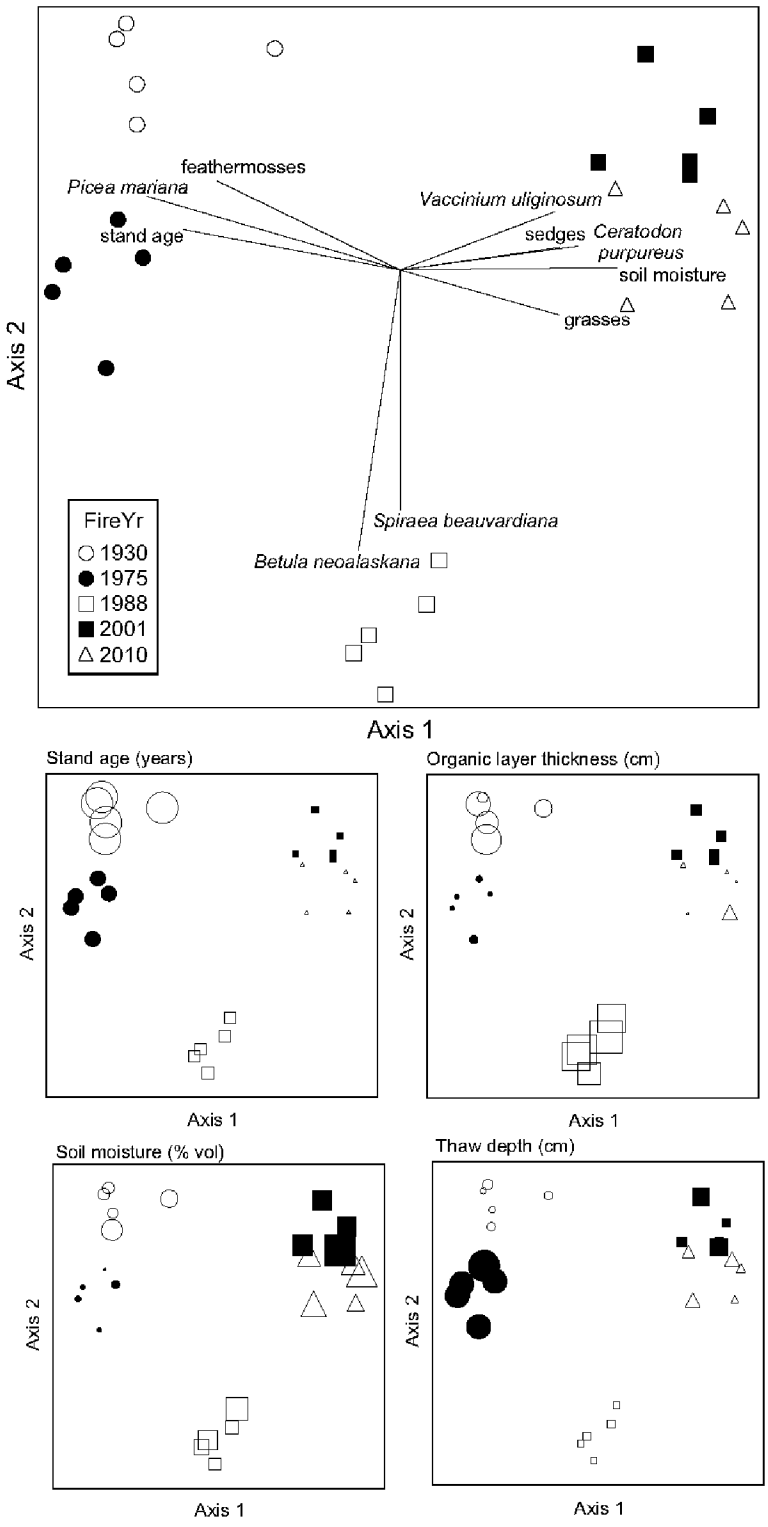

Figure 1.3. Plant community ordination. NMDS ordination of vegetation plots by fire year and correlations (vectors) with vegetation and site variables. Symbols are scaled to site variables in bottom panels.

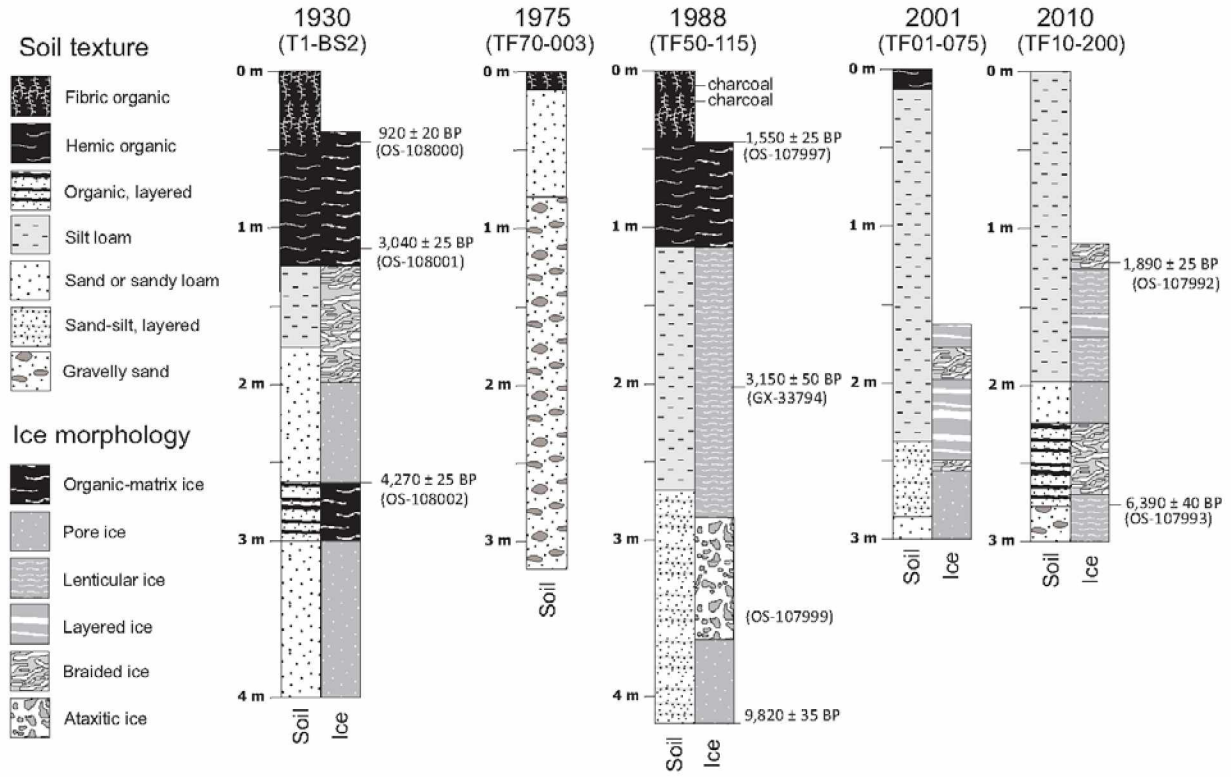

Figure 1.4. Soil texture, permafrost ice morphology, and radiocarbon dates with depth. One representative borehole per fire scar is pictured. Plot and radiocarbon sample IDs are in parentheses.

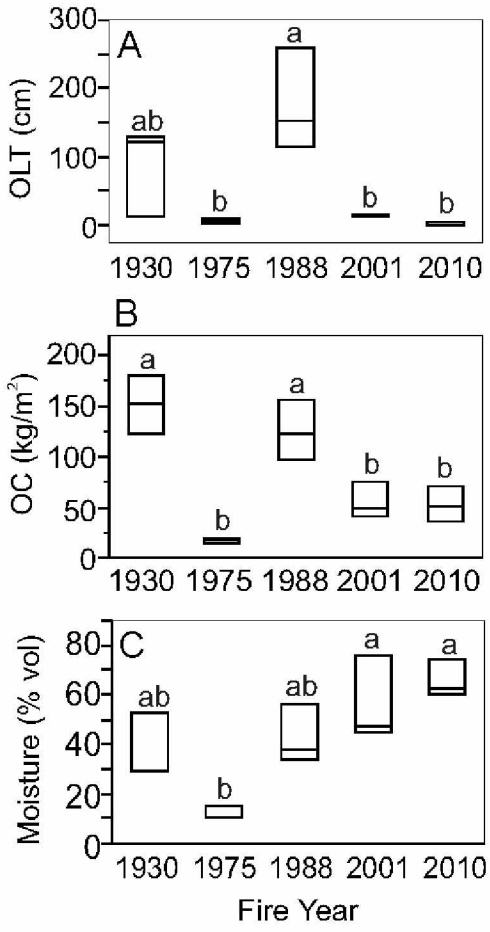

Figure 1.5. Soil physical properties by fire year. Box plots of (a) organic layer thickness (OLT), (b) organic carbon stocks (OC) to 3 m depth, and (c) active layer soil moisture. Tukey-Kramer post hoc results of significant differences ($p < 0.05$) are depicted by lettering. $n = 2$ to 3.

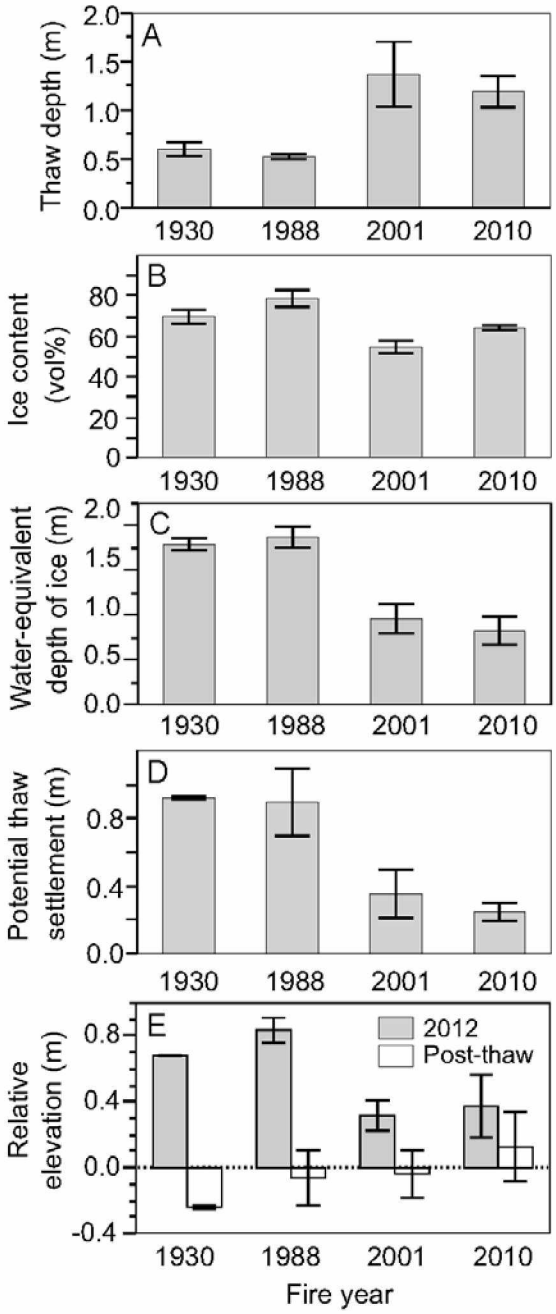

Figure 1.6. Permafrost properties and potential thaw settlement. (a) Thaw depth, (b) permafrost ice content, (c) water-equivalent depth of ice in permafrost, (d) potential thaw settlement, and (e) ground surface elevation in 2012 and predicted post-thaw ground surface elevation relative to surface water level. Data and calculations are based on the upper 3 m of the soil column. Mean ± SE, $n = 3$.

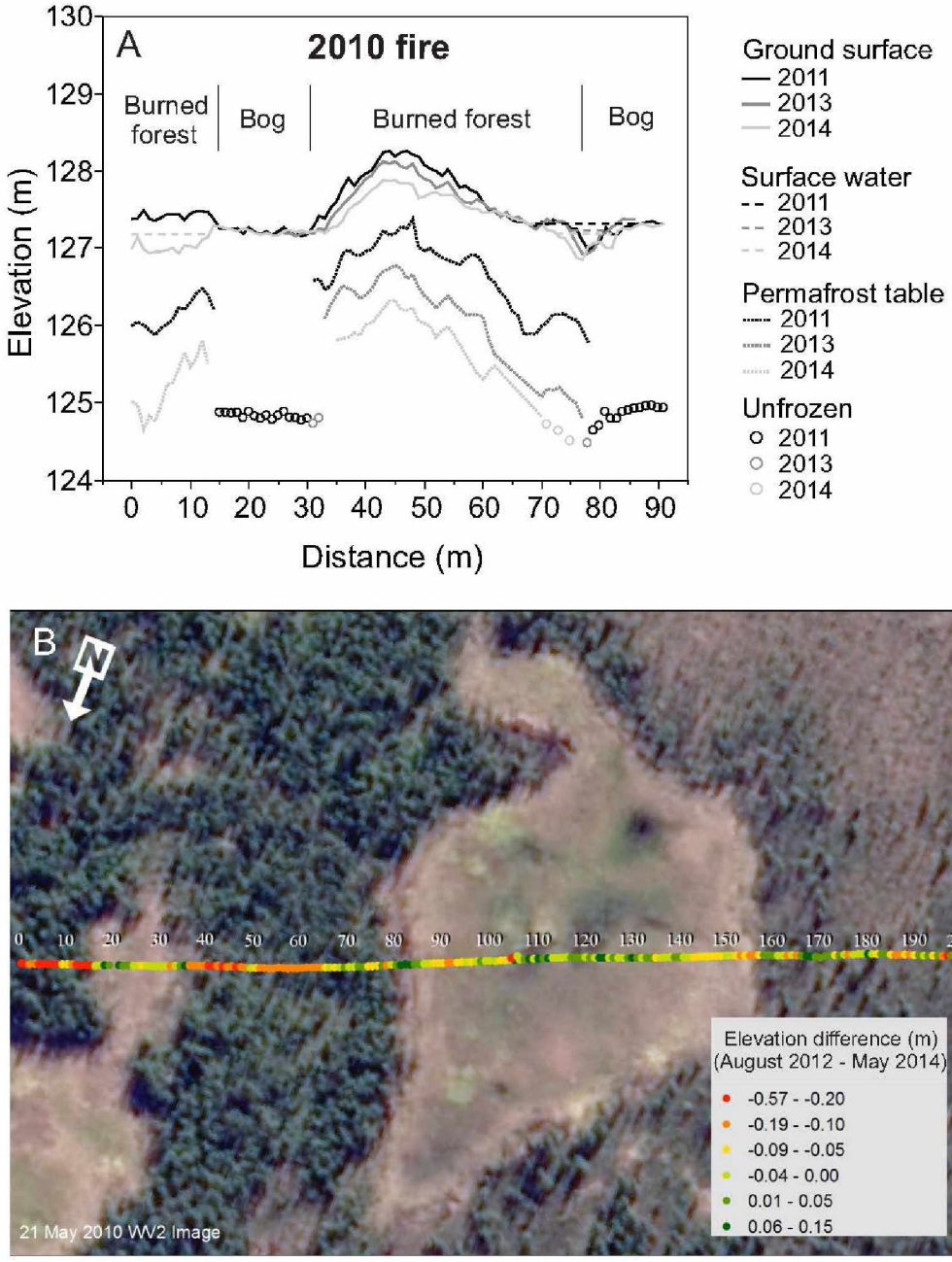

Figure 1.7. Transect through burned black spruce forest and collapse-scar bogs in the 2010 fire scar. (a) A cross-section of a portion of the transect depicts the elevations (m) of the ground surface, surface water, permafrost table, and maximum observed depths of unfrozen ground over time. Measurements for 2013 from transect meters 0 to 25 were excluded due to dGPS inaccuracy. (b) A bird's-eye view of the transect, overlain on prefire imagery (WorldView2, 21 May 2010), shows an independent comparison of surface elevation over time using ground-based dGPS (August 2012) and airborne LiDAR (May 2014).

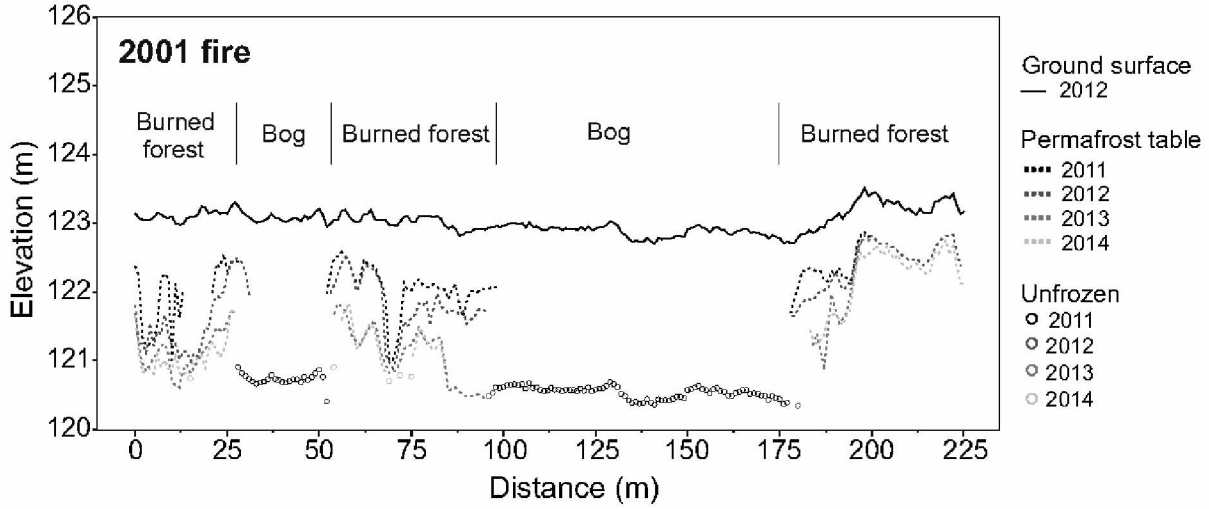

Figure 1.8. Transect through burned black spruce forest and collapse-scar bogs in the 2001 fire scar. Cross-section shows elevations of the ground surface, permafrost table, and maximum observed depths of unfrozen ground over time.

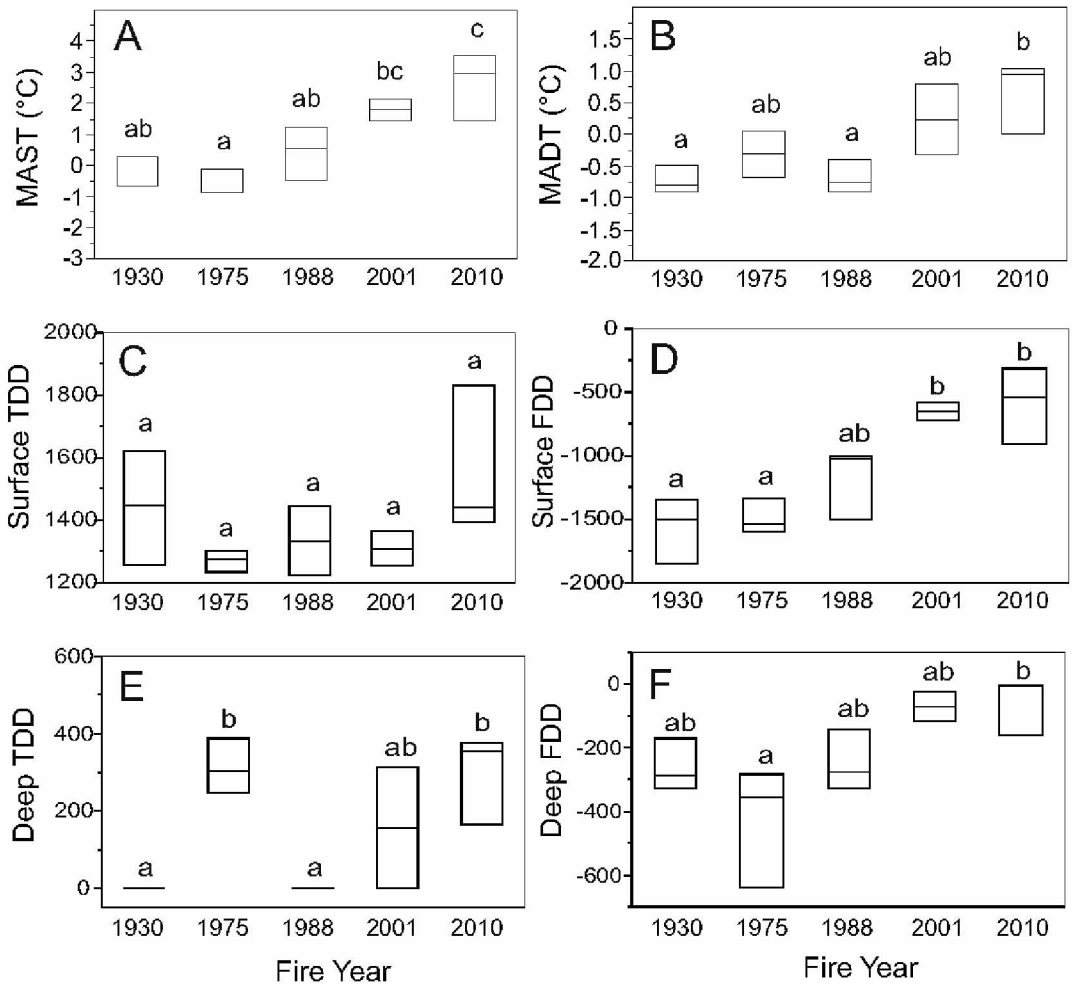

Figure 1.9. Summary of soil thermal regimes. Box plots of (a) mean annual surface temperature (MAST), (b) mean annual deep temperature (MADT), (c) surface thawing degree days (TDD), (d) surface freezing degree days (FDD), (e) deep thawing degree days (TDD), and (f) deep freezing degree days (FDD), by fire scar. Surface and deep measurements were from 5 cm and 1 m depths, respectively, in hydrological year 2013. Tukey-Kramer HSD post hoc tests were conducted following one-way ANOVAs. Significant differences are denoted by lettering. n = 2 to 3.

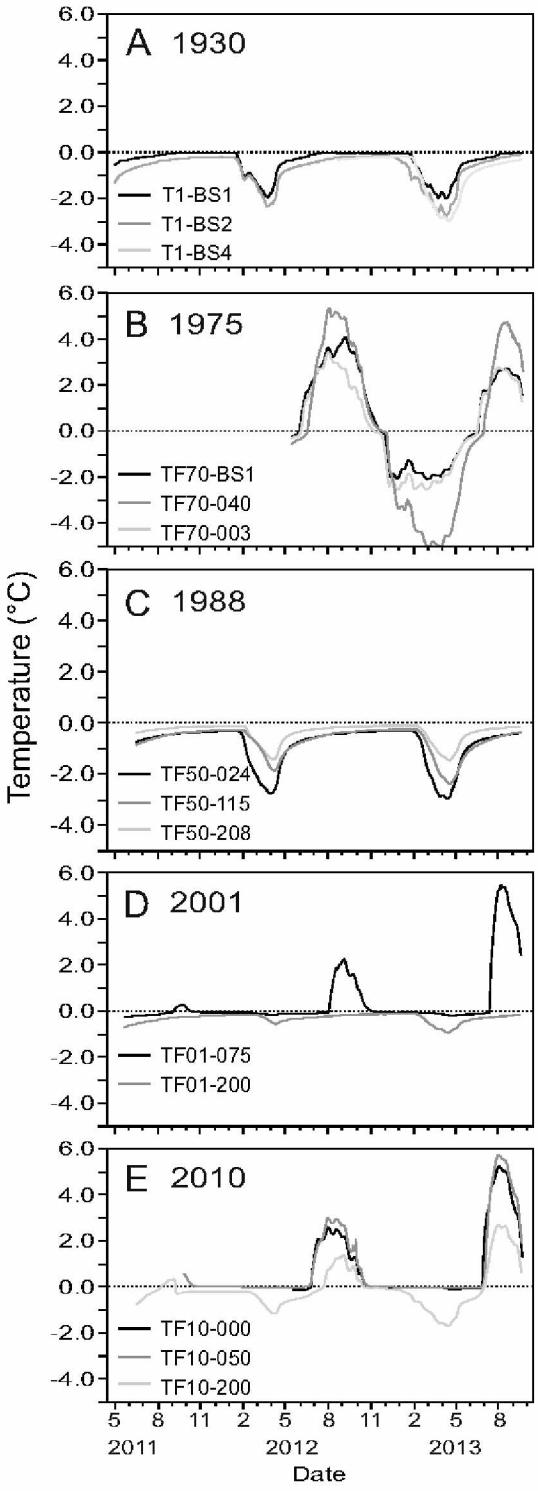

Figure 1.10. Measured daily soil temperatures at 1 m depth. Data are shown for each plot within the (a) 1930, (b) 1975, (c) 1988, (d) 2001, and (e) 2010 fire scars. The *x* axis tick marks depict the first day of each month. The dotted reference lines show 0 ºC.

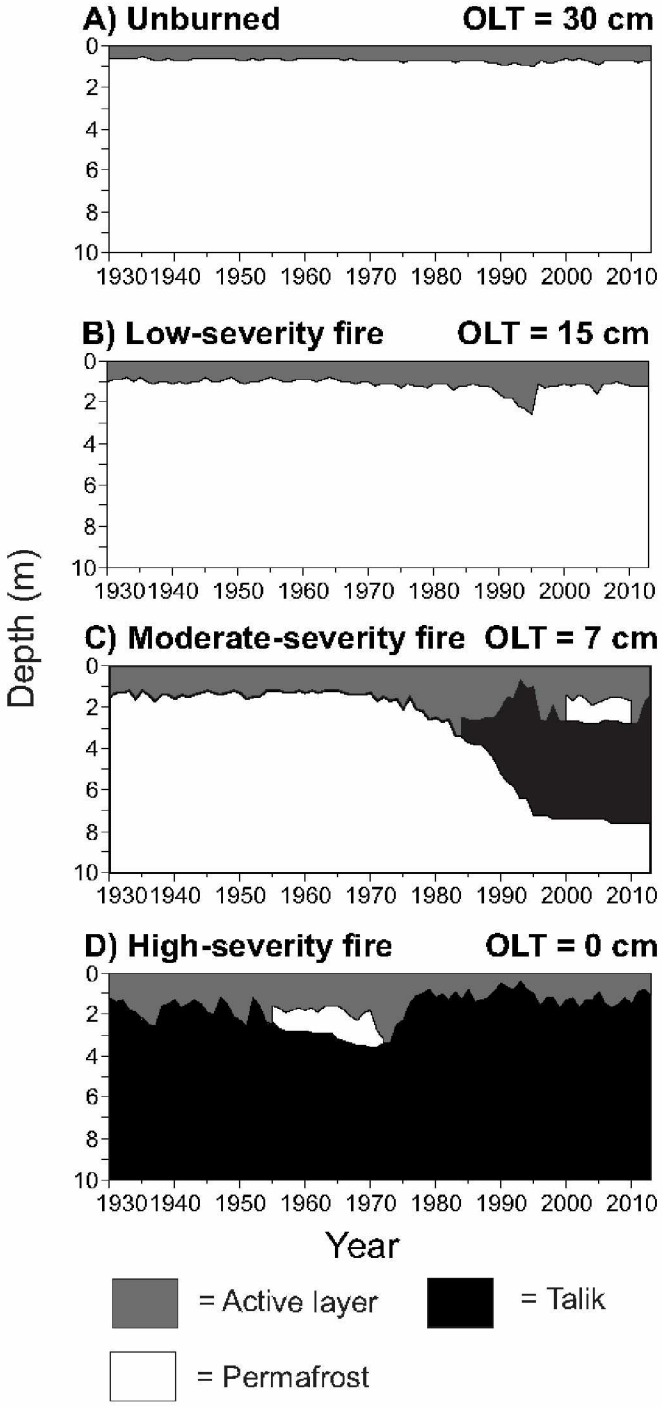

Figure 1.11. Simulated permafrost dynamics from 1930 to 2013. Varied levels of organic layer thickness (OLT) represent (a) unburned conditions, (b) low-severity fire, (c) moderate-severity fire, and (d) high-severity fire.

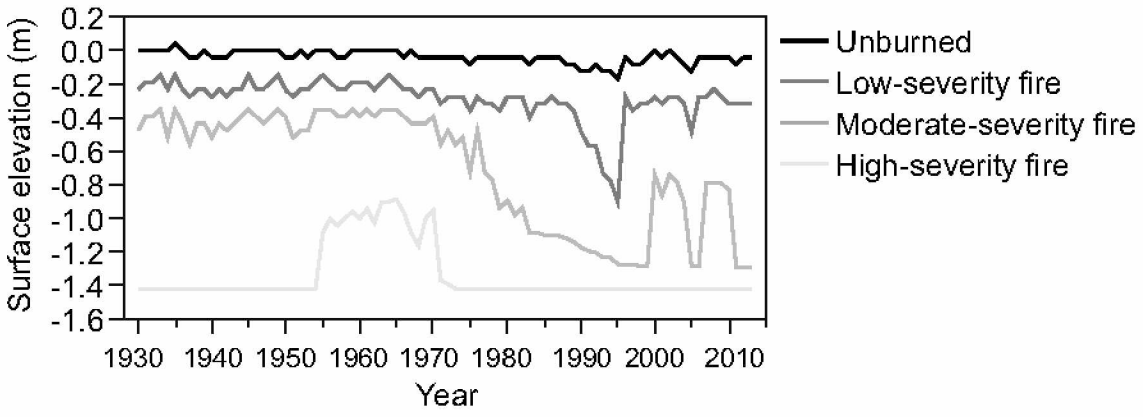

Figure 1.12. Simulated thaw settlement from 1930 to 2013. Surface elevation changes relative to unburned conditions are shown for different levels of fire severity.

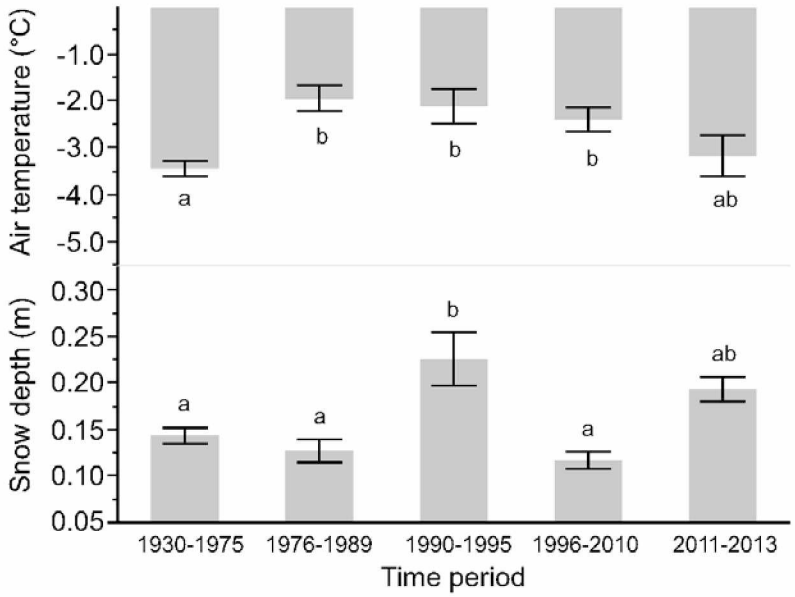

Figure 1.13. Mean annual air temperature and snow depth by time period. Time periods were chosen to represent dominant patterns in simulated permafrost dynamics. Values are means ± SE and significant differences are depicted by lettering.

Tables

Table 1.1. Soil parameters used in model simulations with varying levels of organic layer thickness (OLT). Thickness, volumetric water content (VWC), thermal conductivity (W m^{-1} K^{-1}) of thawed (k_t) and frozen (k_f) soil, and heat capacity (J m^{-3} K^{-1}) of thawed (C_t) and frozen (C_f) soil are shown for each soil layer.

	Thickness of layers for each simulation (m)						
Soil layer	OLT = 30 cm	OLT = 15 cm	OLT = 7 cm	OLT = 0 cm	VWC	k_t/k_f	C_t/C_f (10^6)
Organic	0.30	0.15	0.07	0.00	0.20	0.20/0.60	2.6/2.2
Silt loam/organic	0.09	0.09	0.09	0.09	0.60	0.70/2.10	2.5/1.7
Silt loam	2.74	2.74	2.74	2.74	0.57	1.30/2.10	2.5/1.7
Sand and gravel	96.87	97.02	97.1	97.17	0.33	1.90/2.50	1.8/1.6

Table 1.2. Plant species and percent cover averaged by fire year.

	Species
Trees	*Betula neoalaskana* Sarg.
	Larix laricina (Du Roi) K. Koch
	Picea glauca (Moench) Voss
	Picea mariana (Mill.) Britt., Sterns & Pogg
	Populus balsamifera L.
	Populus tremuloides Michx.
Shrubs	*Alnus viridis* (Chaix) DC ssp. *fruticosa* (Rupr.) Nyman
	Arctostaphylos rubra (Rehd. & Wilson) Fern.
	Betula glandulosa Michx.
	Betula nana L.
	Chamaedaphne calyculata (L.) Moench
	Ledum groenlandicum Oeder
	Linnaea borealis L.
	Oxycoccus microcarpus Turcz. ex Rupr.
	Ribes sp.
	Rosa acicularis Lindl.
	Rubus chamaemorus L.
	Rubus idaeus L.
	Salix alaxensis (Anderss.) Cov.
	Salix arbusculoides Anderss.
	Salix bebbiana Sarg.
	Salix fuscescens Anderss.
	Salix glauca L.
	Salix monticola Bebb

Average % cover by fire scar				
~1930	1975	1988	2001	2010
1.0	36.0	90.2	0.3	1.2
	6.5			
	3.7			
67.6	76.6		2.2	0.3
			0.1	0.1
	19.0		0.1	
0.1				
0.1	2.0			0.6
		6.6	0.6	5.0
			2.6	1.0
			1.0	4.4
16.2	0.3	10.0	9.4	5.5
	2.7			
			0.1	3.5
1.0	0.1			
2.0	0.8			0.1
3.6		2.3		4.0
		0.1		
				0.1
			0.6	0.1
1.0	2.3	1.0	0.6	
				3.0
1.0			1.1	0.7
	1.0			0.6

Table 1.2 continued

	Salix myrtillifolia Anderss.
	Salix novae-angliae Anderss.
	Salix planifolia Pursch. ssp. *pulchra* (Cham.) Argus
	Shepherdia canadensis (L.) Nutt.
	Spiraea beauverdiana Schneid.
	Vaccinium uliginosum L.
	Vaccinium vitis-idaea L.
	Viburnum edule (Michx.) Raf.
Herbaceous	*Adoxa moschatellina* L.
	Chamerion angustifolium (L.) Holub
	Cnidium cnidiifolium (Turcz.) Schischk.
	Cornus canadensis L.
	Epilobium adenocaulon Haussk.
	Equisetum arvense L.
	Equisetum pratense L.
	Equisetum scirpoides Michx.
	Equisetum sylvaticum L.
	Geocaulon lividum (Richards.) Fern.
	Iris setosa Pall. ssp. *setosa*
	Mertensia paniculata (Ait.) G. Don
	Polemonium acutiflorum Willd.
	Potentilla palustris (L.) Scop.
	Stellaria sp.
Graminoid	*Agrostis scabra* Willd.
	Arctagrostis latifolia (R. Br.) Griseb.
	Calamagrostis canadensis (Michx.) Beauv.
	Carex aquatilis Wahlenb.

	0.1			
	0.6			
1.0			0.3	2.3
	0.6			
		7.4		
6.0	0.1		3.2	4.0
8.8	0.9	12.0	9.2	2.6
	0.1			
				3.0
	1.6		1.0	12.0
	2.0			
0.7	0.7	0.1	2.0	
				0.1
			1.3	5.0
3.0	2.6			
2.0	1.0		1.5	13.0
10.5				19.6
7.8	0.6			
			1.0	
0.6	0.8			
			1.1	0.1
			0.1	0.1
0.1			0.1	
				8.0
0.1			1.1	1.3
0.7	1.0	12.4	11.4	10.0
			7.5	0.6

Table 1.2 continued

	Carex canescens L.
	Carex disperma Dew.
	Carex media R. Br.
	Eriophorum vaginatum L.
	Hordeum jubatum L.
	Luzula rufescens Fisch.
Nonvascular	*Aulacomnium palustre* (Hedw.) Schwaegr.
	Ceratodon purpureus (Hedw.) Brid.
	Cladonia amaurocraea (Flörke) Schaerer
	Cladonia gracilis (L.) Willd.
	Cladonia sp.
	Dicranum bonjeanii De Not
	Drepanocladus aduncus (Hedw.) Warnst. s.l.
	Hylocomium splendens (Hedw.) B.S.G.
	Hypnum plicatulum (Lindb.) Jaeg.
	Marchantia polymorpha L.
	Peltigera aphthosa (L.) Willd.
	Peltigera canina (L.) Willd.
	Peltigera didactyla (With.) J. R. Laundon
	Peltigera leucophlebia (Nyl.) Gyelnik
	Peltigera malacea (Ach.) Funck
	Petasites frigidus (L.) Franchet
	Pleurozium schreberi (Brid.) Mitt.
	Polytrichum juniperinum Hedw.
	Sphagnum capillifolium (Ehrh.) Hedw.
	Sphagnum fimbriatum Wils.
	Sphagnum girgensohnii Russ.

			2.0	
			1.1	
			3.7	0.1
			18.2	11.1
				0.1
			0.6	0.3
3.5	2.6	0.1	9.7	1.0
	1.0	0.1	9.5	12.2
1.0				
0.1	0.3			
1.0	0.1	0.1	1.1	
	0.1		1.0	
			3.0	
41.0	8.8	0.1	3.0	
3.8	0.7	0.1		
			0.1	16.2
1.0				2.0
			2.0	
			1.0	
	1.1		1.0	
	0.1			
			0.1	0.1
21.8	2.1	0.4	1.0	
			3.4	0.1
				3.5
3.0			2.0	0.1
4.6				9.0

Table 1.2 continued

Sphagnum magellanicum Brid.
Sphagnum rubellum Wils.
Sphagnum russowii Warnst.
Sphagnum squarrosum Crome
Sphagnum teres (Schimp.) Ångstr. in Hartm.
Tomentypnum nitens (Hedw.) Loeske

				0.1
0.1			0.3	0.1
		5.0		
0.1		0.1	1.0	0.6
			0.8	
	2.0	0.1		

References

Alaska Climate Research Center (2013), Climate normals from the 30-year time period from 1981–2010, provided by the National Climatic Data Center. [Available at http://climate.gi.alaska.edu/Climate/Normals.]

Alaska Climate Research Center (2014), ACIS Daily Data Browser. [Available at http://climate.gi.alaska.edu/acis_data.]

Alaska Interagency Coordination Center (2011), Fire history in Alaska. [Available at http://afsmaps.blm.gov/imf_firehistory/imf.jsp? site=firehistory.]

Barrett, K., E. S. Kasischke, A. D. McGuire, M. R. Turetsky, and E. S. Kane (2010), Modeling fire severity in black spruce stands in the Alaskan boreal forest using spectral and non-spectral geospatial data, *Remote Sens. Environ.*, 114(7), 1494–1503.

Burn, C. R. (1998), The response (1958–1997) of permafrost and near-surface ground temperatures to forest fire, Takhini River valley, southern Yukon Territory, *Can. J. Earth Sci.*, 35(2), 184–199.

Camill, P., and J. S. Clark (2000), Long-term perspectives on lagged ecosystem responses to climate change: Permafrost in boreal peatlands and the grassland/woodland boundary, *Ecosystems*, 3(6), 534–544.

Camill, P., J. A. Lynch, J. S. Clark, J. B. Adams, and B. Jordan (2001), Changes in biomass, aboveground net primary production, and peat accumulation following permafrost thaw in the boreal peatlands of Manitoba, Canada, *Ecosystems*, 4(5), 461–478.

Crory, F. E. (1973), Settlement associated with the thawing of permafrost, in *Proceedings 2nd International Conference on Permafrost, Yakuts, U.S.S.R., North American Contribution*, pp. 599–607, Natl. Acad. Sci., Washington, D. C.

Eugster, W., *et al.* (2000), Land-atmosphere energy exchange in Arctic tundra and boreal forest: Available data and feedbacks to climate, *Global Change Biol.*, 6, 84–115.

Farouki, O. T. (1981), Thermal properties of soils, CRREL Monograph 81-1Rep, United States Army Corps of Engineers, Cold Regions Res. and Eng. Lab., Hanover, N. H.

French, H., and Y. Shur (2010), The principles of cryostratigraphy, *Earth Sci. Rev.*, 101(3–4), 190–206.

Frolking, S., J. Talbot, M. C. Jones, C. C. Treat, J. B. Kauffman, E.-S. Tuittila, and N. Roulet (2011), Peatlands in the Earth's 21st century climate system, *Environ. Rev.*, 19, 371–396.

Genet, H., *et al.* (2013), Modeling the effects of fire severity and climate warming on active layer thickness and soil carbon storage of black spruce forests across the landscape in interior Alaska, *Environ. Res. Lett.*, 8(4), 045016, doi:10.1088/1748-9326/8/4/045016.

Gillett, N. P., A. J. Weaver, F. W. Zwiers, and M. D. Flannigan (2004), Detecting the effect of climate change on Canadian forest fires, *Geophys. Res. Lett.*, 31, L18211, doi:10.1029/2004GL020876.

Harden, J. W., K. L. Manies, M. R. Turetsky, and J. C. Neff (2006), Effects of wildfire and permafrost on soil organic matter and soil climate in interior Alaska, *Global Change Biol.*, 12(12), 2391–2403.

Hartmann, B., and G. Wendler (2005), The significance of the 1976 Pacific climate shift in the climatology of *Alaska, J. Clim.*, 18, 4824–4839.

Hayashi, M., A. McClymont, B. Christensen, L. Bentley, and W. Quinton (2011), Thawing of permafrost peatlands: Effects of water-energy feedback on landscape evolution, paper presented at Proceedings of the joint meeting of the International Association of Hydrogeologists Canadian National Chapter and the Canadian Quaternary Association, Quebec City.

Jafarov, E. E., S. S. Marchenko, and V. E. Romanovsky (2012), Numerical modeling of permafrost dynamics in Alaska using a high spatial resolution dataset, *Cryosphere*, 6(3), 613–624.

Jafarov, E. E., V. E. Romanovsky, H. Genet, A. D. McGuire, and S. S. Marchenko (2013), The effects of fire on the thermal stability of permafrost in lowland and upland black spruce forests of interior Alaska in a changing climate, *Environ. Res. Lett.*, 8(3), 035030, doi:10.1088/1748-9326/8/3/035030.

Johnson, K. D., J. W. Harden, A. D. McGuire, M. Clark, F. Yuan, and A. O. Finley (2013), Permafrost and organic layer interactions over a climate gradient in a discontinuous permafrost zone, *Environ. Res. Lett.*, 8(3), 035028, doi:10.1088/1748-9326/8/3/035028.

Johnston, C. E., S. A. Ewing, J. W. Harden, R. K. Varner, K. P. Wickland, J. C. Koch, C. C.Fuller, K. Manies, and M. T. Jorgenson (2014), Effect of permafrost thaw on CO_2 and CH_4 exchange in a western Alaska peatland chronosequence, *Environ. Res. Lett.*, 9, 085004, doi:10.1088/1748-9326/9/8/085004.

Johnstone, J. F., F. S. Chapin III, T. N. Hollingsworth, M. C. Mack, V. Romanovsky, and M. Turetsky (2010), Fire, climate change, and forest resilience in interior Alaska, *Can. J.For. Res.*, 40(7), 1302–1312.

Jorgenson, M. T., J. E. Roth, M. K. Raynolds, M. D. Smith, W. Lentz, A. L. Zusi-Cobb, and C. H. Racine (1999), An ecological land survey for Fort Wainwright, Alaska, *Rep. CRRELRep. 99–9*, 83 pp., U.S. Army Cold Regions Res. and Eng. Lab., Hanover, N. H.

Jorgenson, M. T., C. H. Racine, J. C. Walters, and T. E. Osterkamp (2001), Permafrost degradation and ecological changes associated with a warming climate in central Alaska, *Clim. Change*, 48(4), 551–579.

Jorgenson, M. T., K. Yoshikawa, M. Kanevskiy, Y. Shur, V. Romanovsky, S. Marchenko, G. Grosse, J. Brown, and B. Jones (2008), *Permafrost Characteristics of Alaska*, Institute of Northern Engineering, Univ. of Alaska Fairbanks.

Jorgenson, M. T., V. Romanovsky, J. Harden, Y. Shur, J. O'Donnell, E. A. G. Schuur, M. Kanevskiy, and S. Marchenko (2010), Resilience and vulnerability of permafrost to climate change, *Can. J. For. Res.*, 40(7), 1219–1236.

Jorgenson, M. T., *et al.* (2013), Reorganization of vegetation, hydrology and soil carbon after permafrost degradation across heterogeneous boreal landscapes, *Environ. Res. Lett.*, 8(3), 035017, doi:10.1088/1748-9326/8/3/035017.

Kanevskiy, M., T. Jorgenson, Y. Shur, J. A. O'Donnell, J. W. Harden, Q. Zhuang, and D. Fortier (2014), Cryostratigraphy and permafrost evolution in the lacustrine lowlands of West-Central Alaska, *Permafrost Periglacial Process.*, 25(1), 14–34.

Kasischke, E. S., *et al.* (2010), Alaska's changing fire regime—Implications for the vulnerability of its boreal forests, *Can. J For. Res.*, 40(7),1313–1324.

Kent, M. (2012), *Vegetation Description and Data Analysis: A Practical Approach*, John Wiley, New York.

Kuhry, P. (1994), The role of fire in the development of Sphagnum-dominated peatlands in western boreal Canada, *J. Ecol.*, 82, 899–910.

Mackay, J. R. (1995), Active layer changes (1968 to 1993) following the forest-tundra fire near Inuvik, N.W.T. Canada, *Arctic Alpine Res.*, 27(4), 323–336.

McCune, B., and J. B. Grace (2002), *Analysis of Ecological Communities*, MjM Software Design, Gleneden Beach, Oreg.

McCune, B., and M. J. Mefford (2011), *PC-ORD. Multivariate Analysis of Ecological Data.Version 6.0*, MjM Software, Gleneden Beach, Oreg.

Myers-Smith, I. H., J. W. Harden, M. Wilmking, C. C. Fuller, A. D. McGuire, and F. S. Chapin III (2008), Wetland succession in a permafrost collapse: Interactions between fire and thermokarst, *Biogeosciences*, 5(5), 1273–1286.

Nelson, D. W., and L. E. Sommers (1996), Total carbon, organic carbon, and organic matter, in *Methods of Soil Analysis, Soil Sci. Soc. Am.*, edited by J. M. Bartels, pp. 963–977, Am. Soc. Agron., Madison, Wis.

Nicolsky, D. J., V. E. Romanovsky, and G. S. Tipenko (2007), Using in-situ temperature measurements to estimate saturated soil thermal properties by solving a sequence of optimization problems, *Cryosphere*, 1(1), 41–58.

Nossov, D. R., M. T. Jorgenson, K. Kielland, and M. Z. Kanevskiy (2013), Edaphic and microclimatic controls over permafrost response to fire in interior Alaska, *Environ. Res. Lett.*, 8, 035013, doi:10.1088/1748-9326/8/3/035013.

O'Donnell, J. A., V. E. Romanovsky, J. W. Harden, and A. D. McGuire (2009), The effect of moisture content on the thermal conductivity of moss and organic soil horizons from black spruce ecosystems in interior Alaska, *Soil Sci.*, 174(12), 646–651.

O'Donnell, J. A., J. W. Harden, A. D. McGuire, and V. E. Romanovsky (2011), Exploring the sensitivity of soil carbon dynamics to climate change, fire disturbance and permafrost thaw in a black spruce ecosystem, *Biogeosciences*, 8(5), 1367–1382.

O'Donnell, J. A., M. T. Jorgenson, J. W. Harden, A. D. McGuire, M. Z. Kanevskiy, and K. P. Wickland (2012), The effects of permafrost thaw on soil hydrologic, thermal, and carbon dynamics in an Alaskan peatland, *Ecosystems*, 15(2), 213–229.

Olefeldt, D., M. R. Turetsky, P. M. Crill, and A. D. McGuire (2013), Environmental and physical controls on northern terrestrial methane emissions across permafrost zones, *Glob Change Biol.*, 19(2), 589–603.

Osterkamp, T. E., and C. R. Burn (2003), Permafrost, in *Encyclopedia of Atmospheric Sciences*, edited by J. R. Holton, J. Pyle, and J. A. Curry, pp. 1717–1729, Academic Press, Oxford, U. K.

Osterkamp, T. E., and V. E. Romanovsky (1999), Evidence for warming and thawing of discontinuous permafrost in Alaska, *Permafrost Periglacial Process.*, 10, 17–37.

Pastick, N. J.,M. T. Jorgenson, B. K.Wylie, J. R. Rose, M. Rigge, and M. A.Walvoord (2014), Spatial variability and landscape controls of near-surface permafrost within the Alaskan Yukon River Basin, *J. Geophys. Res. Biogeosci.*, 119, 1244–1265, doi:10.1002/2013JG002594.

Péwé, T. L. (1975), Quaternary geology of Alaska, *Rep. Prof Pap., 835*, 145 pp., U.S. Geol. Surv., Wash.

Pullman, E. R., M. T. Jorgenson, and Y. Shur (2007), Thaw settlement in soils of the Arctic Coastal Plain, Alaska, *Arct. Antarct. Alp. Res.*, 39(3), 468–476.

Racine, C. H., and J. C. Walters (1991), Groundwater-discharge wetlands in the Tanana Flats, interior Alaska, CRREL Rep. 91–14, U.S. Army Cold Regions Res. and Eng. Lab., Hanover, N. H.

Romanovsky, V. E. (2014), Bonanza Creek 2—Burned: Soils, Geophysical Institute Permafrost Laboratory, Univ. of Alaska Fairbanks. [Available at http://lapland.gi.alaska.edu/vdv/index.html.]

Romanovsky, V. E., and T. E. Osterkamp (2000), Effects of unfrozen water on heat and mass transport processes in the active layer and permafrost, *Permafrost Periglacial Process.*, 11, 219–239.

Romero-Lankao, P., J. B. Smith, D. J. Davidson, N. S. Diffenbaugh, P. L. Kinney, P. Kirshen, P. Kovacs, and L. Villers Ruiz (2014), North America, in *Climate Change 2014: Impacts, Adaptation, and Vulnerability. Part B: Regional Aspects. Contribution of Working Group II to the Fifth Assessment Report of the Intergovernmental Panel on Climate Change*, edited by V. R. Barros et al., pp. 1439–1498, Cambridge Univ. Press, Cambridge, U. K., and New York.

Schuur, E. A., *et al.* (2015), Climate change and the permafrost carbon feedback, *Nature*, 520(7546), 171–179.

Sergueev, D., G. Tipenko, V. Romanovsky, and N. Romanovskii (2003), Mountain permafrost thickness evolution under influence of long-term climate fluctuations (results of numerical simulation), in *The Seventh International Permafrost Conference*, pp. 1017–1021, Swets & Zeitlinger, Lisse.

Shur, Y., K. M. Hinkel, and F. E. Nelson (2005), The transient layer: Implications for geocryology and climate-change science, *Permafrost Periglacial Process.*, 16(1), 5–17, doi:10.1002/ppp.518.

Shur, Y. L., and M. T. Jorgenson (2007), Patterns of permafrost formation and degradation in relation to climate and ecosystems, *Permafrost Periglacial Process.*, 18(1), 7–19.

Thie, J. (1974), Distribution and thawing of permafrost in the southern part of the discontinuous permafrost zone in Manitoba, *Arctic*, 27(3), 189–200.

Turetsky, M. R., R. K. Wieder, D. H. Vitt, R. J. Evans, and K. D. Scott (2007), The disappearance of relict permafrost in boreal North America: Effects on peatland carbon storage and fluxes, *Global Change Biol.*, 13(9), 1922–1934.

Turetsky, M. R., E. S. Kane, J. W. Harden, R. D. Ottmar, K. L. Manies, E. E. Hoy, and E. S. Kasischke (2011), Recent acceleration of biomass burning and carbon losses in Alaskan forests and peatlands, *Nat. Geosci.*, 4, 27–31, doi:10.1038/ngeo1027.

Viereck, L. A., N. R. Werdin-Pfisterer, P. C. Adams, and K. Yoshikawa (2008), Effect of wildfire and fireline construction on the annual depth of thaw in a black spruce permafrost forest in interior Alaska: A 36-year record of recovery, paper presented at Proceedings of the Ninth International Conference on Permafrost, Fairbanks, Alaska.

Viereck, L. A., K. Van Cleve, F. S. Chapin III, and R. W. Ruess (2014), Active layer depths: Bonanza Creek Fireline, (1984 - Present), Bonanza Creek LTER - University of Alaska Fairbanks. BNZ:7. [Available at http://www.lter.uaf.edu/data_detail.cfm?datafile_pkey=7.]

Vitt, D. H., L. A. Halsey, and S. C. Zoltai (1994), The bog landforms of continental western Canada in relation to climate and permafrost patterns, *Arctic Alpine Res.*, 26(1), 1–13.

Wickland, K. P., R. G. Striegl, J. C. Neff, and T. Sachs (2006), Effects of permafrost melting on CO_2 and CH_4 exchange of a poorly drained black spruce lowland, *J. Geophys. Res.*, 111, G02011, doi:10.1029/2005JG000099.

Yoshikawa, K., W. R. Bolton, V. E. Romanovsky, M. Fukuda, and L. D. Hinzman (2003), Impacts of wildfire on the permafrost in the boreal forests of Interior Alaska, *J. Geophys. Res.*, 108(D1), 8148, doi:10.1029/2001JD000438.

Zhang, T. (2005), Influence of the seasonal snow cover on the ground thermal regime: An overview, *Rev. Geophys.*, 43, RG4002, doi:10.1029/2004RG000157.

Zoltai, S. C. (1993), Cyclic development of permafrost in the peatlands of Northwestern Alberta, Canada, *Arc. Alp. Res.*, 25(3), 240–246.

Chapter 2: Edaphic and microclimatic controls over permafrost response to fire in interior Alaska[1]

Abstract

Discontinuous permafrost in the North American boreal forest is strongly influenced by the effects of ecological succession on the accumulation of surface organic matter, making permafrost vulnerable to degradation resulting from fire disturbance. To assess factors affecting permafrost degradation after wildfire, we compared vegetation composition and soil properties between recently burned and unburned sites across three soil landscapes (rocky uplands, silty uplands, and sandy lowlands) situated within the Yukon Flats and Yukon-Tanana Uplands in interior Alaska. Mean annual air temperatures at our study sites from 2011 to 2012 were relatively cold (−5.5 °C) and favorable to permafrost formation. Burning of mature evergreen forests with thick moss covers caused replacement by colonizing species in severely burned areas and recovery of pre-fire understory vegetation in moderately burned areas. Surface organic layer thickness strongly affected thermal regimes and thaw depths. On average, fire caused a five-fold decrease in mean surface organic layer thickness, a doubling of water storage in the active layer, a doubling of thaw depth, an increase in soil temperature at the surface (−0.6 to +2.1 °C) and at 1 m depth (−1.7 to +0.4 °C), and a two-fold increase in net soil heat input. Degradation of the upper permafrost occurred at all burned sites, but differences in soil texture and moisture among soil landscapes allowed permafrost to persist beneath the active layer in the silty uplands, whereas a talik of unknown depth developed in the rocky uplands and a thin talik developed in the sandy lowlands. A changing climate and fire regime would undoubtedly influence permafrost in the boreal forest, but the patterns of degradation or stabilization would vary considerably across the discontinuous permafrost zone due to differences in microclimate, successional patterns, and soil characteristics.

Introduction

North American boreal forests are largely underlain by discontinuous permafrost. Because permafrost temperature in this zone is typically within a few degrees of thawing, it is potentially vulnerable to degradation due to changes in climate or surface disturbance (Osterkamp and Romanovsky 1999, Grosse *et al* 2011). Ecological succession is a strong negative feedback to permafrost degradation (Shur and Jorgenson 2007, Jorgenson *et al* 2010). With the development of evergreen stands with moss understories, surface organic material accumulates and soil moisture increases, creating cold subsurface conditions which support permafrost despite relatively warm air temperatures (Van Cleve and Viereck

[1] Nossov, D R, Jorgenson M T, Kielland K, and Kanevskiy M Z 2013 Edaphic and microclimatic controls over permafrost response to fire in interior Alaska *Environ. Res. Lett.* **8** 035013 doi:10.1088/1748-9326/8/3/035013

1981, Osterkamp and Romanovsky 1999, Johnstone *et al* 2010a). Fire influences the surface energy balance primarily through the combustion of the insulating organic layer, so the response of permafrost to fire is mediated by fire severity (Yoshikawa *et al* 2003). High-severity fires which combust much of the insulating organic layer can increase soil heat flux and cause rapid permafrost degradation (Mackay 1995, Burn 1998, Yoshikawa *et al* 2003, Viereck *et al* 2008, Jiang *et al* 2012). If permafrost thaws beyond the depth of seasonal freezing, a perennially unfrozen layer, or talik, forms above the permafrost table. This talik decouples permafrost from the atmosphere and could continue to develop vertically and laterally over the long term (Osterkamp and Burn 2003, Yoshikawa *et al* 2003). However, degradation could be halted through the recovery of vegetation and the surface organic layer (Mackay 1995, Viereck *et al* 2008, Yi *et al* 2010). Fire severity also mediates the patterns of plant succession, and therefore, the recovery of the surface organic layer and the stabilization of permafrost (Shur and Jorgenson 2007, Viereck *et al* 2008, Johnstone *et al* 2010b, Shenoy *et al* 2011).

Changes in the fire regime, particularly coupled with a warming climate, can impact the distribution of permafrost by controlling the characteristics of the surface organic layer, both directly through combustion and indirectly through plant succession. There is evidence of climatically induced intensification of the fire regime in the North American boreal forest, with increased extent, frequency, and severity of fires, changes which would be expected to be unfavorable to permafrost stability in the marginal climates of the discontinuous permafrost zone (Gillett *et al* 2004, Kasischke and Turetsky 2006, Kasischke *et al* 2010, Johnstone *et al* 2010a, Barrett *et al* 2011). Permafrost degradation impacts hydrology, vegetation, and ecosystem processes which could feedback to influence climate through changes in carbon cycling; therefore, the response of permafrost to fire disturbance could have local, regional, and global-scale implications (Jorgenson *et al* 2010, Grosse *et al* 2011, O'Donnell *et al* 2011, Yuan *et al* 2012). The patterns of resilience or vulnerability of permafrost to the widespread disturbance of fire, though, are likely to differ across the discontinuous permafrost zone depending on numerous site factors that influence soil heat flux.

Variations in microclimate, soils, and vegetation create a wide range of thermal conditions that may modify the permafrost response to fire across the discontinuous permafrost zone. Air temperature and snowfall are important climatic controls on permafrost which vary regionally and topographically (Osterkamp and Romanovsky 1999, Jorgenson *et al* 2010). Soil texture and topography influence soil moisture and ice content, factors which strongly control heat flow through the ground (Shur and Jorgenson 2007). Soil moisture is of particular importance to soil thermal regimes in cold climates largely because the thermal conductivity of ice is four-fold greater than the conductivity of liquid water. Thus, the seasonal variation in the thermal conductivity of moist soils reduces heat conduction into the ground in summer, but enhances heat loss in winter, thereby typically creating colder soil conditions in fine-textured

soils with high water-holding capacities (Williams and Smith 1991). The impermeability of the permafrost surface also contributes to high soil moisture in areas with a thin active layer (Woo *et al* 2008). The effects of permafrost thaw on soil moisture are likely dependent on the underlying soil texture (Jorgenson and Osterkamp 2005). For example, on slopes less susceptible to water impoundment with surface subsidence, the deepening of the active layer into coarse-textured soils would be expected to improve drainage, whereas drainage in fine-textured soils may be less affected by the change in thaw depth. By mediating the soil moisture regime after post-fire permafrost thaw, surficial geology may control the long-term stability of permafrost. Furthermore, the rate of thaw and resilience of permafrost is influenced by ice content (Jorgenson *et al* 2010). Permafrost with low ice content would be expected to thaw more rapidly after fire than permafrost with high ice content, due to differences in latent heat required for thawing. The focus of this research was to test how these edaphic factors influence the vulnerability of permafrost to degradation as a result of fire disturbance.

We examined the patterns of post-fire permafrost degradation in the discontinuous permafrost zone of the interior Alaskan boreal forest, a region with a continental climate and widespread fire disturbance. We compared recently burned and unburned evergreen stands across three soil landscapes (rocky uplands, silty uplands, and sandy lowlands). We examined how the permafrost response to fire, in terms of soil thermal regimes, moisture, and thaw depths, was mediated by vegetation, soil characteristics, and climate. The specific objectives of this study were to: (1) characterize the variation in vegetation composition and surface organic layer thickness in relation to soil properties, succession, and fire; (2) compare soil thermal regimes, moisture regimes, and thaw depths of burned and unburned stands across soil landscapes; and (3) monitor changes in active-layer depth and thaw settlement in ice-rich silty uplands under different disturbance regimes.

Methods

Study area and sampling design

The study area is within the interior Alaskan boreal forest, a region which is bounded by the Brooks Range to the north and the Alaska Range to the south (Figure 2.1). The region is underlain by discontinuous permafrost and is characterized by a continental climate, with low precipitation and wide variation in air temperatures (Figure 2.1, Table 2.1). In interior Alaska, from 1971 to 2000, mean annual air temperature was -3.7 ºC and mean annual precipitation was 323 mm (Alaska Climate Research Center 2013).

Our study focused on three soil landscapes: rocky up lands, silty uplands, and sandy lowlands, which respectively comprise approximately 30%, 5%, and 5% of the boreal region of Alaska (Karlstrom 1964, Jorgenson *et al* 2008) (Figure 2.1, Table 2.1). Within each landscape, we established

three 'unburned' sites in mature evergreen forests (*Picea mariana* or *Picea glauca*), and three recently burned sites. Sites were selected using targeted sampling to establish plots in large homogeneous patches. Accessibility by floatplane or road was also considered in site selection. The range of variation in vegetation, fire severity, and soil characteristics that we captured was limited by the small sample size.

The rocky upland sites were located in the White Mountains National Recreation Area in the Yukon-Tanana Uplands ecoregion (600 m elevation). The colluvial substrate was dominated by channery rocks with fine-textured silt loams. The unburned rocky upland landscape had an ice-rich intermediate layer of permafrost just below the active layer ranging from 0.2 to 1.5 m thick, and was underlain by ice-poor permafrost. The burned rocky upland sites were affected by the 2004 Boundary Fire. The silty upland and sandy lowland study sites were located in the Yukon Flats National Wildlife Refuge, in a region with particularly strong variation in seasonal temperatures and low annual precipitation (170 mm) (Gallant *et al* 1995). The burned silty upland sites were affected by the 2009 Big Creek Fire. The silty upland sites (250 m elevation) were situated on hilly loess deposits. Yedoma deposits such as these were formed by ice-rich syngenetically frozen silt with massive ice wedges in areas that were unglaciated during the late Pleistocene. In interior Alaska, large areas underlain by yedoma have been affected by thermokarst and thermal erosion during the Holocene, which resulted in formation of an ice-poor layer of thawed and refrozen soils up to 4 m thick on top of yedoma sections (Péwé 1975, Kanevskiy *et al* 2012). Our unburned silty upland sites had an ice-rich intermediate layer of permafrost approximately 0.6 m thick, underlain by a 2–3 m ice-poor layer, which was just above the extremely ice-rich yedoma. The sandy lowlands sites (~100 m elevation) had a thin eolian loess cap (0.5–2.5 m) over an eolian sand sheet underlain by fluvial gravel and were ice-poor. The fire-affected sites burned in the 2004 Lower Mouth Fire and the 2010 Canvasback Lake Fire.

Data collection and analysis

Field sampling was conducted from 2009 to 2012. Air temperatures were recorded at one site within each landscape type. Two-channel dataloggers (HoboProV2, Onset Corp.) were installed at each study site to measure soil temperatures at the ground surface (5 cm) and at depth (100 cm). Temperatures were recorded at two-hour intervals and mean monthly air temperatures, mean annual air temperatures (MAAT), mean annual surface temperatures (MAST), and mean annual deep temperatures (MADT) were calculated. Thawing degree days (TDD) and freezing degree days (FDD) were the absolute value of the sum of the daily temperatures above and below 0 ºC, respectively, for a one-year period. Freezing *n*-factors, i.e., the ratio of ground surface FDD to air FDD, were used to assess winter soil surface temperatures relative to local air temperatures to infer surface boundary effects and snow depth (Lunardini 1978). The temperature measurements reported were from the period 1 September 2011 to 31

August 2012. Note that surface temperature data were missing from two sites (in unburned silty uplands and unburned sandy lowlands) due to sensor failure and frost heave.

Soils were sampled near each soil temperature datalogger. Thaw depths were measured with a metal probe in late-August to mid-September. Minimum thaw depths were used for two of the burned sites due to the difficulty of accurately probing the rocky soils. Soil stratigraphy was described according to the methods of the Natural Resources Conservation Service. Soil pH and electrical conductivity were measured with hand-held meters in the field (PCTestr 35, Oakton) and values at 10 cm depth were used for site values. Soil samples were taken for bulk density and volumetric soil moisture, based on wet and oven-dried (60 °C) weights. Water storage (equivalent depth) was calculated as the total water content in the active layer or seasonally frozen layer. The net heat input into the active layer during the thaw season was estimated as the sum of latent and sensible heat in mid-August, based on moisture contents, mineral and organic soil fractions, and temperature gradients of the active layer (Jorgenson 1986). Landscape-level means and results of statistical tests that are reported for the above variables were from the 2012 field data.

Percent cover of each plant species was estimated through point-sampling a 100-point grid within a 5 m × 10 m plot at each site. Species that were present but not captured by the point-sampling were recorded as having trace (0.1%) cover. Vegetation analysis was conducted with a multivariate ordination technique, nonmetric multidimensional scaling (NMDS), using PC-ORD 6.0 (McCune and Grace 2002, McCune and Mefford 2011). Ordination is used as a method of data reduction in which the dominant patterns of the variation in species composition are extracted into few continuous synthetic variables, the ordination axes. After the ordination of plant community data, correlation analyses of the axis scores with species and environmental data were conducted and presented as biplots, in which vectors represent the strength and direction of the correlations. NMDS is an iterative process that finds a low-dimensional representation of the dissimilarity matrix of sample units (sites) while preserving the ranking of distances. Distances between points in the ordination diagram approximate the dissimilarity of vegetation between sites. Species and environmental data were assessed for normality and were transformed as needed prior to ordination analysis.

Two 100–200 m transects were established in the silty uplands area with different fire disturbance histories to monitor annual changes in the permafrost table and thaw settlement through differential leveling and thaw probing (Viereck *et al* 2008, Osterkamp *et al* 2009). The intensive soil and vegetation monitoring sites for the silty uplands described above were located along these transects. Relative elevations were determined using differential leveling at 1 m intervals, and were tied to GPS-derived benchmark elevations to calculate absolute elevations of the ground surface. Thaw depths were measured at the same points and were subtracted from the surface elevations to determine the elevations of the

permafrost table. Sampling dates were: 1–2 September 2009; 3–4 September 2010; 17–18 September 2011; and 7–8 September 2012. Note that initial sampling at the 2009 fire occurred the year following the fire. Changes were analyzed only from 2010 to 2012, the years with complete datasets across both transects.

Two-factor ANOVAs (JMP 10.0.0, SAS 2012) were conducted to determine the effects of landscape type, fire disturbance, and interactive effects on surface organic layer thickness, soil moisture, active-layer water storage, thaw depth, and net heat input. Diagnostic plots of residuals were used to assess normality and homoscedasticity. One outlier, a burned site in the rocky uplands with anomalously low fire severity, was removed from ANOVA analyses and the reported landscape-level means. Least square means differences were calculated using post hoc tests; Tukey HSD for multiple comparisons, and student's *t*-tests for pairs. Linear regression was used to examine relationships between surface organic thickness, thaw depth, and soil moisture. Shapiro–Wilk tests confirmed normal sampling distributions for these variables. Statistical significance was considered with $p < 0.05$. We used only the 2012 data for these analyses, which had a complete set of data across all sites. All datasets associated with this study are archived under the dataset title prefix 'Yukon River Basin Fire and Permafrost' at www.lter.uaf.edu/data b.cfm.

Results and discussion

To evaluate factors controlling permafrost degradation after fire in the discontinuous permafrost zone, we compared ecological and thermal characteristics in burned and unburned forest stands among three soil landscapes in interior Alaska. Rocky upland, silty upland, and sandy lowland landscapes differed in terms of substrate and fire history (timing and severity), factors which influenced vegetation composition and its co-varying soil characteristics, such as surface organic layer thickness, thaw depth, and soil moisture. Fire, vegetation, soil, and topography interacted with climate to create varied soil moisture and thermal regimes and thaw depths that affect the stability of permafrost. Below we describe in detail the ecological, thermal, and physical patterns we observed and discuss the factors influencing permafrost.

Ecological patterns

The ordination shows the variation in plant community composition along gradients associated with edaphic characteristics and fire disturbance (Figure 2.2). The points depicted in the ordination represent the community structure at each site, and the direction and length of the vectors indicate the direction and strength of the correlations of community composition with species cover (Figure 2.2a) and environmental characteristics (Figure 2.2b). The distance between points signifies the degree of

dissimilarity in community composition among sites. The ordination axes were rotated by the treatment variable (fire) to differentiate the effects of fire on species composition from other sources of variation. Therefore, the effects of fire on vegetation were most pronounced along Axis 1, which accounts for most of the variation in community composition (54%). The unburned and burned sites of each soil landscape were clearly separated along this gradient, and the gradient was correlated with fire-related changes, such as decreased vegetation cover, increased cover of bare mineral soil, decreased surface organic layer thickness, increased thaw depth, and deep soil temperature (Figures 2.2a and 2.2b). The increase of bare ground along Axis 1 was accompanied by increased cover of colonizing species that thrive on exposed mineral soils after fire (*Marchantia polymorpha, Ceratodon purpureus, Epilobium angustifolium, Populus tremuloides*) (Figure 2.2a). Given the relationship between Axis 1 and fire, the distance between the unburned and burned sites along Axis 1 suggests the magnitude of change in community composition after fire. Axis 2 represents 39% of the variation in plant community structure. The clustering of the unburned sites by landscape type along this axis and the strong correlations between this axis and plant species found primarily in the unburned stands suggest that the variation along Axis 2 mainly reflects the differences in long-term successional patterns of the mature stands between landscape types (Figure 2.2a). Additionally, Axis 2 was correlated with a number of soil characteristics (organic layer thickness, moisture, pH, electrical conductivity, thaw depth) (Figure 2.2b), which reflect a combination of the underlying environmental characteristics and the influence of vegetation on soils.

The burned and unburned sites of the rocky landscape were clustered along Axis 1, revealing relatively similar community composition before and after the 2004 fire, and suggesting greater survival of pre-fire vegetation and/or greater post-fire recovery. The evergreen canopy (*Picea mariana*) was destroyed and colonizers had invaded, but overall the understory vegetation appeared to be recovering towards pre-fire conditions, increasing the likelihood of permafrost recovery (Viereck *et al* 2008). At two of the burned sites, residual surface organic layer thicknesses were reduced to 4–9 cm. At one tussock-dominated site, fire severity was low, leaving 35 cm of organic material. The unburned sites in the rocky uplands were differentiated from others by the abundance of acidifying *Sphagnum* mosses (mainly *S. fuscum*), acidophilic dwarf birch and ericaceous shrubs, and were associated with strongly acidic soils, thick organic layers, high soil moisture, and shallow active layers (Figures 2.2a and 2.2b).

The sandy lowland sites were affected by severe fires in both 2004 and 2010. Less than 2 cm of surface organic material remained after the first fire. The second fire combusted the remaining organic layer and exposed bare mineral soil over much of the spatial extent of the fire. The magnitude of the effects of the high-severity fire on vegetation in the lowlands was apparent in the wide separation between burned and unburned sites along Axis 1 (Figure 2.2a). The above-ground portions of pre-existing vegetation were virtually all consumed, and cover of mineral soil colonizers increased. The high

abundance of *Populus tremuloides* seedlings after fire in these sites suggests a shift to deciduous successional trajectory, which would be expected to postpone the development of a thick moss layer that facilitates permafrost recovery (Viereck *et al* 2008, Johnstone *et al* 2010a). The unburned sandy lowlands had distinct plant species assemblages, which were likely influenced by the alkaline soils and relatively low soil moisture (20 vol%), as suggested by the correlation of Axis 2 with these environmental variables (Figure 2.2b) and with several indicator species described below (Figure 2.2a). We attribute the low soil moisture to the arid climate and to the good drainage due to the deep active layer and underlying sandy soils. The active layer of these soils was thick even in the unburned sites (~100 cm). In contrast to the other areas where late successional forests were dominated by *Picea mariana*, the unburned evergreen sites were dominated by *Picea glauca*, a species which tends to occupy well-drained soils. *Tomenthypnum nitens*, a common feathermoss indicative of calcareous soils, occurred exclusively in these sites. The calciphilic shrub *Shepherdia canadensis* was common, whereas *Sphagnum* and ericaceous shrubs were notably absent. The surface organic layer was about 15 cm thick and dominated by feathermosses.

In the silty uplands, the 2009 fire reduced surface organic layer thicknesses from 14 to 7 cm on average, and caused a large shift in vegetation, with colonizers establishing on mineral soils and the regrowth of willow species (Figure 2.2a). The exposure of mineral soils and recruitment of deciduous seedlings (*Populus tremuloides*) suggest a shift towards a deciduous successional trajectory. The unburned vegetation was characterized by a high density of *Picea mariana* trees, abundant ericaceous shrubs, and a feathermoss-dominated moss layer. The silt loam soils were weakly acidic, had a moderately thick organic layer and a shallow active layer, and were saturated at depth.

Low-severity fires in which a thick surface organic layer remains typically result in the re-establishment of pre-existing vegetation (Johnstone *et al* 2010b). Many of the dominant species in boreal spruce forest understories are able to resprout after a low-severity fire, thereby speeding the recovery of the pre-fire vegetation (Johnstone *et al* 2010a, Bernhardt *et al* 2011, Hollingsworth et al 2013). Further, the low albedo and high porosity of the charred organic surface create dry conditions unfavorable for the establishment of small-seeded deciduous tree species, which typically have greater success on the moist seedbeds of mineral soils (Johnstone and Chapin 2006). The larger seeds of evergreen trees have greater carbohydrate reserves, which allow rapid root growth and thus a greater ability to access the scarce soil moisture in burned organic seedbeds (Greene and Johnson 1999). The variation in these plant traits helps explain why low-severity fires perpetuate self-replacement and high-severity fires are associated with a shift in the successional trajectory towards deciduous dominance. Deciduous stands are characterized by relatively high rates of evapotranspiration, high litterfall, rapid nutrient cycling, thin organic layers, and limited moss development, factors which contribute to high soil temperatures, low soil moisture, and the absence of, or greater depths to, permafrost (Van Cleve and Viereck 1981, Flanagan and Van Cleve 1983,

Johnstone *et al* 2010a). By contrast, evergreen stands are associated with low litterfall, moss understories, slow rates of decomposition, and the subsequent accumulation of thick organic layers, which insulate soils and reduce heat input.

Moisture and thermal regimes

Fire disturbance and landscape type each had significant effects on a wide range of soil properties, and interactive effects on surface organic thickness, soil moisture, and water stocks were found (Figures 2.3a–e and 2.4). Overall, there was a large decrease in surface organic layer thickness (from 21 to 4 cm) in burned sites across all soil landscapes. There was no significant change in mean volumetric moisture content overall, but there was a large increase in water storage above the permafrost (from 247 to 431 kg m^2) due to increases in thaw depth after fire (from 72 to 152 cm). Fire caused an increase in MAST (from −0.6 to +2.1 ºC), MADT (from −1.7 to +0.4 ºC), and seasonal heat gain (from 86 to 183 MJ m^2). We attribute the higher ground temperatures at the burned sites in winter to the increase in summer ground heat flux after the reduction of the surface organic layer thickness (Figure 2.4). Winter cooling of the soils in the burned sites was likely slowed by the combined effect of snow and an increase of heat released from the deeper active layer. Similar seasonal ground thermal patterns after fire have been observed in other studies (Burn 1998, Yoshikawa *et al* 2003).

The thickness of the surface organic layer was a strong predictor of thaw depth across all landscape types and treatments in our study (Figure 2.5a), underscoring the importance of the interplay between ecological succession, in which organic material accumulates, and fire, which combusts the surface organic material, to the soil thermal regime and permafrost. Increased surface organic layer thickness was also associated with increased volumetric soil moisture content of the active layer/seasonally frozen layer (Figure 2.5b). We attribute this relationship to the high water-holding capacity of organic material and the impermeability of the permafrost table, which causes increased soil moisture in the thin active layer (Woo *et al* 2008, Yi *et al* 2010, Yoshikawa *et al* 2003). It is well documented that organic horizon thickness strongly influences thaw depth in the discontinuous permafrost zone, but there is wide variation in the magnitude of change after fire (Yoshikawa *et al* 2003, Viereck *et al* 2008, O'Donnell *et al* 2011). We suggest that permafrost response to fire disturbance is modified by microclimatic and edaphic variation as we describe in detail below.

Within our study area, we found substantial differences in microclimate, attributed to both region and topography, which influenced the ground thermal regime and the sensitivity of permafrost to degradation after fire (Table 2.1). The climate of the Yukon-Tanana Uplands ecoregion is less continental than the Yukon Flats, a tendency magnified by the higher elevation of the rocky upland sites, which causes cooler summers, warmer winters, and greater snowfall (Table 2.1) (Jorgenson *et al* 2010). More

moderate temperatures were recorded in the rocky upland sites, with lower air TDD and FDD than in the other sites. Freezing *n*-factors, which represent winter soil surface temperatures relative to local air temperatures, can be used to infer the impact of an insulating snow layer on soil temperatures in the absence of direct measurements of snow depth (Lunardini 1978, Karunaratne and Burn 2003). The rocky uplands had significantly lower freezing *n*-factors than the other landscape types, suggesting that greater snowfall in this area may have contributed to warmer winter soil surface temperatures (Table 2.1). The sandy lowland and silty upland sites were located at low elevations in the Yukon Flats area. The greater seasonal variation in the measured values of air TDD and FDD in the Yukon Flats area reflect the strongly continental regional pattern. Within the Yukon Flats area there were climatic differences between the sandy lowland and silty upland sites, which could have been influenced by differences in topography and aspect. The sandy lowland sites had particularly high air TDD. The silty upland sites had MAAT nearly 1 °C colder than the rocky uplands and sandy lowlands. Our study area, near the northern extent of the discontinuous zone, had relatively cold MAATs (−5.2 to −6.1 °C) which helped to minimize the effects of fire. Over the broader discontinuous permafrost zone in Alaska, MAATs typically range from −2 to −6 °C (Jorgenson *et al* 2008).

In the rocky uplands affected by a moderately severe fire in 2004, mean soil volumetric moisture content was 40% lower in burned sites than unburned sites, suggesting that deep thaw into coarse-textured soils improved surface drainage (Figure 2.3b). Total water storage above permafrost, however, increased 20% after fire because of the increase in the volume of thawed soil (Figure 2.3c). Average MAST, which was positive even in the unburned sites with permafrost, was 2.1 °C higher in the burned sites (Figure 2.4). The warmer winter surface soil temperatures, lower freezing *n*-factors, and low amplitude of monthly mean temperatures in the rocky uplands were likely influenced by snow insulation from greater regional snowfall and higher elevations (Table 2.1, Figure 2.4). Average MADT also increased by 2.1 °C after fire (Figure 2.4). Winter temperatures at 1 m depth in the burned sites were constrained at 0 °C, indicating the persistence of unfrozen water throughout the winter and the development of a talik, a perennially unfrozen layer situated between the seasonally frozen layer and permafrost. In the burned sites, permafrost thawed below the 1 m depth of observation in the rocky soil, whereas in unburned sites mean thaw depth was 49 cm (Figure 2.3d). Seasonal heat input increased 67% after fire (Figure 2.3d). Heat input after fire was lower than in the other landscapes, but was still high enough to thaw permafrost beyond the depth of seasonal frost.

In the silty uplands affected by a fire in 2009, mean volumetric moisture content showed little difference between burned and unburned sites as soils remained near saturation (Figure 2.3b), but water storage in the active layer increased more than two-fold with the deepening of the active layer (Figure 2.3c). Average MAST was 3.3 °C higher in burned sites compared to the unburned sites and

average MADT was 3.8 ºC higher (Figure 2.4). The relatively cold winter temperatures at 1 m depth suggest complete refreezing of the deepened active layer. The increase in MADT after fire was greatest in the silty uplands, yet MADT remained the coldest of all soil landscapes after fire. Mean thaw depths were two-fold higher in burned (125 cm) than in unburned sites (59 cm) (Figure 2.3d). Soil heat input was nearly three-fold higher in the burned sites compared to unburned sites (Figure 2.3e). Despite these large changes in soil temperature, heat input, and thaw depth, there was no evidence of talik development after fire. Soil heat loss was likely exacerbated by the cold air temperatures, low snowfall, and high thermal conductivity of the active layer during winter associated with the high moisture content.

In the sandy lowlands after severe fires in 2004 and 2010, mean soil volumetric moisture content was 27% lower in burned than unburned sites (Figure 2.3b). Accompanying a nearly two-fold increase in thaw depth between unburned (109 cm) and burned (196 cm) sites (Figure 2.3d) was a 29% increase in mean water storage after fire (Figure 2.3c). This landscape was unusual with its lower moisture contents and greater thaw depths, likely due to the sandy soils beneath the thin loess caps and the aridity of the climate. Average MAST was 3.7 ºC higher in burned than unburned sites, which had the highest surface temperatures of the study (Figure 2.4). The magnitude of increase in summer surface temperatures after fire was greatest in this landscape, which we attribute to the severity of the fires, exposure of mineral soils, and low soil moisture. Average MADTs were 1.5 ˚C higher in the burned sites, due mostly to warmer summer temperatures (Figure 2.4). Mean soil heat input after the fires increased by 86% (Figure 2.3e). Although the winter temperatures at 1-m depth in the burned sites were below 0 ˚C, observations of seasonal frost above underlying unfrozen soil, and deep thaw depths, indicate that thin taliks developed at two, and possibly three, of the burned sites.

These findings suggest that the underlying mineral soil texture mediates the soil moisture regime after fire-initiated permafrost thaw, thus influencing the vulnerability of permafrost to long-term degradation. The sensitivity of permafrost to fire disturbance is further modified by landscape position, which controls microclimate. The recovery of permafrost is likely impacted by the rate of thaw in relation to the recovery of vegetation. The ecosystem response to changing climatic and fire regimes will be largely impacted by the response of permafrost. Because boreal forest soils function as an important terrestrial carbon sink, changes in carbon cycling in this region are of particular significance to global climate (McGuire *et al* 2009, Grosse *et al* 2011, O'Donnell *et al* 2011, Yuan *et al* 2012). Decomposition, nutrient cycling, and productivity are largely temperature and moisture dependent (Chapin *et al* 2010); thus, the differential response in soil thermal and moisture regimes to fire will likely mediate the impact of changing climatic and fire regimes on carbon cycling throughout the discontinuous permafrost zone.

Thaw settlement

The resilience of permafrost in the silty uplands was further assessed through monitoring changes in thaw depths and surface elevations along transects encompassing different disturbance regimes (Figure 2.6). Transect 1 was located in an area that burned around 1925 (previously considered 'unburned'), and Transect 2 was located in the 2009 bum. Both transects were partially affected by a fire in 1967, which resulted in an increase in deciduous tree cover. The 1967 fire left a legacy of deeper thaw in both of the transects, but the persistence of near-surface permafrost indicates stability and resilience to fire.

From 2010 to 2012, changes in the ground surface and permafrost table in the combined 1925 and 1967 bums were negligible. At the 1925 burn, declines in surface and permafrost elevation along a portion of the transect near a meteorological tower site were attributed to trampling of the thick mossy organic mat by researchers. Compaction was visually observed along this portion of the transect. Transect 2 was less vulnerable to compaction due to the thin residual surface organic layer (~0-10 cm) and the minimal use by researchers. The 2009 fire lowered the permafrost table throughout the transect and caused thaw settlement in the portion of the transect that had shallow active layers in 2010. The effects of the 2009 fire on the permafrost table and thaw settlement were most pronounced between the first and second year after fire. By the third year after fire, the permafrost table had largely stabilized. From 2010 to 2012, the permafrost table at the 2009 fire (only) was lowered by an average of 41 cm (max. 75 cm). Ground surface elevations declined on average by 9 cm (max. 39 cm), which is consistent with the expected thaw settlement due to the degradation of ice-rich permafrost. Along the portion of this transect that had previously burned in 1967, the permafrost table was lowered by an average of 25 cm (max. 35 cm) with no detectable thaw settlement, suggesting that the ice-rich intermediate layer of the upper permafrost had degraded as a result of the 1967 fire and had not recovered in the ~45 years of succession after the fire.

Overall, these results indicate that permafrost in the silty uplands was resilient to fire, as the fires of 1925, 1967, and 2009 did not result in a talik indicative of significant degradation. We attribute this to the ability of the active layer to adjust and absorb the additional soil heat flux after fire due to its high moisture content, the recovery of vegetation that reduces soil heat flux, and the high latent heat contents of the ice-rich permafrost that slows surface thawing.

Conclusions

Regional climate and topography interacted to create microclimates that influenced the ground thermal regime and permafrost, but this effect was strongly mediated by surface and subsurface conditions, which are products of disturbance history, ecological succession, and substrate. Successional patterns varied depending on fire severity and pre-fire species composition, which influence the recovery

of the surface organic layer. Surface organic layer thickness was an important variable controlling the ground thermal regime and thaw depth. The reduction of the surface organic layer through moderate to severe burning caused the warming and thawing of upper permafrost across all soil landscapes, but talik initiation was observed only in the rocky uplands and sandy lowlands. The sensitivity of the rocky uplands and sandy lowlands was influenced by soil texture, whereby increased thaw depths after fire resulted in a reduction in soil moisture contents, as well as by greater snowfall at high elevations in the rocky uplands. Permafrost in the silty uplands was resilient to fire because of the high moisture content of the active layer and the high latent heat associated with the ground ice, which slows thaw and allows the deeper active layer to absorb more heat while vegetation recovery changes surface characteristics. Long-term permafrost degradation after fire is more likely in areas of the discontinuous permafrost zone with warmer climates and greater snowfall, whereas cold areas and continental climates in the northern portion of the discontinuous permafrost zone can allow permafrost to persist even after severe fire. A warming climate alone is expected to cause widespread permafrost degradation in the discontinuous permafrost zone (Grosse *et al* 2011, Jafarov e*t al* 2012), and the impact of fire could hasten such degradation (Shur and Jorgenson 2007, Jorgenson *et al* 2010, Jiang *et al* 2012), though response will vary considerably depending on complex interactions of climate, topography, soil properties, vegetation, and fire severity.

Acknowledgments

This study was funded by the US Geological Survey, through their Yukon River Basin studies, and through the Changing Arctic Ecosystems Initiative of the US Geological Survey's Ecosystem Mission Area. We thank Mark Waldrop and Tony DeGange for managing the research grants, Eric Jorgenson, Mark Winterstein, Jack McFarland, and Katie Nicolato for their assistance with fieldwork, and Vladimir Romanovsky for discussions that helped to improve this letter. We thank the Bonanza Creek Long-Term Ecological Program for in-kind support.

Figures

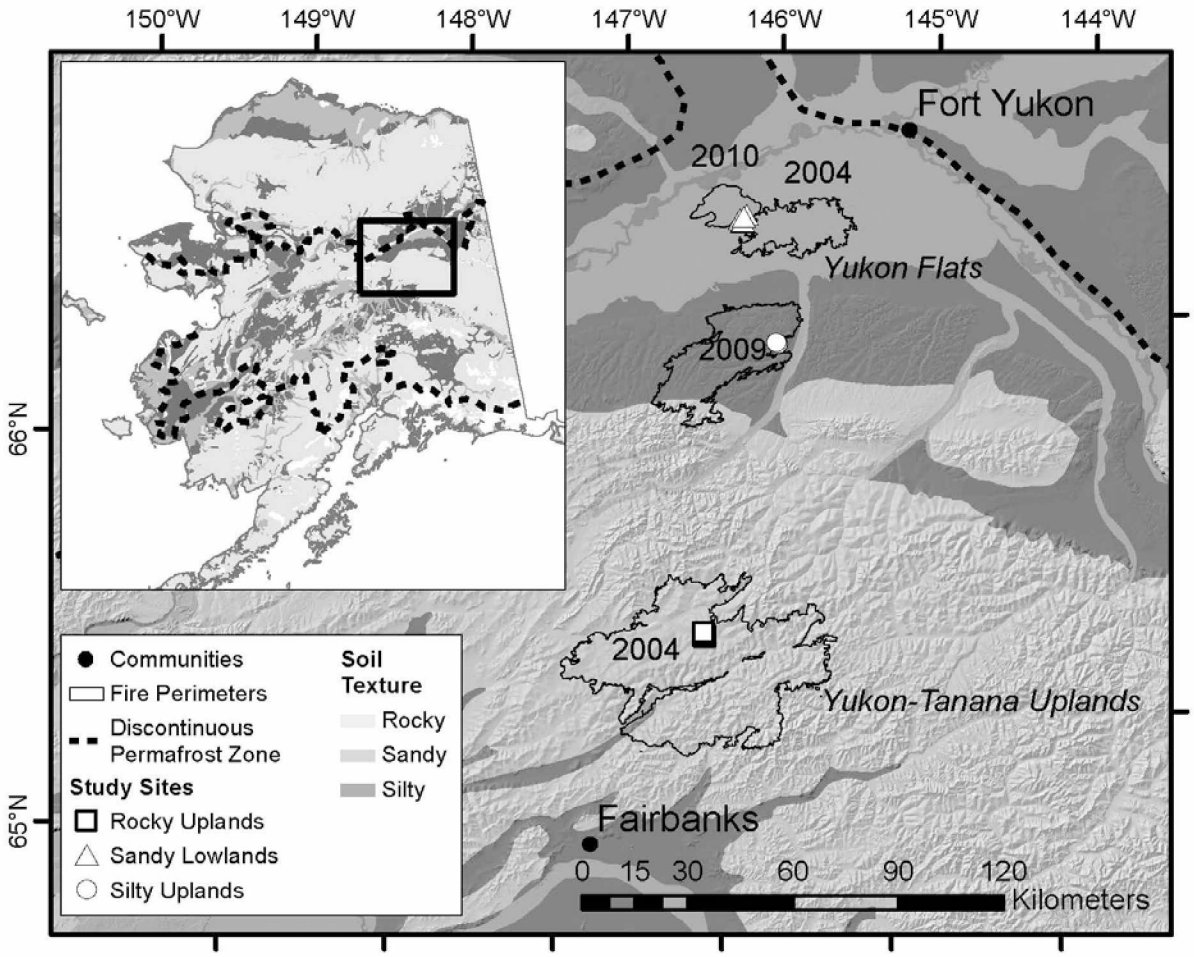

Figure 2.1. Topographic map of study area in interior Alaska. Dominant mineral soil textures are mapped with gray-scale symbology based on Karlstrom (1964) and Jorgenson *et al* (2008). The northern and southern boundaries of the discontinuous permafrost zone, from Jorgenson *et al* (2008), are represented with dashed lines. Study sites (n = 18) are indicated by open squares (rocky uplands), triangles (sandy lowlands), and circles (silty uplands). Fire perimeters and year of burn are shown for the recent fires studied.

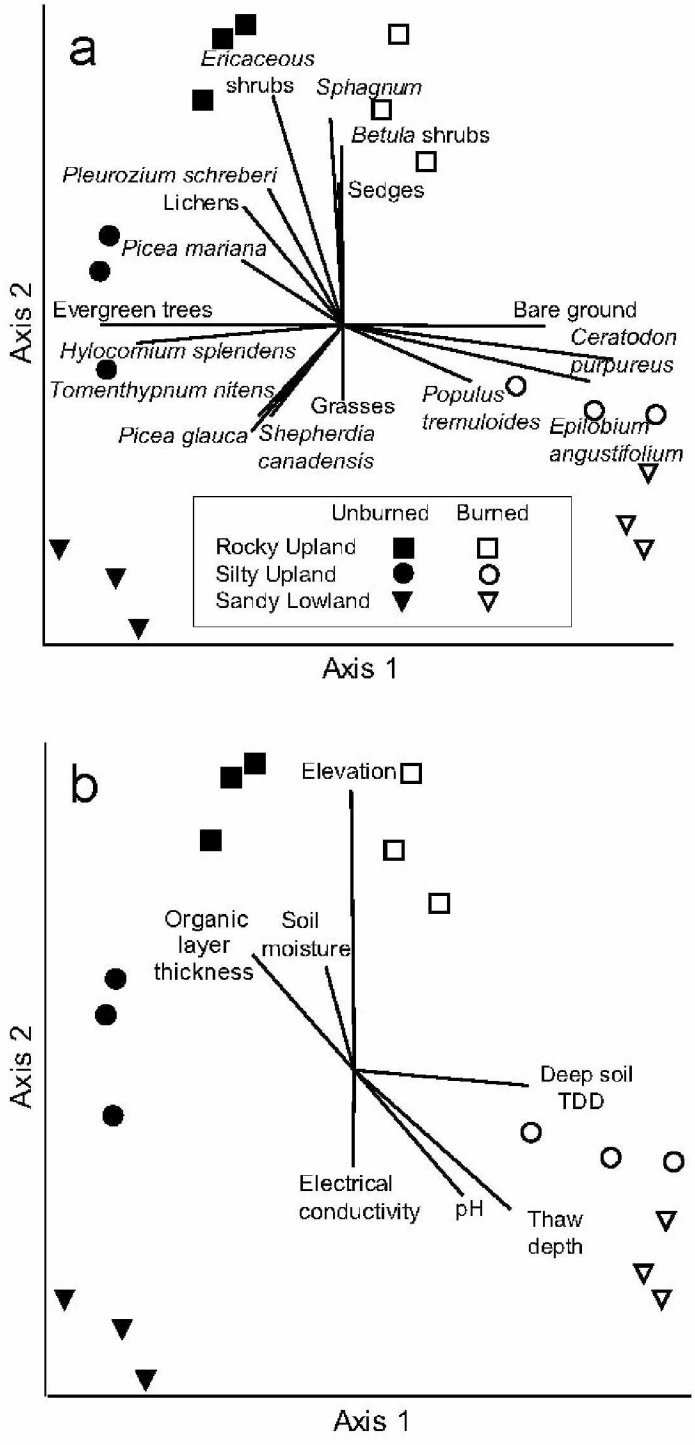

Figure 2.2. Plant community ordination and relationships with vegetation and environment. Nonmetric multidimensional scaling (NMDS) ordination of plant communities and correlations with (a) vegetation and (b) environmental characteristics. Points represent plant communities at each site. Symbols indicate landscape type and treatment. Vectors show direction and strength of correlations.

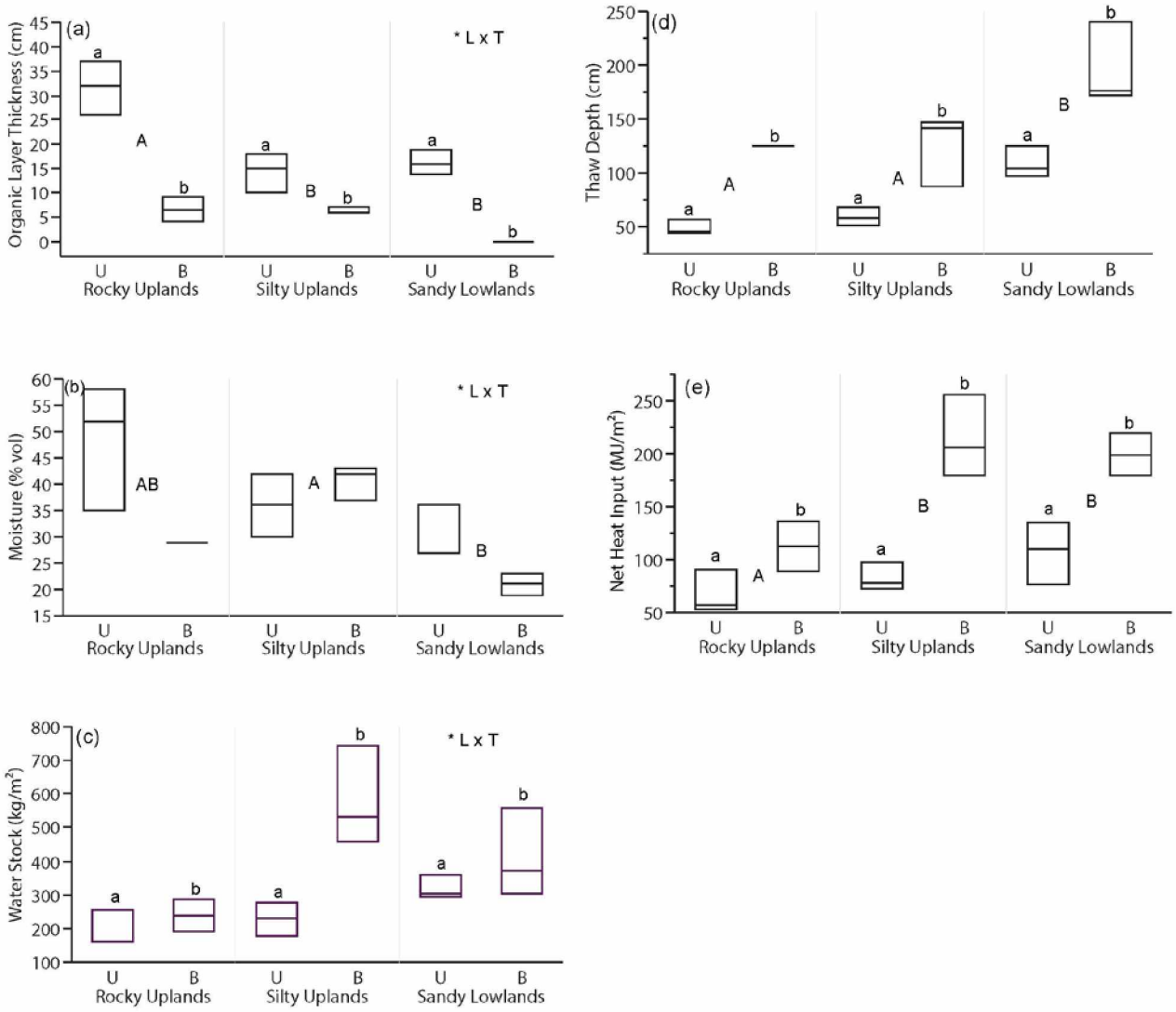

Figure 2.3. Soil physical properties by landscape and treatment. Box plots of (a) surface organic layer thickness, (b) volumetric soil moisture, (c) water stock, (d) thaw depth, (e) and net heat input (n = 17). One outlier from a low-severity burn in the rocky uplands was excluded. Two-way ANOVAs and post hoc test (Tukey HSD and student's t-tests) were conducted. Significant differences between means are denoted by lowercase letters for treatment and uppercase letters for landscape. Positioning of uppercase letters indicate the landscape-level means on the y-axes. Interactive effects (* L x T) are displayed when significant.

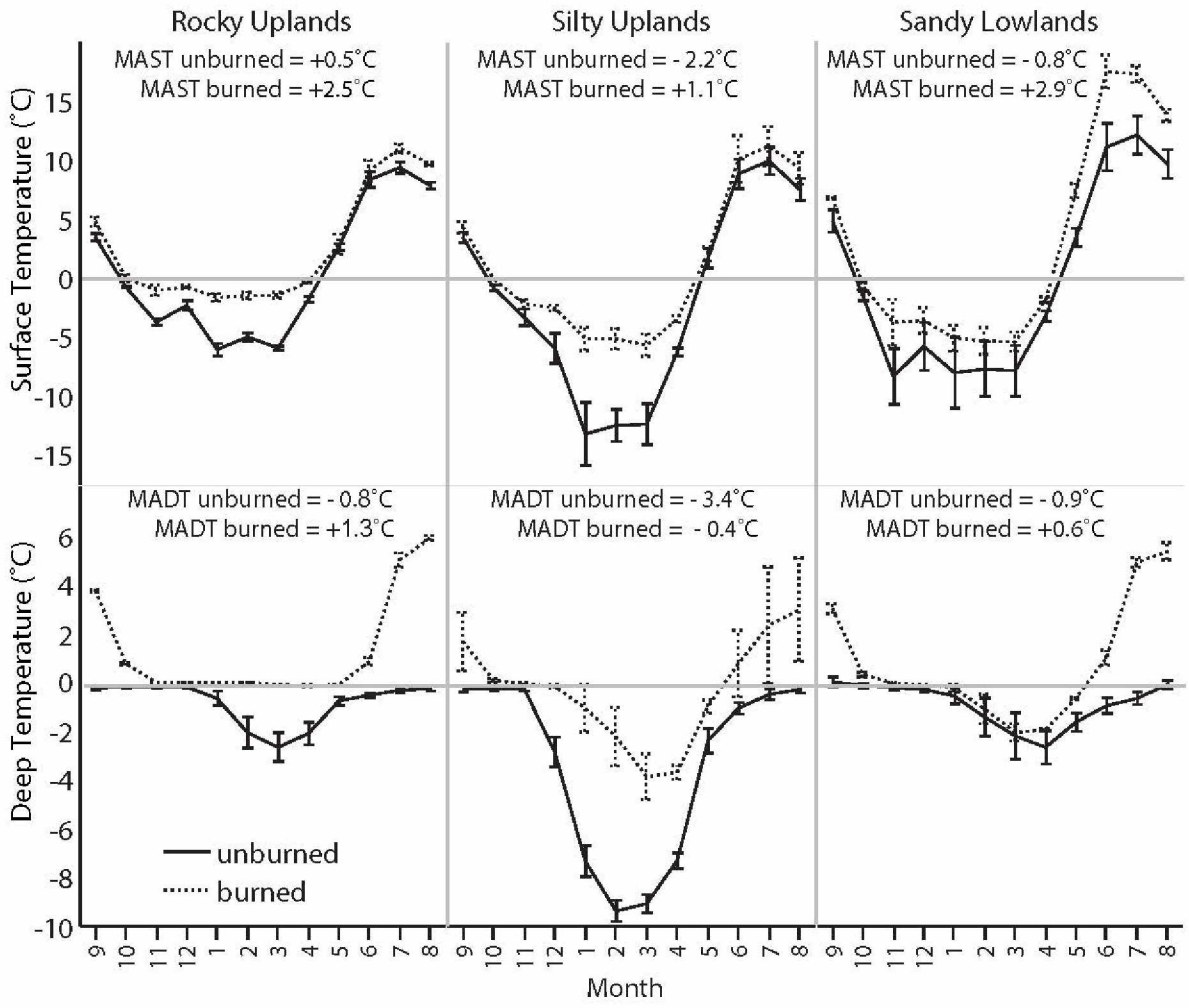

Figure 2.4. Monthly soil temperatures by landscape and treatment. Data shown are monthly means (± SE) soil temperatures at the surface (5 cm) and at depth (100 cm) for unburned (solid line) and burned (dotted line) sites from September 2011 to August 2012 (n = 17). One outlier from a low-severity burn in the rocky uplands was excluded. Mean annual surface temperatures (MAST) and mean annual deep temperatures (MADT) are displayed in text boxes.

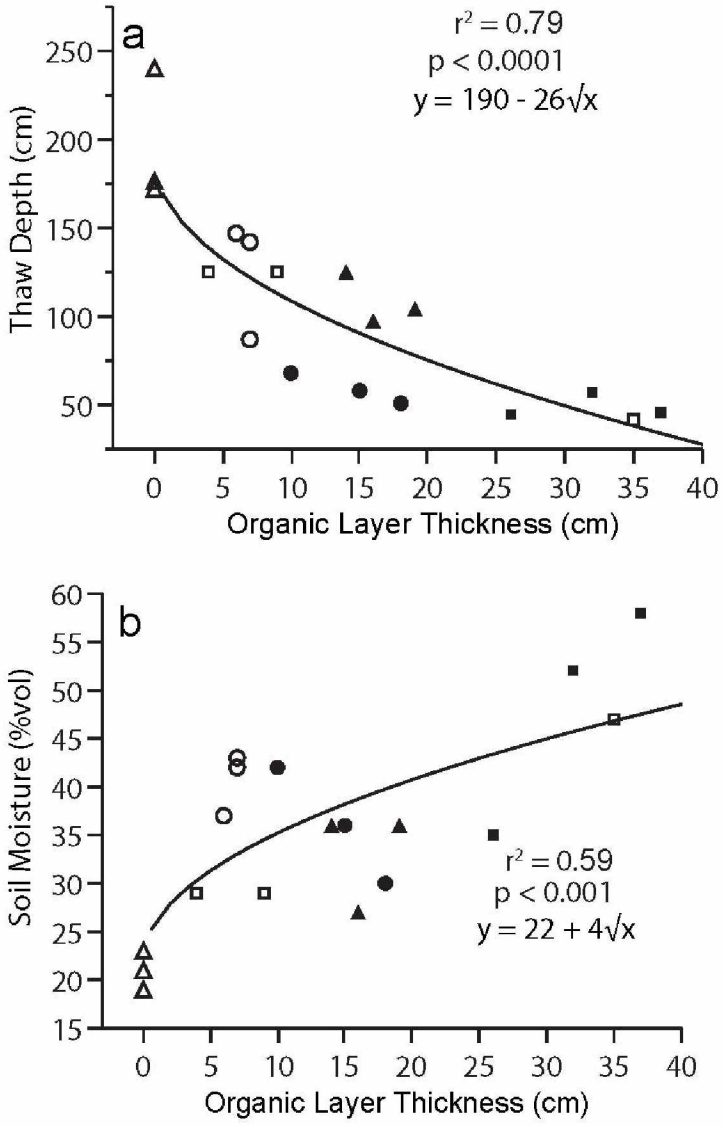

Figure 2.5. Relationships among soil physical properties. (a) Thaw depth and organic layer thickness, and (b) volumetric soil moisture and organic layer thickness (n = 18). Solid markers = unburned; open markers = burned. Triangles = sandy lowlands; circles = silty uplands; squares = rocky uplands.

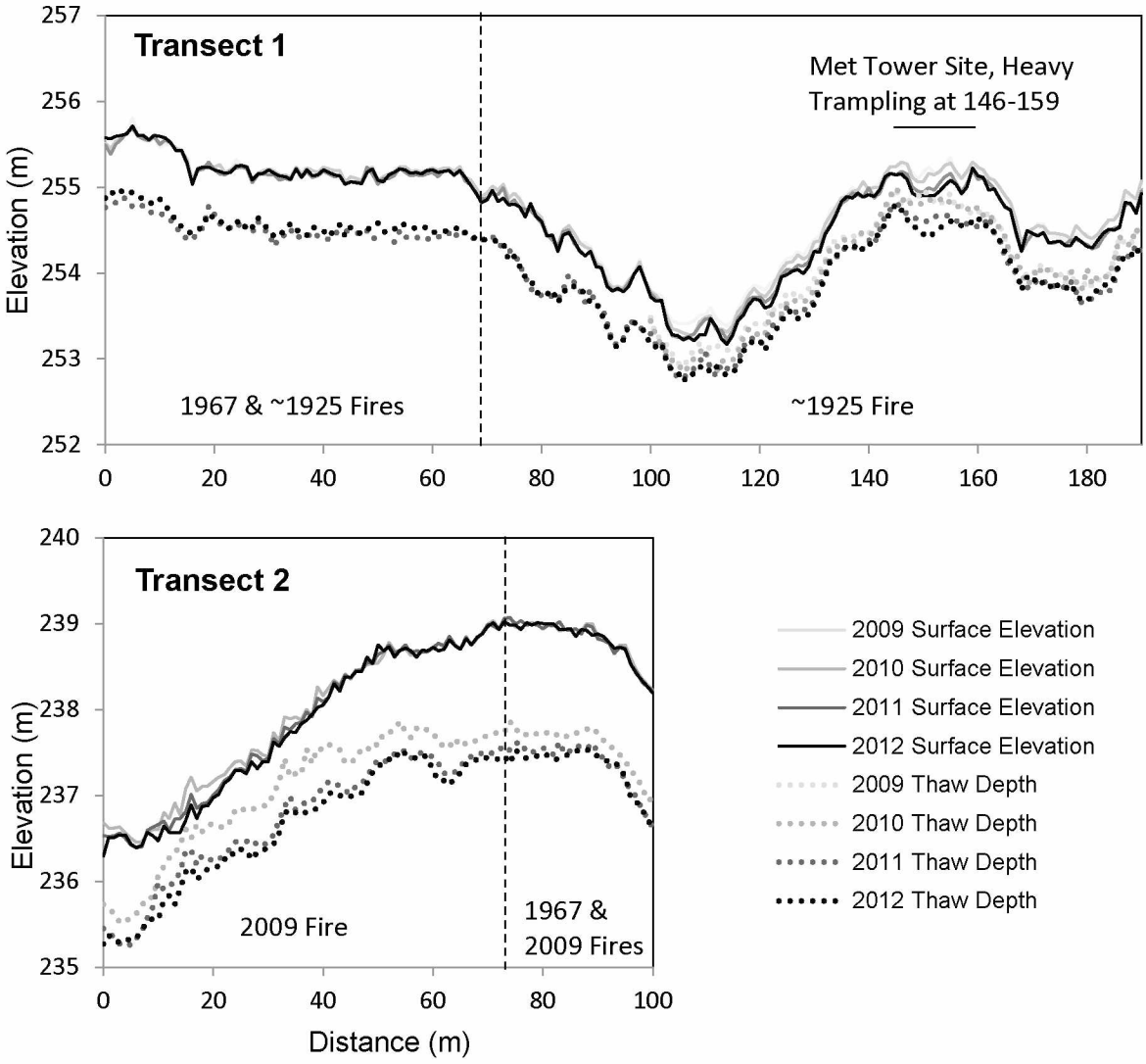

Figure 2.6. Cross-section of transects in silty uplands under different disturbance regimes. Ground surface elevation and thaw depths are shown from 2009 to 2012. Transect 1 burned around 1925 and a portion of it re-burned in 1967. Transect 2 in 2009, and a portion of it had previously burned in 1967. The organic mat was compacted by human disturbance in Transect 1, with heavy trampling near a meteorological tower site.

Tables

Table 2.1. Summary of environmental characteristics by landscape type. Region, mean elevation, mean annual air temperature (MAAT), air freezing degree days (FDD), air thawing degree days (TDD), and freezing n-factor (ratio of soil surface FDD to air FDD) are shown. The n-factor values are the least square means ± SE from a Tukey HSD post hoc test conducted after a significant effect of landscape type was found with a two-way ANOVA ($p = 0.01$); significant differences between means are denoted by different letters.

Landscape type	Region	Elevation (m)	MAAT (°C)	Air FDD	Air TDD	N_f-factor
Rocky Uplands	Yukon-Tanana Uplands	604	-5.3	3437	1518	0.1 ± 0.0 *A*
Silty Uplands	Yukon Flats	249	-6.1	4018	1780	0.3 ± 0.0 *B*
Sandy Lowlands	Yukon Flats	123	-5.2	3904	1997	0.3 ± 0.0 *B*

References

Alaska Climate Research Center 2013 *Climate Normals for Interior Alaska* (available: http://climate.gi.alaska.edu/Climate/ Normals/interior.html, accessed 17 April 2013)

Barrett K, McGuire A D, Hoy E E and Kasischke E S 2011 Potential shifts in dominant forest cover in interior Alaska driven by variations in fire severity *Ecol. Appl.* **21** 2380–96

Bernhardt E L, Hollingsworth T N and Chapin F S III 2011 Fire severity mediates climate-driven shifts in understorey community composition of black spruce stands of interior *Alaska J. Veg. Sci.* **22** 32–44

Burn C R 1998 The response (1958–1997) of permafrost and near-surface ground temperatures to forest fire, Takhini River valley, southern Yukon Territory Can. *J. Earth Sci.* **35** 184–99

Chapin F S III *et al* 2010 Resilience of Alaska's boreal forest to climatic change *Can. J. Forest Res.* **40** 1360–70

Flanagan P W and Van Cleve K 1983 Nutrient cycling in relation to decomposition and organic matter quality in taiga forest ecosystems *Can. J. Forest Res.* **13** 795–817

Gallant A L, Binnian E F, Omernik J M and Shasby M B 1995 Ecoregions of Alaska *US Geological Survey Professional Paper 1567* (Washington, DC: US Department of Interior)

Gillett N P, Weaver A J, Zwiers F W and Flannigan M D 2004 Detecting the effect of climate change on Canadian forest fires *Geophys. Res. Lett.* **31** L18211

Greene D F and Johnson E A 1999 Modelling recruitment of Populus tremuloides, Pinus banksiana, and Picea mariana following fire in the mixedwood boreal forest *Can. J Forest Res.* **29** 462–73

Grosse G *et al* 2011 Vulnerability of high-latitude soil organic carbon in North America to disturbance *J Geophys. Res.***116** G00K06

Hollingsworth T N, Johnstone J F, Bernhardt E L and Chapin F S III 2013 Fire severity filters regeneration traits to shape community assembly in Alaska's boreal forest *PLoS One* **8** e56033

Jafarov E E, Marchenko S S and Romanovsky V E 2012 Numerical modeling of permafrost dynamics in Alaska using a high spatial resolution dataset *Cryosphere* **6** 613–24

Jiang Y, Zhuang Q and O'Donnell J A 2012 Modeling thermal dynamics of active layer soils and near-surface permafrost using a fully coupled water and heat transport model *J. Geophys. Res.* **117** D11110

Johnstone J F and Chapin F S III 2006 Effects of soil burn severity on post-fire tree recruitment in boreal forest *Ecosystems* **9** 14–31

Johnstone J F, Chapin F S III, Hollingsworth T N, Mack M C, Romanovsky V and Turetsky M 2010a Fire, climate change, and forest resilience in interior Alaska *Can. J. Forest Res.* **40** 1302–12

Johnstone J F, Hollingsworth T N, Chapin F S III and Mack M C 2010b Changes in fire regime break the legacy lock on successional trajectories in Alaskan boreal forest *Glob. Change Biol.* **16** 1281–95

Jorgenson M T 1986 Biophysical factors influencing the geographic variability of soil heat flux near Toolik Lake, Alaska: implications for terrain sensitivity *MS Thesis* University of Alaska, Fairbanks

Jorgenson M T and Osterkamp T E 2005 Response of boreal ecosystems to varying modes of permafrost degradation *Can. J. Forest Res.* **35** 2100–11

Jorgenson M T, Romanovsky V, Harden J, Shur Y, O'Donnell J, Schuur E A G, Kanevskiy M and Marchenko S 2010 Resilience and vulnerability of permafrost to climate change *Can. J. Forest Res.* **40** 1219–36

Jorgenson M T, Yoshikawa K, Kanevskiy M, Shur Y, Romanovsky V, Marchenko S, Grosse G, Brown J and Jones B 2008 *Permafrost Characteristics of Alaska* (Fairbanks, AK: Institute of Northern Engineering, University of Alaska)

Kanevskiy M, Shur Y, Connor B, Dillon M, Stephani E and O'Donnell J 2012 Study of the ice-rich syngenetic permafrost for road design (interior Alaska) *Proc. 10th Int. Conf Permafrost* pp 25–9

Karlstrom T N V 1964 Surficial geology of Alaska 1:1,584,000 *US Geological Survey Miscellaneous Geologic Investigations Map 357*

Karunaratne K C and Burn C R 2003 Freezing *n*-factors in discontinuous permafrost terrain, Takhini River, Yukon Territory, Canada *Proc. 8th Int. Conf on Permafrost, 2003 (Zurich)* ed M Phillips, S M Springman and L U Arenson, pp 519–24

Kasischke E S and Turetsky M R 2006 Recent changes in the fire regime across the North American boreal region—spatial and temporal patterns of burning across Canada and Alaska *Geophys. Res. Lett.* **33** L09703

Kasischke E S *et al* 2010 Alaska's changing fire regime—implications for the vulnerability of its boreal forests *Can. J. Forest Res.* **40** 1313–24

Lunardini V J 1978 Theory of *n*-factors and correlation of data *Proc. 3rd Int. Conf on Permafrost (July 1978)* (Edmonton: National Research Council Canada) pp 41–6

Mackay J R 1995 Active layer changes (1968 to 1993) following the forest-tundra fire near Inuvik, N.W.T., Canada *Arctic Alpine Res.* **27** 323–36

McCune B and Grace J B 2002 *Analysis of Ecological Communities* (Gleneden Beach, OR: MjM Software Design)

McCune B and Mefford M J 2011 PC-ORD *Multivariate Analysis of Ecological Data. Version 6.0* (Gleneden Beach, OR: MjM Software)

McGuire A D, Anderson L G, Christensen T R, Dallimore S, Guo L, Hayes D J, Heimann M, Lorenson T D, Macdonald R W and Roulet N 2009 Sensitivity of the carbon cycle in the Arctic to climate change *Ecol. Monogr.* **79** 523–55

O'Donnell J A, Harden J W, McGuire A D, Kanevskiy M Z, Jorgenson M T and Xu X 2011 The effect of fire and permafrost interactions on soil carbon accumulation in an upland black spruce ecosystem of interior Alaska: implications for post-thaw carbon loss *Glob. Change Biol.* **17** 1461–74

Osterkamp T E and Burn C R 2003 Permafrost *Encyclopedia of Atmospheric Sciences* 1st edn, ed J R Holton, J Pyle and J A Curry (Oxford: Academic)

Osterkamp T E, Jorgenson M T, Schuur E A G, Shur Y L, Kanevskiy M Z, Vogel J G and Tumskoy V E 2009 Physical and ecological changes associated with warming permafrost and thermokarst in interior Alaska *Permafrost Periglac. Process.* **20** 235–56

Osterkamp T E and Romanovsky V E 1999 Evidence for warming and thawing of discontinuous permafrost in Alaska *Permafrost Periglac. Process.* **10** 17–37

Péwé T L 1975 *Quaternary Geology of Alaska* (Washington, DC: United States Geological Survey)

Shenoy A, Johnstone J F, Kasischke E S and Kielland K 2011 Persistent effects of fire severity on early successional forests in interior Alaska Forest Ecol. Manag. 261 381–90

Shur Y L and Jorgenson M T 2007 Patterns of permafrost formation and degradation in relation to climate and ecosystems *Permafrost Periglac. Process.* **18** 7–19

Van Cleve K and Viereck L A 1981 Forest succession in relation to nutrient cycling in the boreal forest of Alaska *Forest Succession: Concepts and Application* ed D C West, H H Shugart and D B Botkin (New York: Springer)

Viereck L A, Werdin-Pfisterer N R, Adams P C and Yoshikawa K 2008 Effect of wildfire and fireline construction on the annual depth of thaw in a black spruce permafrost forest in interior Alaska: a 36-year record of recovery *Proc. 9th Int. Conf. Permafrost (Fairbanks, AK)* ed D L Kane and K M Hinkel, pp 1845–50

Williams P J and Smith M W 1991 *The Frozen Earth: Fundamentals of Geocryology* (Cambridge: Cambridge University Press)

Woo M-K, Kane D L, Carey S K and Yang D 2008 Progress in permafrost hydrology in the new millennium *Permafrost Periglac. Process.* **19** 237–54

Yi S, McGuire A D, Kasischke E, Harden J, Manies K, Mack M and Turetsky M 2010 A dynamic organic soil biogeochemical model for simulating the effects of wildfire on soil environmental conditions and carbon dynamics of black spruce forests *J. Geophys. Res.* **115** G04015

Yoshikawa K, Bolton W R, Romanovsky V E, Fukuda M and Hinzman L D 2003 Impacts of wildfire on the permafrost in the boreal forests of interior Alaska *J. Geophys. Res.* **108** 8148

Yuan F-M, Yi S-H, McGuire A D, Johnson K D, Liang J, Harden J, Kasischke E S and Kurz W 2012 Assessment of boreal forest historical C dynamics in the Yukon River Basin: relative roles of warming and fire regime change *Ecol. Appl.* **22** 2091–109

Chapter 3: Landscape effects of wildfire on permafrost distribution in interior Alaska derived from remote sensing[1]

Abstract

Climate change coupled with an intensifying wildfire regime is becoming an important driver of permafrost loss and ecosystem change in the northern boreal forest. There is a growing need to understand the effects of fire on the spatial distribution of permafrost and its associated ecological consequences. We focus on the effects of fire a decade after disturbance in an upland landscape in the interior Alaskan boreal forest. We establish post-fire relationships of soil properties, vegetation, topography, and remote sensing data with the ultimate goal of mapping and analyzing patterns of subsurface permafrost distribution and drainage conditions. Of the remote sensing metrics we considered, ranging from optical (Landsat), L-band radar (ALOS-PALSAR), and topographic (LiDAR) datasets, indices using the near-infrared and shortwave infrared bands were most closely related to field-based data. The strong empirical relationships between the normalized difference infrared index (NDII) and post-fire vegetation, soil moisture, and soil temperature enabled us to indirectly map subsurface properties using regression-based models. The thickness of the insulating surface organic layer after fire, a measure of burn severity, was an important control over the extent of permafrost degradation. According to our classifications, 90% of the area considered a high severity burn (using the difference normalized burn ratio (dNBR)) lacked permafrost after fire. Permafrost thawing, in turn, increased drainage and resulted in drier surface soils. Burn severity also influenced plant community composition, which was tightly linked to soil temperature and moisture. Overall, interactions between burn severity, topography, and vegetation appear to control the distribution of near-surface permafrost and associated drainage conditions after disturbance.

Introduction

Permafrost is vulnerable to thawing with continued climate warming, particularly in the boreal forest region where the mean annual permafrost temperature is close to 0 °C [1]. Permafrost degradation has begun in some areas, and widespread thawing over the next century is predicted under future climate scenarios [2,3]. The resilience of permafrost to climate change is enhanced where it is insulated by the accumulation of thick layers of organic material on the ground surface [4,5]. Conversely, the loss of this protective organic layer through wildfire combustion is a major positive feedback to permafrost degradation [6]. Fire is a widespread disturbance of the boreal forest, and the fire impacts in Alaska

[1] Brown, DRN, MT Jorgenson, K Kielland, DL Verbyla, A Prakash, and JC Koch. Submitted. Landscape effects of wildfire on permafrost distribution in interior Alaska derived from remote sensing Remote Sensing.

appear to have recently intensified as a result of climate warming, with increased fire frequency, extent, and severity [7,8]. Climate change coupled with the intensifying wildfire regime is becoming a significant driver of permafrost loss and ecosystem change in the northern boreal forest [6,9-11].

Permafrost strongly influences ecosystem processes and hydrology, and plays a significant role in the global climate system by sequestering massive quantities of carbon [12-14]. The thawing of permafrost allows for the release of carbon that was previously immobilized in frozen soils. Permafrost thawing can also cause changes in microtopography and drainage. The effects of permafrost thawing vary spatially depending upon factors such as soil texture, permafrost ice content, and topography [15]. For example, fine-textured soils with high ice content are likely to subside with thawing, potentially leading to surface water impoundment in flat, low-lying areas [10,16] or greater drainage and further permafrost erosion in upland areas [17]. Thawing in coarse-textured soils, and especially on slopes, is likely to cause increased drainage [18,19]. These contrasting effects of thawing can lead to either wetter or drier soil environments [20]. Loss of permafrost and change in soil moisture regimes influence the rates and pathways of biogeochemical cycling, which in turn impact nutrient availability to plants and carbon release to the atmosphere [12]. The degradation of permafrost therefore has ecological impacts that can range from local to global in scope.

Changes in permafrost distribution after fire are largely mediated by the spatial variation in burn severity [21]. The thickness of the surface organic layer of soil remaining after fire is a critical control on the magnitude of permafrost degradation [6,9,10]. Here, we consider the thickness of the residual surface organic layer to be a proxy for burn severity. Burn severity is influenced by a multitude of factors that govern fire behavior and the characteristics of fuel sources [7]. The seasonality of the fire as it relates to snowmelt and seasonal thawing of frozen ground impacts the moisture content of surface vegetation and organic soils, and thus the depth of burning [22]. Surface drainage, influenced by topography, soil texture, and permafrost, exerts a strong control on burn severity, both through direct effects on surface soil moisture and indirect effects on vegetation and the accumulation of organic soils [21,23].

Spatial models of current and future permafrost distribution have indicated the need to better capture the influence of fire on permafrost [2,24]. As a subsurface thermal condition of soil, permafrost status remains a challenge to detect remotely, and diverse approaches and techniques to sensing and mapping permafrost are being developed [25]. A geophysical study mapped subsurface permafrost at depth through the contrasting electrical resistivity of frozen and unfrozen soils utilizing airborne electromagnetic (AEM) data [26]. Several recent studies have modelled ground temperatures using Land Surface Temperature (LST) products from Moderate Resolution Imaging Spectroradiometers (MODIS) to produce regional scale permafrost maps [27-29]. Empirical relationships with topography, vegetation, and spectral indices have been used to indirectly map permafrost presence or active layer thickness [30-32]. Synthetic aperture

radar (SAR) backscatter has been used for remote sensing of surface soil moisture after boreal forest wildfires, which has been related to thaw depth and permafrost presence [33,34].

Here, we analyze post-fire relationships of soil properties, vegetation and topography; and use empirical relationships with remote sensing data to map near-surface permafrost distribution and associated drainage conditions a decade after disturbance in a rocky upland landscape in the interior Alaskan boreal forest. There is a paucity of post-fire permafrost information from rocky boreal uplands due to the difficulty of probing for permafrost in these landscapes. Yet these rocky upland landscapes comprise approximately 30% of the boreal region of Alaska [35,36], and are likely to experience accelerated thawing after wildfire, depending on fire severity [11,18,21]. Post-fire soil moisture is also likely to decline in this environment as permafrost thaws [18]. We considered a variety of remotely sensed metrics in our analysis from optical (Landsat 8 Operational Land Imager (OLI)), L-band radar (ALOS-PALSAR), and topographic (Light Detection and Ranging (LiDAR)) datasets. Based on this evaluation, we analyzed the best predictor of soil temperature and moisture, the normalized difference infrared index (NDII), and applied these relationships to map permafrost distribution and surface soil moisture classes within a burn scar.

Materials and methods

Study area and design

The ~100 km^2 study area is within the boundaries of the 2004 Boundary Fire in the Nome Creek portion of the White Mountains National Recreation Area in the Yukon-Tanana Uplands ecoregion of interior Alaska (Figure 3.1). The climate of this region is characterized by cold winters, warm summers, and low precipitation. The vegetation mosaic of this region is strongly influenced by disturbance legacies (primarily wildfire) and topographic control of microclimate. Across the region, black spruce forests dominate colder sites, such as valley bottoms and north-facing slopes, and are typically underlain by permafrost. White spruce occurs on warmer sites, such as active floodplains and south-facing slopes. Deciduous forest (aspen, birch, and balsam poplar) also occur on warmer sites, especially following disturbance. After severe fire which exposes mineral soil, early successional vegetation is often dominated by colonizing species (e.g. *Marchantia polymorpha*, *Ceratodon purpureus*, *Chamerion angustifolium, Salix* spp., *Populus tremuloides*), whereas low severity burns have a greater proportion of surviving and resprouting pre-fire vegetation (e.g. *Sphagnum* spp., *Eriophorum vaginatum*, *Rubus chamaemorus, Rhododendron tomentosum*) [37,38].

In 2014, we established 30 field sites in burned black spruce stands representing a range of topographic positions where we sampled vegetation and soils, and for which we extracted remote sensing data (Figure 3.1, Table 3.1). Within our study area, black spruce stands occurred in most landscape

positions, including south-facing slopes. Our sites had relatively high elevations fairly close to treeline. Additionally, 5 unburned patches of black spruce forest were sampled, confirming the presence of near-surface permafrost before fire in these locations. Other studies in the study area have documented contrasting permafrost status between burned and unburned areas [18,39].

Vegetation sampling

At each site we described plant species composition in detail and classified vegetation type coarsely following Viereck [40]. Percent cover of each plant species was determined within a 10 x 5 m area using either visual estimates or point-sampling, when time allowed. For visual estimates, a Braun-Blanquet cover class was assigned to each species [41]. For point-sampling, we recorded each species occurrence along a 100-point grid. Species present in the sampling area, but not encountered in point-sampling, were given a trace cover value of 0.1%. For consistency in analysis, percent cover values derived from point-sampling were converted to Braun-Blanquet cover classes. If plant species was uncertain, taxa were aggregated to the genus-level for analysis.

Soil sampling

Soils were sampled to determine stratigraphy, surface soil moisture, and presence of shallow permafrost. Soil moisture, temperature, and thaw depths were determined during a precipitation-free period during September 11–13, 2014. Descriptions of soil stratigraphy to ~40 cm depth were conducted for 2–3 soil plugs per site. Surface organic layer thickness (OLT) was considered a proxy for burn severity. OLT was measured at 1-m intervals along the 10-m transect at each site. Volumetric water content of the upper 20 cm of the soil profile was also measured at 1-m intervals using a Campbell Scientific Hydrosense sensor. An additional dataset of surface soil moisture from a severely burned site was used to assess temporal patterns of soil moisture in relation to remote sensing indices. Soil moisture at 7 cm depth was measured at 15 minute intervals using moisture sensors (M005, Onset Computer Corporation, Fort Collins, CO) attached to a data logger (H21-002, Onset Computer Corporation, Fort Collins, CO). Data from the snow-free seasons of 2014 and 2015 were used in this analysis.

Permafrost presence, usually identified through mechanical probing with a metal rod, was difficult to determine at most of our sites due to the rocky soils. Instead, soil temperature at 1 m depth was used as an indicator of near-surface (1 m) permafrost presence. If soil temperature was above 0 °C at 1 m depth, shallow permafrost at this depth was considered absent, although permafrost may be present at greater depths. One to three boreholes were drilled to ~1 m depth at each site in the summer in preparation for soil temperature determination in fall, the time of maximum seasonal thaw. A 1.3-cm-diameter drill bit was used with a portable Bosch Litheon hammer drill. The full length of each borehole was plugged with

hollow polyethylene (PEX) tubing sealed at both ends with silicon and epoxy to prevent water pooling. Sites were revisited in the fall for temperature determination. The upper seal of the tubes were cut, thermistor sensors were slowly lowered to two depths (50 cm and the bottom depth), and temperatures were recorded after equilibration using an Omega HH41 thermistor thermometer.

If the bottom depth was not exactly 100 cm, we used the temperature gradient from 50 cm to the bottom depth to estimate the temperature at 1 m. Borehole depths ranged from 80 to 120 cm, so the maximum extrapolation of temperatures was 20 cm beyond the deepest temperature measurement. The temperature gradients were similar across most boreholes (n = 50), ranging from -0.035 to -0.003 °C /cm, with a mean of -0.013 °C /cm (SE = 0.001). At the 3 boreholes where thaw depth could be determined by frost probing, it was used to validate the gradients used to estimate 1 m temperatures, whereby the depth of 0 °C along the temperature gradient should approximate the measured thaw depth. Our predicted thaw depths deviated from measured thaw depths by 1 to 6 cm (mean = 3.7 cm).

Remote sensing

The remote sensing involved use of a digital elevation model (DEM) derived from airborne Light Detection and Ranging (LiDAR) for topographic metrics, Landsat optical imagery, and synthetic aperture radar (SAR) (Table 3.2). Geospatial data processing was conducted using ERDAS Imagine 2014 and ArcMap 10.

The following topographic metrics were derived from the 2.5-m resolution DEM: elevation, aspect, slope, curvature, direct solar radiation [42], and compound topographic index (CTI), a steady state wetness index calculated using catchment area and slope [43]. Bilinear interpolation was used for extraction of topographic indices.

For optical data we used Landsat 8 OLI Surface Reflectance products (30-m resolution) processed by the U.S. Geological Survey. The primary scene for analysis was acquired on September 9, 2014, within 4 days of field soil sampling. This scene was used for correlation analyses with ground-based data and for mapping. Fourteen additional scenes from the snow-free seasons of 2013–2015 were used for subsequent analysis of temporal variation in surface reflectance relative to plant phenology and soil moisture. Dimensionless band indices, which maximize the contrast between bands and reduce noise (i.e. topographic effects on illumination, atmospheric effects), were calculated. The normalized difference vegetation index (NDVI) and normalized difference infrared index (NDII) were computed as follows using the red, near infrared (NIR), and shortwave infrared (SWIR) bands of the OLI sensor:

$$NDVI = (NIR - red) / (NIR + red) \quad \text{(eq. 1)}$$

$$NDII = (NIR - SWIR) / (NIR + SWIR) \quad \text{(eq. 2)}$$

where red is band 4 (0.64–0.67 μm) and NIR is band 5 (0.85–0.88 μm). NDII6 was calculated using SWIR1 band 6 (1.57–1.65 μm), and NDII7 was calculated using SWIR2 band 7 (2.11–2.29 μm). Vegetation highly reflects electromagnetic energy in the NIR region, and water absorbs electromagnetic energy in the SWIR region.

NDII is calculated the same way as the normalized burn ratio (NBR) [44,45]. The differenced normalized burn ratio (dNBR) is often used as an indicator of burn severity, and is calculated as:

$$\text{dNBR} = \text{pre-fire NBR} - \text{post-fire NBR} \qquad \text{(eq. 3)}$$

We used dNBR products acquired from the Monitoring Trends in Burn Severity (MTBS) program of the U.S. Geological Survey for the Boundary Fire (ID: BLM-AKAFS-A4SZ-20040613). The dNBR dataset was calculated from Landsat 7 ETM+ imagery acquired before and after fire. We used the dNBR index for correlations with soil and vegetation properties, and used the thematic map to exclude unburned areas from our mapping and to differentiate levels of burn severity (low, moderate, and high).

Microwave remote sensing has been successful in mapping soil moisture because radar backscatter varies as soil moisture changes during the growing season in burned boreal forest [33,34]. In this study, we used L-band synthetic aperture radar (SAR) data from ALOS-PALSAR in fine beam dual polarization mode (HH and HV polarizations). Radiometric and terrain corrected (RTC) products (20-m resolution) were processed by the Alaska Satellite Facility. Because backscatter is influenced by topography, surface roughness, and vegetation cover, multi-temporal observations (August 2009, September 2009, August 2010, September 2010) were used to isolate the soil moisture signal. This approach assumes that moisture is the major time-variant factor within a season, and other influences on backscatter are somewhat constant, an assumption which appears to be valid in boreal forests after fire [33]. A principal components analysis (PCA) was conducted for the time series of HH and HV polarized data.

Data analysis

Vegetation

Analysis of plant communities and relationships with environmental and remote sensing variables were conducted using nonmetric multidimensional scaling (NMDS) (PC-ORD 6, MjM Software). This multivariate ordination technique extracts the dominant patterns of plant species composition across sites into two continuous synthetic variables represented by the ordination axes. In the ordination diagram, each point represents the plant community composition at a site. The distance between points represents

the dissimilarity between plant communities. Relationships between plant communities (NMDS ordination axis scores) and environmental and remote sensing variables were examined with correlation analyses. The strength and direction of these relationships are depicted by vectors in the ordination diagram.

Soils

Statistical analyses were conducted using JMP Pro 11. The distributions of field data were assessed for normality. Soil temperature at 1 m depth exhibited a non-normal bimodal distribution, precluding parametric statistical analyses. Sites were thus grouped into "cold" and "warm" classes based on the bimodal soil temperature distribution. The cold soil class was defined by temperatures $\leq 1.0\ ^{\circ}C$ (n = 13) and the warm soil class had temperatures $\geq 2.5\ ^{\circ}C$ (n = 17). Relationships among variables were assessed using a combination of nonparametric correlation analyses (Spearman's rank), t-tests among soil temperature classes, and regression analyses when statistical assumptions were met. Results were considered statistically significant at alpha = 0.05.

Remote sensing

A suite of remote sensing indices in relation to soil moisture and temperature were tested using nonparametric correlation analyses (Spearman's rank), and the strongest indicator of subsurface properties, NDII7, was used in mapping. To better understand the extent to which vegetation and/or soil properties were driving the observed NDII7 response, we conducted analyses of the seasonal patterns of NDII7 and its components (NIR and SWIR reflectance) at our field sites in relation to plant phenology and soil moisture from May through September of 2013, 2014, and 2015 for warm and cold soil temperature classes. We also analyzed variation in surface soil moisture (7 cm depth) over time at a monitoring site in a severely burned area in relation to reflectance.

Mapping

The empirical relationships between NDII7, soil moisture, and soil temperature were used to map drainage conditions and permafrost distribution in our study area a decade after fire. Unburned areas, as determined by dNBR, were excluded from thematic maps. The linear relationship between NDII7 and surface soil moisture (upper 20 cm) was applied to each 30-m pixel in the study area to estimate volumetric water content of soils. The pixels were grouped into soil moisture classes based on volumetric water content using the Jenks optimization method [46]. Soil water content fluctuates temporally and this map is based on single-date measurements; therefore, it is intended to represent relative drainage conditions rather than absolute water content. For the permafrost map, thresholds of NDII7 values were

used to divide soil temperature predictions into 3 classes that reflect the probability of near-surface (1 m) permafrost presence.

Results

Vegetation

The vegetation structure of the majority (73%) of our sites consisted of low shrub communities dominated by *Rhododendron tomentosum*, *Vaccinium uliginosum*, or *Betula glandulosa* (Table 3.1). 13% of the sites were bryoid herbaceous meadows that had a mix of shrubs, forbs, graminoids, and mosses, but had the greatest cover of mosses *Ceratodon purpureus* and *Polytrichum juniperinum*. 10% of the sites were shrub-tussock meadows dominated by *Eriophorum vaginatum* and *Rhododendron tomentosum*. One outlier graminoid herbaceous site dominated by grasses (*Calamagrostis canadensis*) was excluded from the NMDS analysis.

In the NMDS ordination, sites with similar vegetation structure were grouped closely together, with shrub-tussock meadows and bryoid herbaceous meadows each clustered on opposing extremes of Axis 1 (Figure 3.2a). Axis 1 was negatively correlated with sedge tussock (r = -0.62), low shrub (r = -0.63), and dwarf shrub cover (r = -0.55); and was positively correlated with grass cover (r = 0.66) (Figure 3.2a, Table 3.3). Cover of other growth forms (evergreen tree, deciduous tree, tall shrub, moss, forbs, sedges, lichens) were not associated with either axis.

Numerous individual species/genera were associated with the ordination axes (Figure 3.2b, Table 3.3). The strongest correlations were related to Axis 1: *Rubus chamaemorus* (r = -0.72), *Ceratodon purpureus* (r = 0.69), *Rhododendron* spp. (r = -0.69), *Eriophorum vaginatum* (r = -0.62), *Cornus canadensis* (r = 0.60), and *Sphagnum* spp. (r = -0.58) (Figure 3.2b, Table 3.3). The strongest correlations with Axis 2 were *Chamerion angustifolium* (r = 0.56), *Alnus viridis* ssp. *crispa* (r = -0.52), *Rosa acicularis* (r = 0.49), and *Vaccinium uliginosum* (r = 0.49).

Soils

There were strong relationships among surface organic layer thickness (OLT), soil temperature, and moisture after the 2004 fire (Table 3.3). OLT was inversely related to soil temperature at 1 m depth (Figure 3.3a, n = 30, Spearman's $\rho = -0.51$, $p = 0.004$). A strong inverse relationship between soil temperature at 1 m depth and surface soil moisture of the upper 20 cm was found across our sites (Figure 3.3b, n = 30, Spearman's $\rho = -0.71$, $p < 0.0001$). The warm soil class (≥ 2.5 °C) had a lower mean OLT (10.6 cm vs 16.5 cm) and volumetric soil moisture (19.0 % vs 41.9 %) than the cold soil class (≤ 1.0 °C) (Figure 3.4). These soil properties were also related to the NMDS ordination of plant communities

(Figure 3.2c, Table 3.3). NMDS Axis 1 had a strong positive correlation with soil temperature (r = 0.84) and a negative correlation with soil moisture (r = -0.53) and OLT (r = -0.62).

Remote sensing

Topographic variables derived from the DEM were related to soil moisture and temperature (Table 3.4). Elevation and slope were significantly correlated with both moisture (ρ = -0.53, p = 0.0025; ρ = -0.38, p = 0.0395; respectively) and temperature (ρ = 0.54, p = 0.0023; ρ = 0.48, p = 0.0078; respectively). No significant correlations were found for aspect, CTI, curvature, or solar radiation. Of the topographic variables, only elevation was associated with the plant community ordination (Figure 3.2d, Table 3.3). Elevation had a negative correlation with NMDS Axis 2 (r = -0.62) and a positive correlation with Axis 1 (r = 0.47).

From the SAR dataset, the first principal component of the HV polarization time series was significantly correlated with soil moisture (ρ = 0.42, p = 0.0200), but only weakly correlated with soil temperature (ρ = -0.36, p = 0.0516) (Table 3.4). No additional relationships were found between soil properties and other principal components of the HH or HV polarizations. The SAR-derived variables were not associated with either axis of the plant community ordination.

Landsat-derived indices, particularly those within the infrared region, showed strong relationships with soil properties and vegetation (Tables 3.3, 3.4, Figure 3.2d). dNBR was negatively correlated with soil moisture (ρ = -0. 53; p = 0.0026) and positively correlated with temperature (ρ = 0.64, p = 0.0001). NDVI was positively associated with soil moisture (ρ = 0.39, p = 0.0345), and negatively associated with soil temperature (ρ = -0.57, p = 0.0009). The infrared indices (NDII6 and NDII7) were the remote sensing metrics most highly correlated with measured soil properties. NDII7, in particular, emerged as the best predictor of both surface soil moisture (ρ = 0.69, $p < 0.0001$) and soil temperature (ρ = -0.83, $p < 0.0001$) at depth. All of the infrared remote sensing indices that were correlated with soil properties were also correlated with the plant community ordination axes. NMDS Axis 1 was negatively correlated with NDII7 (r = -0.73) and NDVI (r = -0.67), and positively correlated with dNBR (r = 0.60). Based on the strength of the correlations, NDII7 was chosen for regression-based spatial modeling of soil properties and more detailed analyses of relationships with soils and vegetation.

Sites from both soil temperature classes exhibited similar seasonal reflectance patterns, though the cold sites had higher NDII7 values, higher NIR reflectance, and lower SWIR reflectance (Figure 3.5). The seasonal reflectance patterns were generally consistent during 2013–2015. SWIR reflectance typically decreased from springtime through the summer, and slightly increased in fall. NDII7 and NIR reflectance both increased from springtime to mid-late summer and decreased in fall. An additional dataset of surface soil moisture from a severely burned site was used to assess temporal patterns of moisture in

relation to spectral reflectance. Variation in surface soil moisture (at 7 cm depth) had a strong negative relationship with SWIR reflectance, and to a lesser extent with NDII7, and no significant relationship to NIR reflectance (Figure 3.6).

Mapping

The linear relationship between NDII7 and surface soil moisture (upper 20 cm) was used to map volumetric soil moisture content (Figure 3.7a). The pixels were grouped into 6 soil moisture classes (Figure 3.8a).

The majority of the burned portion of the study area was classified as poorly drained (61%), 24% was considered moderately drained, and 15% was well drained (Figure 3.9a). Well drained and moderately drained classes were located primarily on ridgetops and upper hill slopes; whereas poorly drained classes occurred mainly on lower lying areas, in concave drainage areas, and along linear water tracks (Figure 3.8a). There were exceptions to this overall pattern; with poorly drained areas occurring on hilltops and well drained areas on lower hillslopes.

The permafrost map was produced using thresholds of NDII7 values, which were indicative of soil temperatures at 1 m depth (Figure 3.7b). At NDII7 values < 0.21, 100% of sites had soil temperatures greater than 2.5 °C; therefore, with high certainty, this class was designated as unfrozen. Although permafrost is not expected within the upper meter in this class, permafrost may be present at greater depths. At NDII7 values > 0.24, 89% of sites had soil temperatures between -0.3 and 0.3 °C; therefore, this class was considered to have a high probability of permafrost near 1 m depth. At intermediate NDII7 values, soil temperatures ranged from 0.3 to 5.1 °C, with half the sites having temperatures > 4 °C and half having temperatures <0.5 °C. This group likely includes a mixture of permafrost conditions at 1 m depth, and therefore was classified as unknown permafrost status.

According to our mapping classifications, 51% of the study area was underlain by near-surface permafrost (within 1 m depth), 37% lacked permafrost, and 12% had unknown permafrost status (Figure 3.9b). Near-surface permafrost was distributed mainly on lower hillslopes, but also was found on hilltops and upper slopes (Figure 3.8b). Conversely, areas without near-surface permafrost occurred mainly on hilltops and upper slopes, but also on lower hillslopes. Areas of unknown permafrost status usually occurred on the boundaries between the areas with permafrost and without permafrost.

Permafrost status was related to burn severity class, as delineated by dNBR (Figure 3.10). 79% of the low burn severity area was underlain by near-surface permafrost according to our classification. 89% of the high burn severity area was classified as lacking near-surface permafrost. The moderate burn severity area had a relatively even mixture of permafrost classes (46% absent; 37% present).

Discussion

Remote sensing indicators of soil properties

Of the remote sensing indices considered, we found relationships of ground-based data with elevation and slope from the DEM, with the first principal component of the HV polarization from the ALOS-PALSAR time series, and with multiple indices from Landsat.

We expected to find stronger relationships of soil moisture with the SAR data. Microwave sensors measure the dialectric constant of soils, which is directly related to the soil water content [47]. Promising relationships between post-fire soil moisture and SAR backscatter time series have been found elsewhere using the C-band radar signal [33,34]. The greater wavelength of the L-band radar signal of ALOS-PALSAR allows it to more readily penetrate the vegetation canopy and enter deeper into the soil surface. However, in this study there was a several year time lag between the SAR data acquisition and our field data collection which may have weakened the strength of the associations. Considering the sensitivity of the radar signal to soil moisture, and the strong relationships between surface moisture and permafrost properties, the use of SAR data has been identified as a high research priority for permafrost mapping [25].

Soil temperature, soil moisture, and plant community composition were related to numerous Landsat-derived indices, including dNBR, NDVI, NDII6, and NDII7. The effectiveness of dNBR in quantifying burn severity has been inconsistent in the boreal forest [48]. That this index derived from pre-fire and immediate post-fire imagery was closely related to evolving soil properties a decade after fire suggests that it was able to capture an aspect of burn severity that was important to predicting permafrost degradation in our study area. Burn severity, as indicated by dNBR, was positively associated with soil temperature, negatively associated with soil moisture, and positively correlated with the primary axis of plant community variation.

An opposing pattern was found with NDVI, a measure of vegetation phytomass or health. NDVI was negatively associated with soil temperature, positively associated with soil moisture, and negatively correlated with the primary axis of plant community variation. The inverse relationship between NDVI and dNBR, and the direction of the relationships with soil properties and plant community composition, together suggest that higher NDVI values were due to lower burn severity. Within this early successional environment, high NDVI values indicated a high proportion of unburned patches or resprouting vegetation typical of low severity burns [38]. We expect the relationship between NDVI and soil temperature to evolve over time with plant succession. Indeed, an inverse relationship between NDVI and permafrost presence was found at a broad regional scale [32], likely because warm soils tend to support productive vegetation types such as deciduous forests.

The infrared indices (NDII6 and NDII7), which incorporate both the NIR and SWIR bands, were the remote sensing metrics most highly correlated with measured soil properties and plant communities. Vegetation reflects highly in the NIR region, and water (on the soil surface or within plant leaves) absorbs electromagnetic radiation in the SWIR region. High NIR reflectance and low SWIR reflectance were indicative of cold, moist soils. NDII7 was the strongest indicator of both surface soil moisture and soil temperature at depth, and was therefore chosen for regression-based spatial modeling of these soil properties and more detailed analyses. NDII was also found to be closely related to permafrost presence at the regional scale, presumably because of its sensitivity to water content of vegetation or soils [32]. NDII is sensitive to leaf water content and is commonly considered a vegetation index [44,49], although it is influenced by soils when they are not obscured by vegetation cover, as is the case after fire disturbance [50]. Therefore, surface soil moisture, which strongly influences SWIR reflectance [51], and vegetation properties are both likely to contribute to NDII in our post-fire study area.

We analyzed seasonal reflectance patterns over several years to determine the extent to which soil moisture versus vegetation properties influenced NDII. Sites with and without near-surface permafrost had the same seasonal patterns of NDII7, NIR, and SWIR reflectance, although reflectance values varied in magnitude. Our interpretation is that the sites with colder soils had greater NIR reflectance due to higher vegetation cover resulting from lower burn severity, and lower SWIR reflectance due to higher water content in plant leaves or the soil surface.

The seasonal surface soil moisture dynamics in this region are driven by spring snowmelt and the seasonal thawing of frozen ground. Surface moisture is typically highest at the time of spring snowmelt and gradually declines through the summer as thaw depth increases [52]. If SWIR were sensitive predominantly to surface soil moisture, we would expect to see SWIR reflectance increase from springtime to fall. Instead, SWIR reflectance decreased from springtime through the summer, and slightly increased in fall. The wide variations in precipitation from 2013–2015, with 2014 a summer of a record-breaking high rainfall, would have influenced surface moisture, yet the seasonal reflectance patterns we observed at our field sites were generally consistent each year [53]. The seasonal patterns of NDII7 and NIR reflectance were, however, consistent with expected plant phenology. As vegetation grows and leaves expand from springtime through the summer we see increased NDII7 and NIR reflectance, and subsequent declines in fall as leaves senesce. Across our sites, it therefore appears that the relationship between NDII7 and soil moisture was predominantly an indirect relationship driven by variations in vegetation properties, which reflect burn severity and co-vary with soil properties.

Within severe burns, which have a greater proportion of soil exposure relative to plant cover, direct relationships between SWIR reflectance and surface soil moisture are more likely, however. Our time-series of surface soil moisture from a field monitoring site in a severe burn had a strong negative

relationship with SWIR reflectance, suggesting a sensitivity of SWIR reflectance to surface soil moisture. We conclude that NDII7 performed well at predicting subsurface properties because it is an integrative index sensitive both to vegetation properties and surface moisture, both of which are correlated with soil moisture and temperature at depths beyond the reach of optical sensors.

Controls over permafrost distribution and drainage class

It has been well documented that the loss of the insulating surface organic layer of soil through wildfire can initiate rapid permafrost degradation [6,54]. The level of degradation is directly related to the thickness of the surface organic layer remaining after disturbance, and thus to burn severity. As expected, an inverse relationship between surface organic layer thickness and soil temperature at 1 m depth was found, demonstrating the positive influence of burn severity over permafrost degradation at our study sites. Soil temperature was also correlated with a remote sensing indicator of burn severity, dNBR.

The strong negative relationship we found between shallow soil moisture (upper 20 cm) and deep temperature (1 m) supports our conjecture that permafrost thawing after fire would result in increased drainage and subsequently drier surface soils [18], since the permafrost table, impermeable to water, strongly controls water table depth, hydrology, and soil moisture regimes [14,20].

Topography also influenced soil properties, as elevation and slope were both positively correlated with soil temperature and negatively with soil moisture. The association of upper slopes with warmer and drier soils and flatter bottomlands with wetter and colder soils are consistent with our understanding of topographic controls over soil properties [55]. Elevation influences microclimate primarily because of the pronounced wintertime temperature inversions, which cause mean annual air temperatures of lowlands to be significantly lower than adjacent hilltops [6]. Because of the low solar angles at high latitudes, slope and aspect are especially important in mediating solar input, affecting air temperatures, evaporation, and snowmelt [56,57]. Slope further influences the soil environment by controlling the mass flow of water. Mineral soil stratigraphy, soil texture, and loess thickness also tend to co-vary with topography due to differences in material redistribution, typically resulting in thicker deposits of fine-grained soils in lower positions [23,56,58]. The accumulation of thick organic layers in cold and poorly drained landscape positions reinforces cold and wet soil conditions through the development of a shallow permafrost table and through resilience to deep burning and subsequent permafrost degradation [11,21,23,59].

According to our mapping results, 37% of the study area lacked permafrost in the upper meter. Whereas permafrost-free areas occurred on hilltops and upper slopes, they also occurred in lower bottomland landscape positions, where permafrost conditions would be most expected. The inconsistency of topographic controls on permafrost presence suggests that other factors also strongly influence the spatial pattern of permafrost distribution after disturbance. The consistent relationships between burn

severity class and mapped permafrost presence provide compelling evidence that burn severity was a key control over the spatial distribution of permafrost. Nearly 90% of the high-severity burn area lacked near-surface permafrost, whereas permafrost persisted across ~80% of the low-severity burn. Some of the deviations from the expected topographic control over permafrost distribution and burn severity could be the result of temporally dynamic factors that influence fire behavior, such as previous precipitation affecting fuel moisture, wind speed/direction, humidity, etc. [59]; or to variation in vegetation and the properties of the surface organic layer, which influence the vulnerability to deep burning [60].

Topography and burn severity both influence the post-fire distribution of permafrost, which in turn impacts soil moisture regimes and landscape hydrology. The prevalent water tracks in our study area are evidence of surface flow due to permafrost. The presence of near-surface permafrost restricts subsurface infiltration, limiting flow to the shallow active layer, and resulting in active layer soils that are wet to saturated [61]. Permafrost dominated watersheds are thus characterized by flashy near-surface flow, with high peaks of stream discharge responsive to precipitation, and low base flow [62]. As permafrost thaws in a watershed, the water holding capacity of soils increases and flowpaths deepen, which cause higher base flow and less responsiveness to precipitation [63].

Burn severity is also tightly linked to vegetation, with the post-fire plant community reflecting the level of disturbance and the pre-fire vegetation [37,64]. Our ordination analysis shows that most of the variation in plant communities occurred along the first axis, which we interpret as a gradient of burn severity due to its close relationships to surface organic layer thickness and dNBR, as well as to patterns of plant species cover. This axis was strongly associated with soil temperature at 1 m depth, and to a lesser extent with surface soil moisture. Low shrub communities were the dominant post-fire vegetation type and encompassed a wide range of permafrost and moisture conditions. Extensive cover of dwarf shrubs (e.g. *Vaccinium vitis-idaea*), low shrubs (e.g. *Rhododendron tomentosum*), sedge tussocks, *Sphagnum* spp., and *Rubus chamaemorus* were indicative of low burn severity and colder, wetter soils. Over the broader interior Alaskan region, these particular species have been found to comprise the early successional vegetation of low severity burns as remnants or resprouts from surviving vegetation, whereas colonizing species regenerating by seed dominate in high severity burns [37,38]. Likewise, we found high cover of grasses and colonizing mosses (e.g. *Ceratodon purpureus*) to be associated with high burn severity and warmer, drier soils. Elevation was positively correlated with the primary axis of plant communities, suggesting a topographic control over burn severity and species composition. Topographic impacts on soil moisture likely interacted with pre-fire vegetation to influence burn severity, creating a range of post-fire early successional communities. These communities were closely related to the infrared remote sensing indices. The strong associations between post-fire vegetation, soil properties, and remote sensing indices enabled us to indirectly map subsurface properties.

Conclusions

With increasing fire extent and severity, there is a growing need for spatial characterization of permafrost within burned areas, particularly within rocky landscapes, which comprise a third of the Alaskan boreal region but for which spatial permafrost data are sparse. Our approach to modeling permafrost status and drainage conditions after fire used the associations among permafrost, soil moisture, and vegetation by establishing empirical relationships between field-based and remotely sensed data. We examined these relationships and landscape-level patterns to identify the possible controls over post-fire permafrost distribution.

We found that burn severity, topography, and vegetation strongly interacted to control permafrost distribution and influence soil moisture after fire. Burn severity influenced the extent of permafrost degradation, which in turn impacted drainage conditions, resulting in drier surface soils. Burn severity also influenced plant community composition, which therefore was closely related to these soil conditions. Topography and vegetation also affect the pre-fire soil environment and thus the vulnerability to deep burning.

Because soil temperature at depth was closely linked to post-fire vegetation and surface moisture, remote sensing indices that could capture these surface properties were presumed to perform best as indicators of subsurface permafrost status. Whereas remote sensing indices from all sensors were correlated with measured soil properties, the Landsat-derived infrared index NDII7 was most strongly related to field data. The temporal patterns of NDII7, and its components SWIR and NIR reflectance, suggest that this index was sensitive primarily to vegetation properties linked with burn severity, but also to surface soil moisture in severe burns where soil exposure was less obscured by plant cover.

This study enabled us to model the spatial distribution of permafrost and drainage characteristics after fire by relating satellite data to the surface characteristics of vegetation and soils. Moreover, the analysis of resulting maps allowed us to identify the mechanisms underlying the landscape scale patterns and characterize the ecological and hydrological impacts of fire.

Acknowledgments

This research was funded by the Changing Arctic Ecosystems Initiative of the US Geological Survey's Ecosystem Mission Area and through the US Geological Survey's Land Carbon Program, through the Alaska Cooperative Fish and Wildlife Research Unit and the Institute of Arctic Biology at the University of Alaska Fairbanks. We thank A. Marsh for help with fieldwork, B. K. Wylie for providing the LiDAR data, R. Gens for assistance with SAR data processing, S. Ewing and K. Wickland for contributing soil moisture data, and S. E. Euskirchen, N. J. Pastick, V. E. Romanovsky, and R.W. Ruess

for insightful reviews of the manuscript. Any use of trade names is for descriptive purposes only and does not imply endorsement by the U.S. Government.

Figures

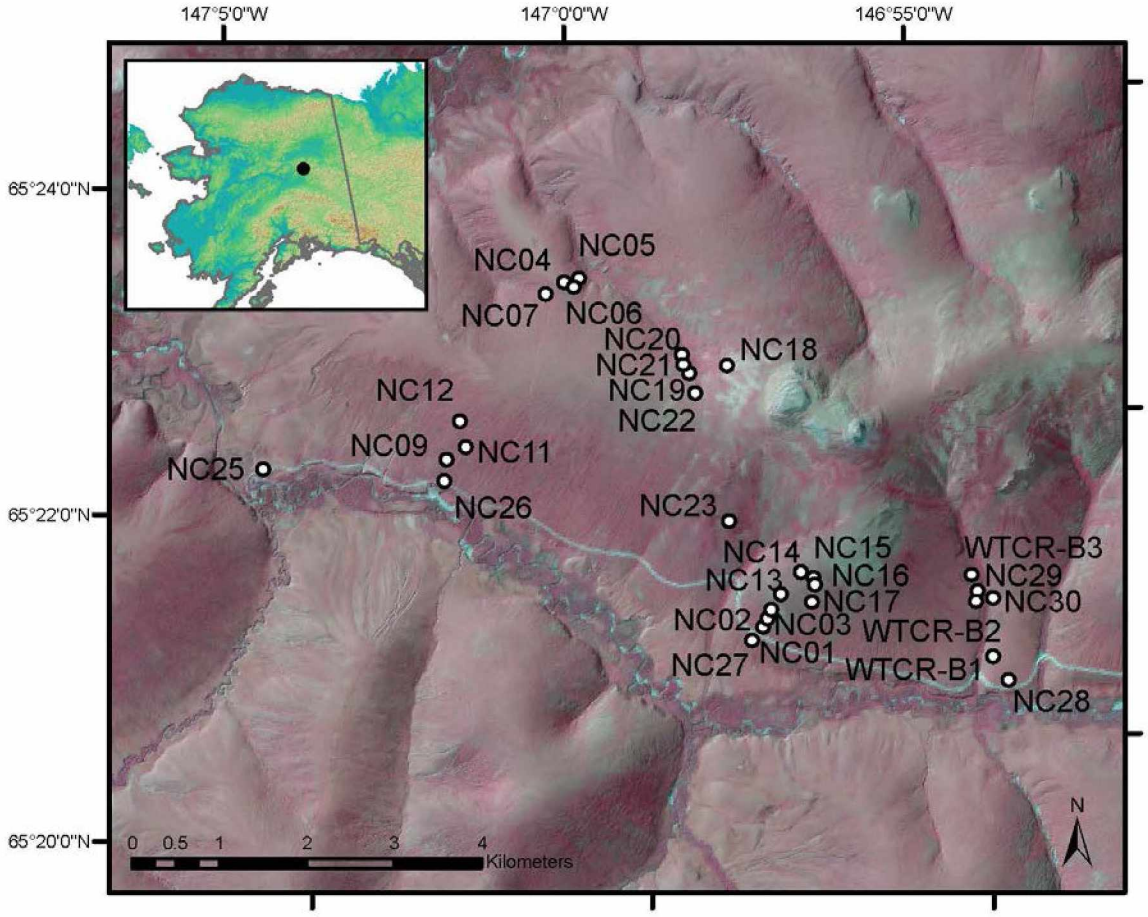

Figure 3.1. Map of study area and field sites. Study area is within the White Mountains National Recreation Area in interior Alaska. Imagery is a Landsat 8 OLI false color composite draped over a 2.5-m DEM.

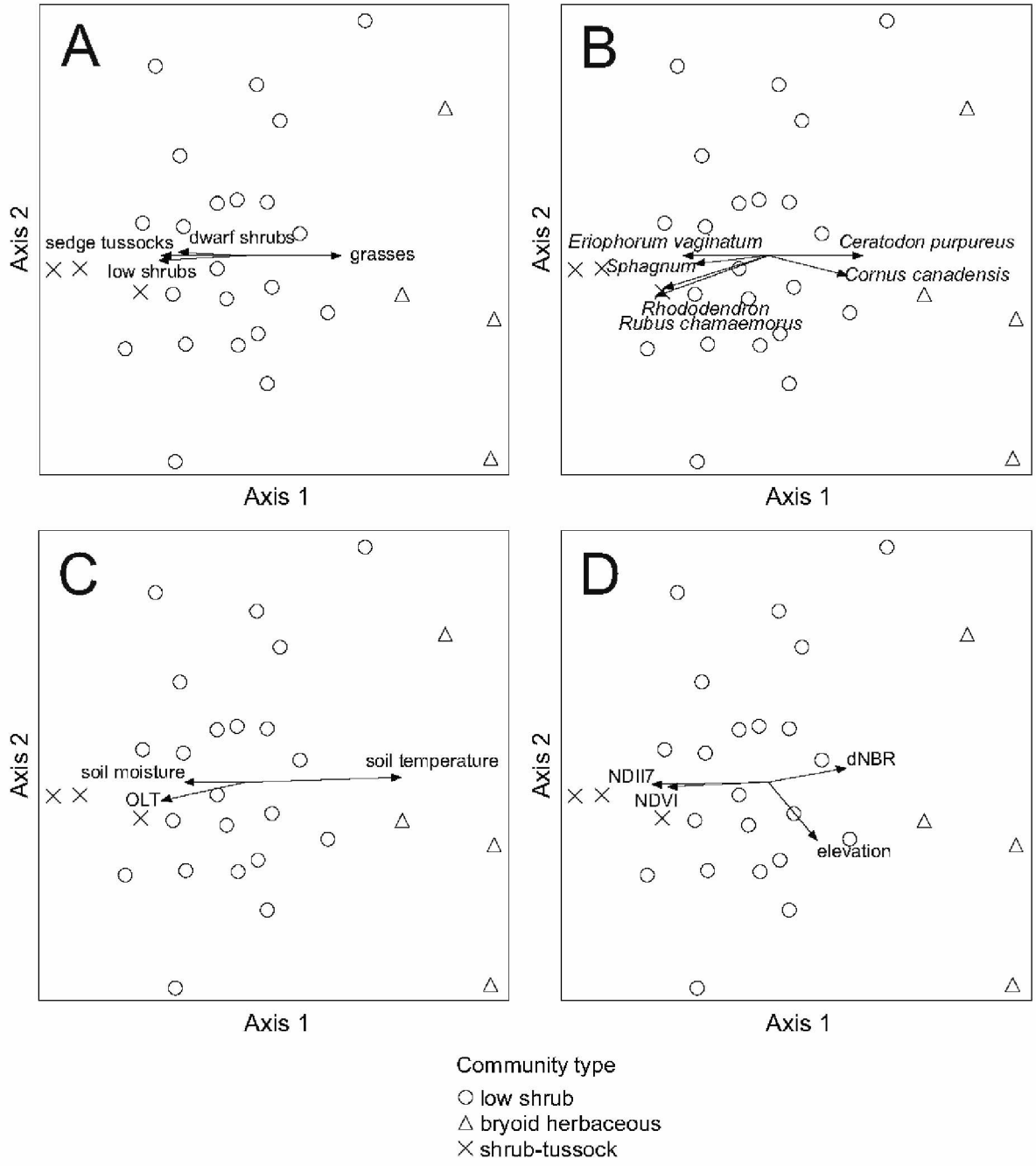

Figure 3.2. Plant community analysis. NMDS ordination of plant communities and relationships with (a) vegetation cover by growth form, (b) vegetation cover by species or genus, (c) soil properties, and (d) remote sensing variables. One outlier was excluded (n = 29).

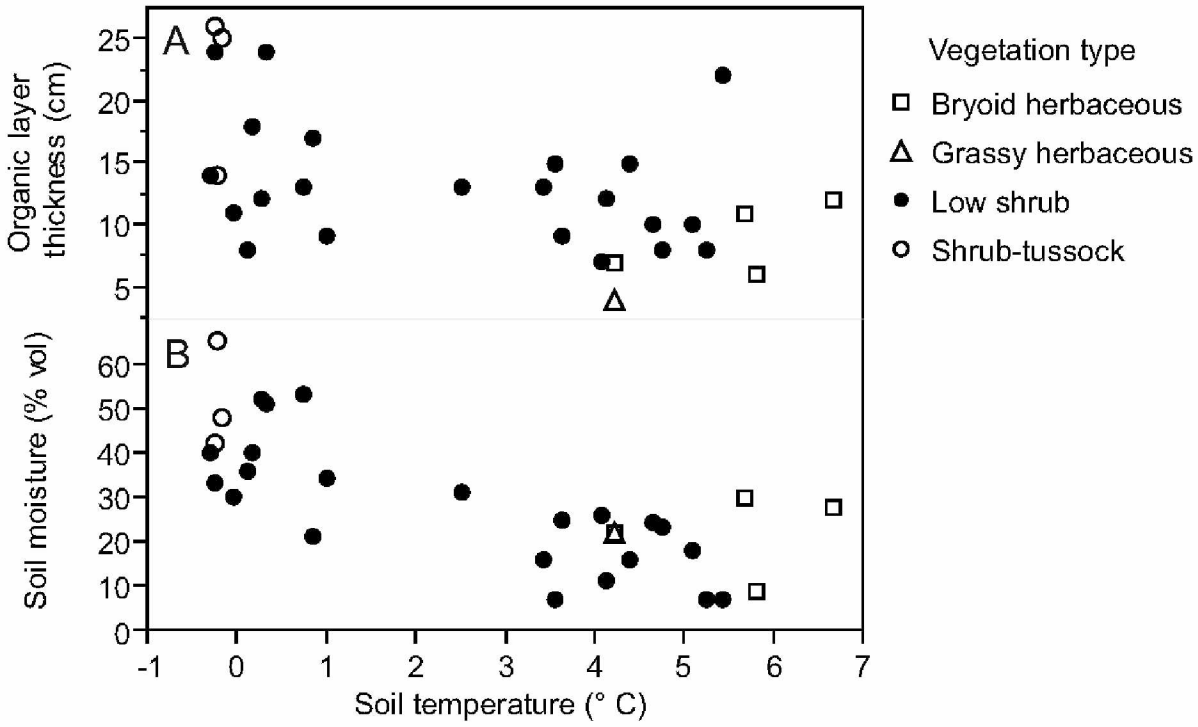

Figure 3.3. Relationships among soil temperature and physical properties by vegetation type. (a) Soil temperature (1 m depth) and organic layer thickness, and (b) soil temperature and soil moisture (upper 20 cm) (n = 30).

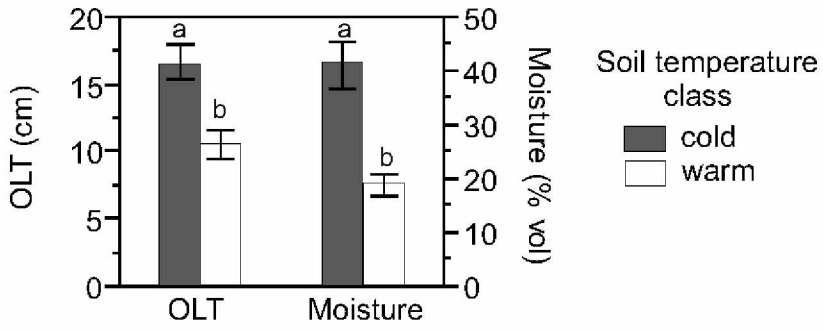

Figure 3.4. Variation in soil physical properties by soil temperature class. Mean ± SE organic layer thickness (OLT) and soil moisture by soil temperature class. Significant differences between cold (≤ 1.0 ° C, n = 13) and warm (≥ 2.5 ° C, n = 17) groups were determined with two-tailed t-tests and denoted by lettering.

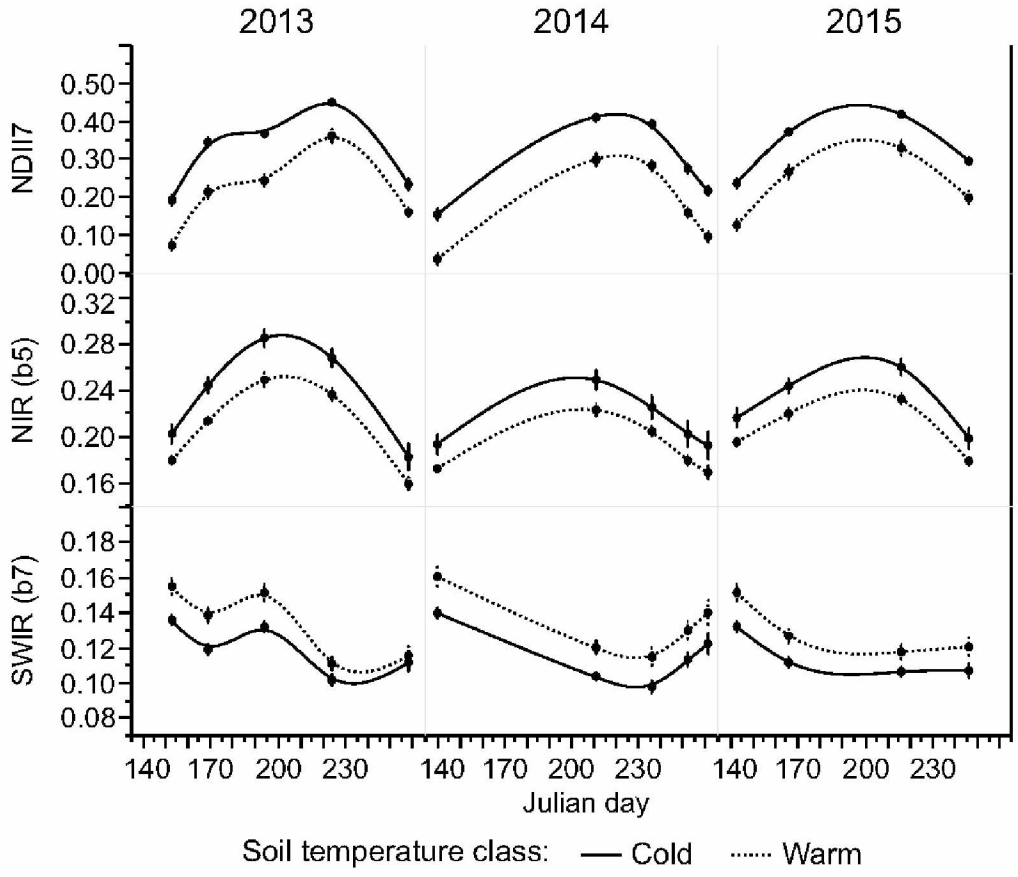

Figure 3.5. Inter-annual variation in seasonal reflectance patterns by soil temperature class. NDII7, NIR, and SWIR reflectance (Landsat 8 OLI) from May–September of 2013–2015. Points represent means ± SE for field sites in cold (≤ 1.0 °C, n = 13) and warm (≥ 2.5 °C, n = 17) soil temperature classes.

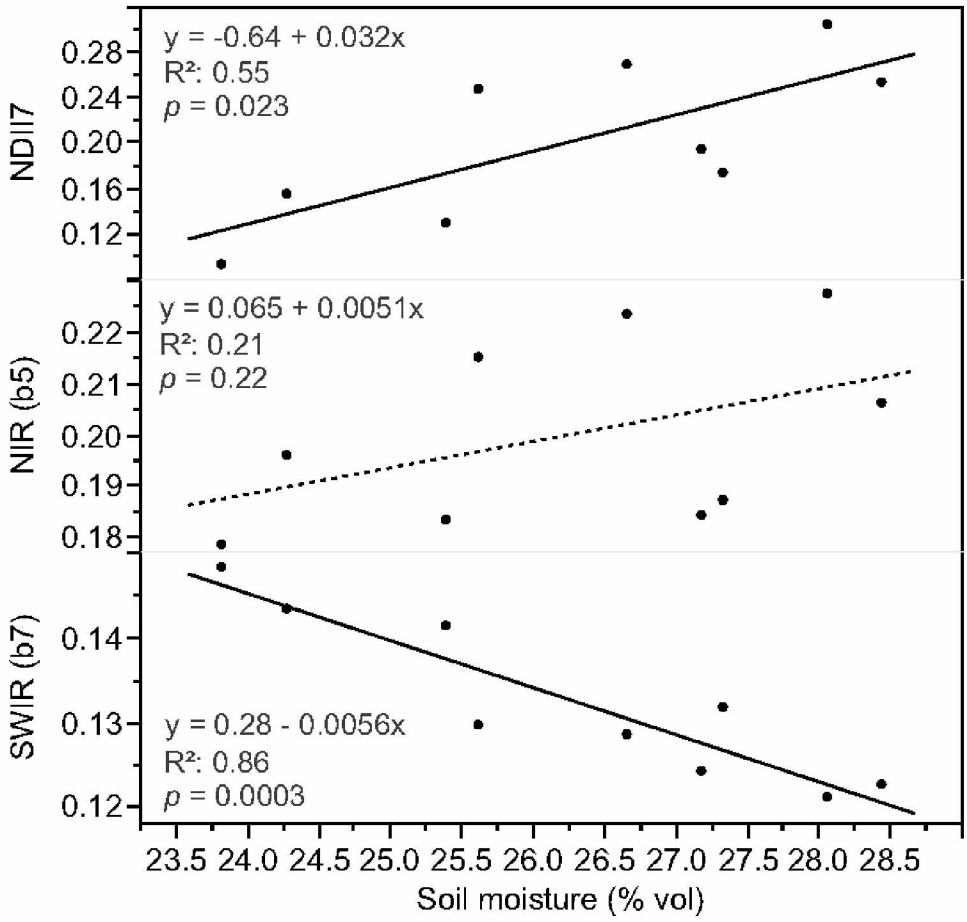

Figure 3.6. Relationships between spectral reflectance and soil moisture over time. NDII7, NIR, and SWIR reflectance (Landsat 8 OLI) and surface soil moisture (7 cm depth) at a field monitoring site in a severe burn. Each data point is from a different day in the 2014─2015 snow-free seasons (n = 9). Solid lines depict significant regressions; dashed lines depict insignificant regressions.

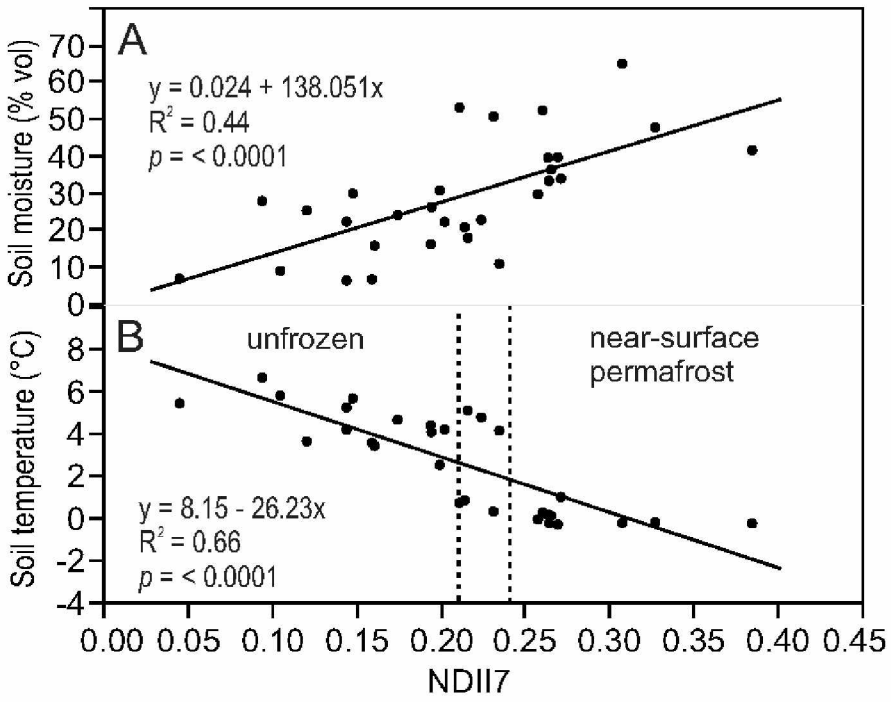

Figure 3.7. Relationships between NDII7, soil moisture, and soil temperature across field sites. NDII7 (Landsat 8 OLI) and (a) soil moisture (upper 20 cm), and (b) soil temperature (1 m, n = 30). Vertical dashed lines represent cut-points used to delineate unfrozen from near-surface permafrost classes in mapping.

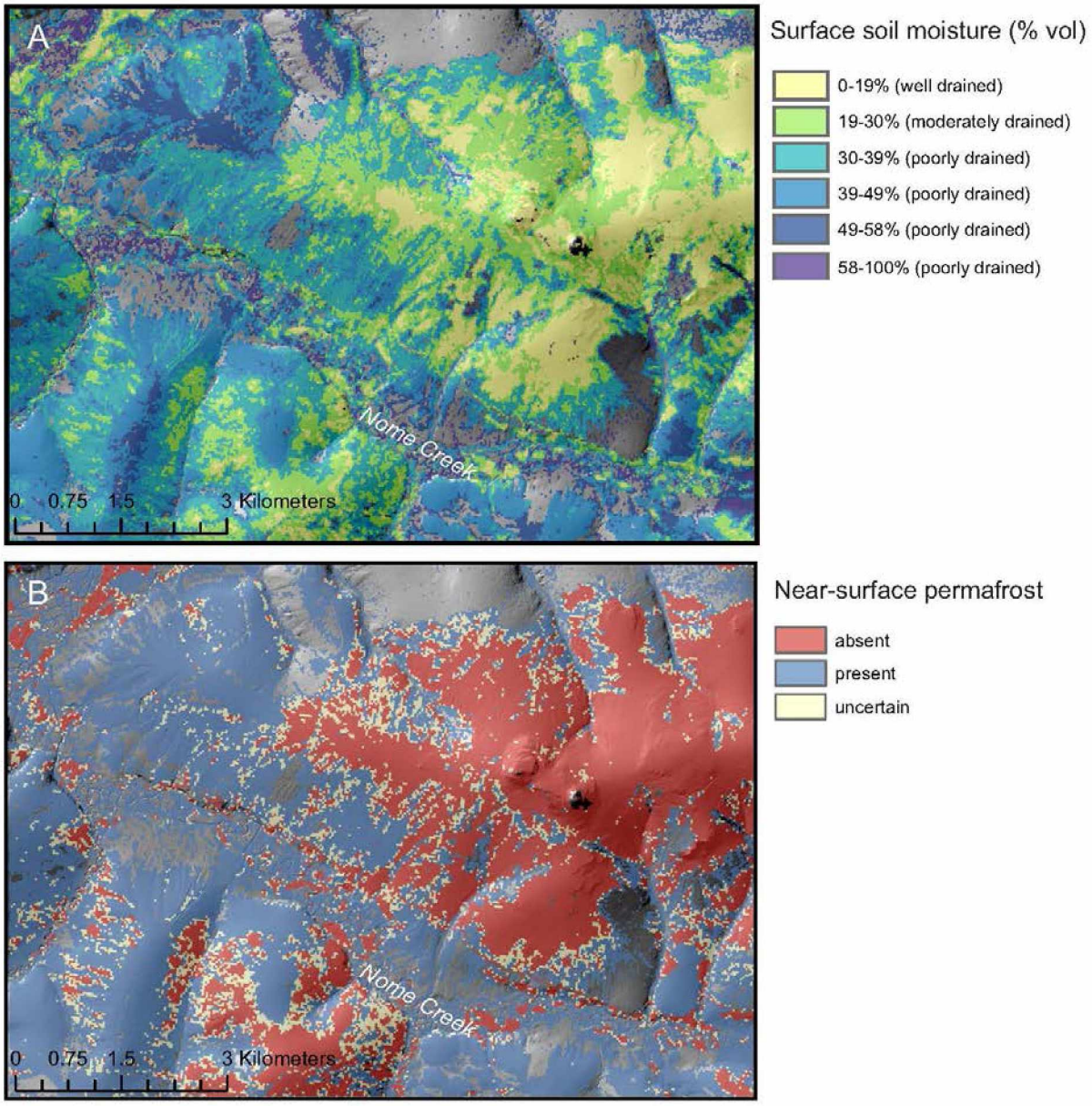

Figure 3.8. Maps of post-fire drainage classes and permafrost status. (a) Surface soil moisture (% vol) of upper 20 cm and (b) near-surface permafrost (~1 m) distribution a decade after the 2004 Boundary Fire in interior Alaska. Thematic maps are based on NDII7 calculations from a Landsat 8 OLI scene acquired September 9, 2014. Unburned areas are excluded.

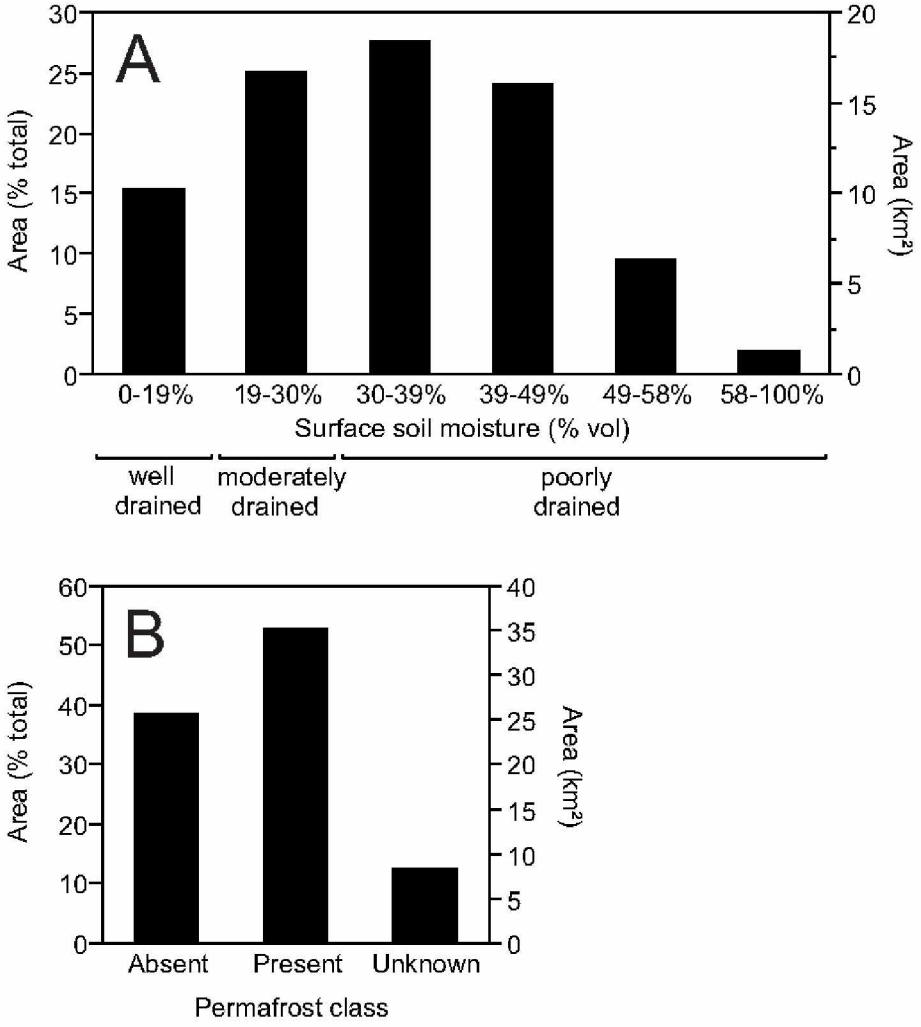

Figure 3.9. Distribution of mapped (a) drainage and (b) permafrost classes.

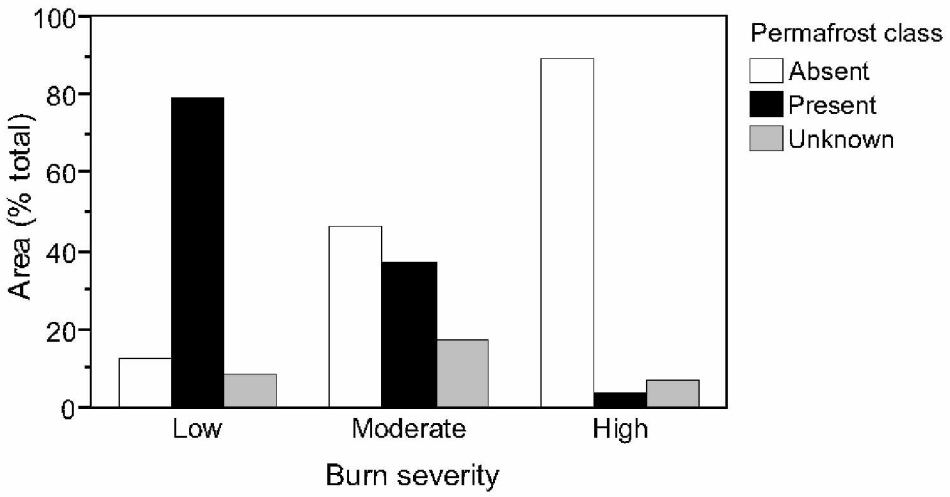

Figure 3.10. Distribution of mapped permafrost classes by burn severity. Burn severity was derived from dNBR (Landsat 7 ETM+).

Tables

Table 3.1. Site-level environmental data (n = 30).

Site	Elevation (m)	Slope (°)	Organic layer thickness (cm)	Soil temperature at 1 m (° C)	Soil moisture (% vol)	Vegetation type
NC01	599	13	24	-0.24	33	Low shrub
NC02	613	12	22	5.44	7	Low shrub
NC03	626	15	8	5.25	7	Low shrub
NC04	632	8	11	-0.04	30	Low shrub
NC05	617	20	8	4.77	23	Low shrub
NC06	633	13	13	3.43	16	Low shrub
NC07	633	12	9	1.01	34	Low shrub
NC09	565	9	13	0.74	53	Low shrub
NC11	588	10	14	-0.29	40	Low shrub
NC12	608	12	18	0.18	40	Low shrub
NC13	653	13	9	3.65	25	Low shrub
NC14	698	12	6	5.81	9	Bryoid herbaceous
NC15	700	11	15	3.57	7	Low shrub
NC16	690	13	12	6.65	28	Bryoid herbaceous
NC17	658	15	10	4.66	24	Low shrub
NC18	778	29	4	4.20	22	Grassy herbaceous
NC19	738	16	17	0.85	21	Low shrub
NC20	701	26	10	5.11	18	Low shrub
NC21	724	16	24	0.33	51	Low shrub
NC22	776	16	7	4.20	22	Bryoid herbaceous
NC24	680	14	11	5.68	30	Bryoid herbaceous
NC25	506	2	7	4.09	26	Low shrub
NC26	544	9	12	0.28	52	Low shrub
NC27	579	11	14	-0.22	65	Shrub-tussock
NC28	584	8	26	-0.24	42	Shrub-tussock
NC29	609	13	13	2.53	31	Low shrub
NC30	601	16	8	0.12	36	Low shrub
WTCR-B1	590	9	25	-0.17	48	Shrub-tussock
WTCR-B2	606	13	12	4.14	11	Low shrub
WTCR-B3	619	14	15	4.40	16	Low shrub

Table 3.2. Satellite remote sensing scenes used in analysis.

Satellite/Sensor	Scene Identifier	Date	Path	Row
Landsat 8 OLI	LC80690142013153LGN00	6/2/2013	69	14
Landsat 8 OLI	LC80690142013169LGN00	6/18/2013	69	14
Landsat 8 OLI	LC80680142013194LGN00	7/13/2013	68	14
Landsat 8 OLI	LC80700142013224LGN00	8/12/2013	70	14
Landsat 8 OLI	LC80680142013258LGN00	9/15/2013	68	14
Landsat 8 OLI	LC80690142014140LGN00	5/20/2014	69	14
Landsat 8 OLI	LC80700142014211LGN00	7/30/2014	70	14
Landsat 8 OLI	LC80690142014236LGN00	8/24/2014	69	14
Landsat 8 OLI	LC80690142014252LGN00	9/9/2014	69	14
Landsat 8 OLI	LC80680142014261LGN00	9/18/2014	68	14
Landsat 8 OLI	LC80690142015143LGN00	5/23/2015	69	14
Landsat 8 OLI	LC80700142015166LGN00	6/15/2015	70	14
Landsat 8 OLI	LC80680142015216LGN00	8/4/2015	68	14
Landsat 8 OLI	LC80700142015246LGN00	9/3/2015	70	14
Landsat 7 ETM+	7069014000214750	5/27/2002	69	14
Landsat 7 ETM+	7069014000520350	7/22/2005	69	14
	Granule	Date	Frame	Path
ALOS-PALSAR	ALPSRP188501300	8/8/2009	1300	253
ALOS-PALSAR	ALPSRP195211300	9/23/2009	1300	253
ALOS-PALSAR	ALPSRP242181300	8/11/2010	1300	253
ALOS-PALSAR	ALPSRP248891300	9/26/2010	1300	253

Table 3.3. Correlations with plant community ordination axes. Pearson and Kendall correlations of NMDS ordination axes with vegetation cover (by type and species), soil properties, and remote sensing metrics. Variables correlated with at least one axis with $R^2 > 0.2$ are shown, with values in bold. One outlier was excluded (n = 29).

		Axis 1			Axis 2		
		r	r-sq	tau	r	r-sq	tau
	Vegetation type (% cover)						
	Dwarf shrubs	-0.55	**0.31**	-0.37	0.12	0.01	0.05
	Low shrubs	-0.63	**0.39**	-0.40	-0.14	0.02	-0.04
	Grasses	0.66	**0.43**	0.51	0.05	0.00	-0.07
	Plant species (% cover)						
Tall shrubs	*Alnus incana* ssp. *crispa*	0.22	0.05	0.08	-0.52	**0.27**	-0.37
Low shrubs	*Rhododendron* spp.	-0.69	**0.47**	-0.46	-0.38	0.15	-0.28
	Rosa acicularis	0.40	0.16	0.30	0.49	**0.24**	0.34
	Vaccinium uliginosum	-0.53	**0.28**	-0.37	0.49	**0.24**	0.43
Dwarf shrubs	*Vaccinium vitis-idaea*	-0.51	**0.26**	-0.43	0.12	0.02	0.11
Forbs	*Aster sibirica*	0.55	**0.30**	0.34	-0.07	0.01	-0.03
	Cornus canadensis	0.60	**0.36**	0.47	-0.30	0.09	-0.35
	Chamerion angustifolium	0.46	**0.21**	0.40	0.56	**0.31**	0.44
	Rubus chamaemorus	-0.72	**0.52**	-0.59	-0.43	0.19	-0.30
Sedges	*Carex bigelowii*	0.53	**0.28**	0.48	-0.18	0.03	-0.20
Sedge tussocks	*Eriophorum vaginatum*	-0.62	**0.39**	-0.68	0.02	0.00	0.19
Mosses	*Ceratodon purpureus*	0.69	**0.48**	0.45	-0.07	0.01	0.05
	Polytrichum juniperinum	0.47	**0.22**	0.43	0.01	0.00	-0.19
	Sphagnum spp.	-0.58	**0.33**	-0.55	-0.19	0.04	-0.21
	Soil properties						
	OLT	**-0.62**	**0.38**	**-0.49**	-0.15	0.02	-0.01
	Soil moisture, 20 cm	**-0.53**	**0.28**	**-0.43**	0.22	0.05	0.22
	Soil temperature, 1 m	**0.84**	**0.71**	**0.69**	0.03	0.00	-0.03
	Remote sensing variables						
	Elevation	0.44	0.19	0.35	**-0.62**	**0.38**	**-0.45**
	NDII7	**-0.73**	**0.54**	**-0.57**	0.02	0.00	0.03
	NDVI	**-0.68**	**0.46**	**-0.42**	-0.04	0.00	-0.03
	dNBR	**0.60**	**0.35**	**0.52**	0.02	0.00	0.03

Table 3.4. Relationships between remote sensing variables and soil properties. Spearman's rank correlations (ρ) between remote sensing metrics, volumetric soil moisture (upper 20 cm), and soil temperature (1 m). Significant relationships are highlighted in bold (n = 30).

	Soil moisture		Soil temperature	
	p	Prob>|p|	p	Prob>|ρ|
Topographic				
Aspect	0.21	0.2638	-0.12	0.5271
CTI	-0.15	0.4409	0.08	0.6611
Curvature	0.22	0.2476	-0.04	0.8336
Elevation	**-0.53**	**0.0025**	**0.54**	**0.0023**
Slope	**-0.38**	**0.0395**	**0.48**	**0.0078**
Solar radiation	-0.07	0.7042	0.20	0.2975
Radar				
HH-PC1	-0.21	0.2764	-0.03	0.8923
HH-PC2	0.08	0.6697	0.02	0.9015
HH-PC3	0.29	0.1251	-0.29	0.1234
HH-PC4	0.07	0.7042	-0.10	0.6084
HV-PC1	**0.42**	**0.0200**	-0.36	0.0516
HV-PC2	0.12	0.5419	-0.03	0.8573
HV-PC3	0.22	0.2486	-0.03	0.8812
HV-PC4	-0.07	0.7164	-0.08	0.6894
Optical				
dNBR	**-0.53**	**0.0026**	**0.64**	**0.0001**
NDII6	**0.66**	**<0.0001**	**-0.81**	**<0.0001**
NDII7	**0.69**	**<0.0001**	**-0.83**	**<0.0001**
NDVI	**0.39**	**0.0345**	**-0.57**	**0.0009**

References

1. Osterkamp, T.E.; Romanovsky, V.E. Evidence for warming and thawing of discontinuous permafrost in Alaska. *Permafrost and Periglacial Processes* **1999**, *10*, 17-37.

2. Jafarov, E.E.; Marchenko, S.S.; Romanovsky, V.E. Numerical modeling of permafrost dynamics in Alaska using a high spatial resolution dataset. *The Cryosphere* **2012**, *6*, 613-624.

3. Zhang, Y.; Chen, W.; Riseborough, D.W. Transient projections of permafrost distribution in Canada during the 21st century under scenarios of climate change. *Global and Planetary Change* **2008**, *60*, 443-456.

4. Jorgenson, M.T.; Romanovsky, V.; Harden, J.; Shur, Y.; O'Donnell, J.; Schuur, E.A.G.; Kanevskiy, M.; Marchenko, S. Resilience and vulnerability of permafrost to climate change. *Canadian Journal of Forest Research* **2010**, *40*, 1219-1236.

5. Johnson, K.D.; Harden, J.W.; David McGuire, A.; Clark, M.; Yuan, F.; Finley, A.O. Permafrost and organic layer interactions over a climate gradient in a discontinuous permafrost zone. *Environmental Research Letters* **2013**, *8*, 035028.

6. Yoshikawa, K.; Bolton, W.R.; Romanovsky, V.E.; Fukuda, M.; Hinzman, L.D. Impacts of wildfire on the permafrost in the boreal forests of interior Alaska. *Journal of Geophysical Research* **2003**, *108*, 8148.

7. Kasischke, E.S.; Verbyla, D.L.; Rupp, T.S.; McGuire, A.D.; Murphy, K.A.; Jandt, R.; Barnes, J.L.; Hoy, E.E.; Duffy, P.A.; Calef, M., *et al.* Alaska's changing fire regime — implications for the vulnerability of its boreal forests. *Canadian Journal of Forest Research* **2010**, *40*, 1313-1324.

8. Calef, M.P.; Varvak, A.; McGuire, A.D.; Chapin, F.S.; Reinhold, K.B. Recent changes in annual area burned in interior Alaska: The impact of fire management. *Earth Interactions* **2015**, *19*, 1-17.

9. Jafarov, E.E.; Romanovsky, V.E.; Genet, H.; McGuire, A.D.; Marchenko, S.S. The effects of fire on the thermal stability of permafrost in lowland and upland black spruce forests of interior Alaska in a changing climate. *Environmental Research Letters* **2013**, *8*, 035030.

10. Brown, D.R.N.; Jorgenson, M.T.; Douglas, T.A.; Romanovsky, V.E.; Kielland, K.; Hiemstra, C.; Euskirchen, E.S.; Ruess, R.W. Interactive effects of wildfire and climate on permafrost degradation in Alaskan lowland forests. *Journal of Geophysical Research: Biogeosciences* **2015**, *120*, 1619-1637.

11. Genet, H.; McGuire, A.D.; Barrett, K.; Breen, A.; Euskirchen, E.S.; Johnstone, J.F.; Kasischke, E.S.; Melvin, A.M.; Bennett, A.; Mack, M.C., *et al.* Modeling the effects of fire severity and climate warming on active layer thickness and soil carbon storage of black spruce forests across the landscape in interior Alaska. *Environmental Research Letters* **2013**, *8*, 045016.

12. Schuur, E.A.; McGuire, A.D.; Schadel, C.; Grosse, G.; Harden, J.W.; Hayes, D.J.; Hugelius, G.; Koven, C.D.; Kuhry, P.; Lawrence, D.M., *et al.* Climate change and the permafrost carbon feedback. *Nature* **2015**, *520*, 171-179.

13. Chapin, F.S., III; McGuire, A.D.; Ruess, R.W.; Hollingsworth, T.N.; Mack, M.C.; Johnstone, J.F.; Kasischke, E.S.; Euskirchen, E.S.; Jones, J.B.; Jorgenson, M.T., *et al.* Resilience of Alaska's boreal forest to climatic change. *Canadian Journal of Forest Research* **2010**, *40*, 1360-1370.

14. Woo, M.-K.; Kane, D.L.; Carey, S.K.; Yang, D. Progress in permafrost hydrology in the new millennium. *Permafrost and Periglacial Processes* **2008**, *19*, 237-254.

15. Jorgenson, M.T.; Osterkamp, T.E. Response of boreal ecosystems to varying modes of permafrost degradation. *Canadian Journal of Forest Research* **2005**, *35*, 2100-2111.

16. Jorgenson, M.T.; Racine, C.H.; Walters, J.C.; Osterkamp, T.E. Permafrost degradation and ecological changes associated with a warming climate in central Alaska. *Climatic Change* **2001**, *48*, 551-579.

17. Koch, J.C.; Ewing, S.A.; Striegl, R.; McKnight, D.M. Rapid runoff via shallow throughflow and deeper preferential flow in a boreal catchment underlain by frozen silt (Alaska, USA). *Hydrogeology Journal* **2013**, *21*, 93-106.

18. Nossov, D.R.; Jorgenson, M.T.; Kielland, K.; Kanevskiy, M.Z. Edaphic and microclimatic controls over permafrost response to fire in interior Alaska. *Environmental Research Letters* **2013**, *8*, 035013.

19. Koch, J.C.; Kikuchi, C.P.; Wickland, K.P.; Schuster, P. Runoff sources and flow paths in a partially burned, upland boreal catchment underlain by permafrost. *Water Resources Research* **2014**, *50*, 8141-8158.

20. Jorgenson, M.T.; Harden, J.; Kanevskiy, M.; O'Donnell, J.; Wickland, K.; Ewing, S.; Manies, K.; Zhuang, Q.; Shur, Y.; Striegl, R., *et al.* Reorganization of vegetation, hydrology and soil carbon after permafrost degradation across heterogeneous boreal landscapes. *Environmental Research Letters* **2013**, *8*, 035017.

21. Swanson, D.K. Susceptibility of permafrost soils to deep thaw after forest fires in interior Alaska, U.S.A., and some ecologic implications. *Arctic and Alpine Research* **1996**, *28*, 217-227.

22. Kasischke, E.S.; Johnstone, J.F. Variation in postfire organic layer thickness in a black spruce forest complex in interior Alaska and its effects on soil temperature and moisture. *Canadian Journal of Forest Research* **2005**, *35*, 2164-2177.

23. Ping, C.L.; Michaelson, G.J.; Packee, E.C.; Stiles, C.A.; Swanson, D.K.; Yoshikawa, K. Soil catena sequences and fire ecology in the boreal forest of Alaska. *Soil Science Society of America Journal* **2005**, *69*, 1761.

24. Grosse, G.; Harden, J.; Turetsky, M.; McGuire, A.D.; Camill, P.; Tarnocai, C.; Frolking, S.; Schuur, E.A.G.; Jorgenson, T.; Marchenko, S., *et al.* Vulnerability of high-latitude soil organic carbon in North America to disturbance. *Journal of Geophysical Research* **2011**, *116*, G00K06.

25. Gogineni, P.; V. Romanovsky; J. Cherry; C. Duguay; S. Goetz; M. T. Jorgenson; Moghaddami, M. *Opportunities to use remote sensing in understanding permafrost and related ecological characteristics: Report of a workshop*. National Academy of Science: Washington, D.C., 2014; p 84.

26. Minsley, B.J.; Abraham, J.D.; Smith, B.D.; Cannia, J.C.; Voss, C.I.; Jorgenson, M.T.; Walvoord, M.A.; Wylie, B.K.; Anderson, L.; Ball, L.B., *et al.* Airborne electromagnetic imaging of discontinuous permafrost. *Geophysical Research Letters* **2012**, *39*.

27. Hachem, S.; Allard, M.; Duguay, C. Using the modis land surface temperature product for mapping permafrost: An application to Northern Quebec and Labrador, Canada. *Permafrost and Periglacial Processes* **2009**, *20*, 407-416.

28. Langer, M.; Westermann, S.; Heikenfeld, M.; Dorn, W.; Boike, J. Satellite-based modeling of permafrost temperatures in a tundra lowland landscape. *Remote Sensing of Environment* **2013**, *135*, 12-24.

29. Westermann, S.; Østby, T.I.; Gisnås, K.; Schuler, T.V.; Etzelmüller, B. A ground temperature map of the North Atlantic permafrost region based on remote sensing and reanalysis data. *The Cryosphere* **2015**, *9*, 1303-1319.

30. Nelson, F.E.; Shiklomanov, N.; Mueller, G.R.; Hinkel, K.M.; Walker, D.A.; Bockheim, J.G. Estimating active-layer thickness over a large region: Kuparuk river basin, Alaska, U.S.A. *Arctic and Alpine Research* **1997**, *29*, 367-378.

31. Panda, S.K.; Prakash, A.; Solie, D.N.; Romanovsky, V.E.; Jorgenson, M.T. Remote sensing and field-based mapping of permafrost distribution along the alaska highway corridor, interior Alaska. *Permafrost and Periglacial Processes* **2010**, *21*, 271-281.

32. Pastick, N.J.; Jorgenson, M.T.; Wylie, B.K.; Nield, S.J.; Johnson, K.D.; Finley, A.O. Distribution of near-surface permafrost in Alaska: Estimates of present and future conditions. *Remote Sensing of Environment* **2015**, *168*, 301-315.

33. Bourgeau-Chavez, L.L.; Kasischke, E.S.; Riordan, K.; Brunzell, S.; Nolan, M.; Hyer, E.; Slawski, J.; Medvecz, M.; Walters, T.; Ames, S. Remote monitoring of spatial and temporal surface soil moisture in fire disturbed boreal forest ecosystems with ERS SAR imagery. *International Journal of Remote Sensing* **2007**, *28*, 2133-2162.

34. Kasischke, E.S.; Bourgeau-Chavez, L.L.; Johnstone, J.F. Assessing spatial and temporal variations in surface soil moisture in fire-disturbed black spruce forests in interior Alaska using spaceborne synthetic aperture radar imagery - implications for post-fire tree recruitment. *Remote Sensing of Environment* **2007**, *108*, 42-58.

35. Karlstrom, T.N.V. Surficial geology of Alaska In *U.S. Geological Survey Miscellaneous Geologic Investigations Map 357*, 1964

36. Jorgenson, M.T.; Yoshikawa, K.; Kanevskiy, M.; Shur, Y.; Romanovsky, V.; Marchenko, S.; Grosse, G.; Brown, J.; Jones, B. *Permafrost characteristics of Alaska*. Institute of Northern Engineering, University of Alaska Fairbanks: 2008.

37. Bernhardt, E.L.; Hollingsworth, T.N.; Chapin, F.S., III. Fire severity mediates climate-driven shifts in understorey community composition of black spruce stands of interior Alaska. *Journal of Vegetation Science* **2011**, *22*, 32-44.

38. Hollingsworth, T.N.; Johnstone, J.F.; Bernhardt, E.L.; Chapin, F.S., 3rd. Fire severity filters regeneration traits to shape community assembly in Alaska's boreal forest. *PloS one* **2013**, *8*, e56033.

39. Minsley, B.J.; Pastick, N.J.; Wylie, B.K.; Brown, D.R.N.; Andy Kass, M. Evidence for nonuniform permafrost degradation after fire in boreal landscapes. *Journal of Geophysical Research: Earth Surface* **2016**, *121*, 320-335.

40. Viereck, L.A.D., C.T.; Batten, A.R.; Wenzlick, K.J. The Alaska vegetation classification. General technical report pnw-gtr-286. Portland, or: U.S. Department of Agriculture, Forest Service, Pacific Northwest Research Station. 278 p. **1992**.

41. Braun-Blanquet, J. *Plant sociology: The study of plant communities*. Hafner: London, 1965.

42. Rich, P.M., R. Dubayah, W. A. Hetrick, and S. C. Saving. Using viewshed models to calculate intercepted solar radiation: Applications in ecology. *American Society for Photogrammetry and Remote Sensing Technical Papers* **1994**, 524–529.

43. Moore, I.D., Grayson, R.B. and Ladson, A.R. Digital terrain modelling: A review of hydrological, geomorphological, and biological applications. *Hydrological Processes* **1991**, *5*, 3-30.

44. Ji, L.; Zhang, L.; Wylie, B.K.; Rover, J. On the terminology of the spectral vegetation index (NIR − SWIR)/(NIR + SWIR). *International Journal of Remote Sensing* **2011**, *32*, 6901-6909.

45. Hardisky, M.A.; Klemas, V.; Smart, R.M. The influence of soft salinity, growth form, and leaf moisture on the spectral reflectance of *Spartina alterniflora* canopies. *Photogramm. Eng. Remote Sens.* **1983**, *49*, 77-83.

46. Jenks, G.F. The data model concept in statistical mapping. *International Yearbook of Cartography* **1967**, *7*, 186-190.

47. Kerr, Y.H. Soil moisture from space: Where are we? *Hydrogeology Journal* **2006**, *15*, 117-120.

48. French, N.H.F.; Kasischke, E.S.; Hall, R.J.; Murphy, K.A.; Verbyla, D.L.; Hoy, E.E.; Allen, J.L. Using landsat data to assess fire and burn severity in the north american boreal forest region: An overview and summary of results. *International Journal of Wildland Fire* **2008**, *17*, 443-462.

49. Kimes, D.S.; Markham, B.L.; Tucker, C.J.; McMurtrey III, J.E. Temporal relationships between spectral response and agronomic variables of a corn canopy. *Remote Sensing of Environment* **1981**, *11*, 401-411.

50. Wang, L.; Qu, J.J. NMDI: A normalized multi-band drought index for monitoring soil and vegetation moisture with satellite remote sensing. *Geophysical Research Letters* **2007**, *34*.

51. Weidong, L.; Baret, F.; Xingfa, G.; Qingxi, T.; Lanfen, Z.; Bing, Z. Relating soil surface moisture to reflectance. *Remote Sensing of Environment* **2002**, *81*, 238-246.

52. Romanovsky, V.E. Bonanza Creek 2 - burned: Soils, geophysical institute permafrost laboratory, University of Alaska Fairbanks, http://lapland.Gi.Alaska.Edu/vdv/index.Html. 2016.

53. Alaska Climate Research Center. ACIS daily data browser <http://climate.Gi.Alaska.Edu/acis_data>. 2016; Vol. 2016.

54. Viereck, L.A. In *Effects of fire and firelines on active layer thickness and soil temperatures in interior Alaska*, Proceedings of the 4th Canadian Permafrost Conference, The Roger J. E. Brown Memorial Volume, 1982; Natural Resource Council of Canada: 1982; pp 123-134.

55. Van Cleve, K.; F. S. Chapin III; P. W. Flanagan; L. A. Viereck; Dyrness, C.T. *Forest ecosystems in the Alaskan taiga: A synthesis of structure and function*. Springer-Verlag: New York, 1986; p 57.

56. Péwé, T.L. *Quaternary geology of alaska*; Professional Paper 835; United States Geological Survey: Washington, D.C., 1975; p 145.

57. Hinzman, L.D.; Viereck, L.A.; Adams, P.C.; Romanovsky, V.E.; Yoshikawa, K. Climate and permafrost dynamics of the alaskan boreal forest. In *Alaska's changing boreal forest*, Chapin, I., F. S.; Oswood, M.W.; Van Cleve, K.; Viereck, L.A.; Verbyla, D.L., Eds. Oxford University Press: New York, New York, 2006.

58. Rieger, S., J.A. DeMent, D. Sanders. Soil survey of Fairbanks area, Alaska. USDA Soil Conservation Service. U.S. Gov. Print. Office, Washington, DC. 1963.

59. Barrett, K.; Kasischke, E.S.; McGuire, A.D.; Turetsky, M.R.; Kane, E.S. Modeling fire severity in black spruce stands in the Alaskan boreal forest using spectral and non-spectral geospatial data. *Remote Sensing of Environment* **2010**, *114*, 1494-1503.

60. Kane, E.S.; Kasischke, E.S.; Valentine, D.W.; Turetsky, M.R.; McGuire, A.D. Topographic influences on wildfire consumption of soil organic carbon in interior Alaska: Implications for black carbon accumulation. *Journal of Geophysical Research* **2007**, *112*.

61. Hinzman, L.D.; Bolton, W.R.; Petrone, K.C.; Jones, J.B.; Adams, P.C. Watershed hydrology and chemistry in the Alaskan boreal forest: The central role of permafrost. In *Alaska's changing boreal forest*, Chapin Iii, F.S.; Oswood, M.W.; Van Cleve, K.; Viereck, L.A.; Verbyla, D., Eds. Oxford University Press: New York, NY, 2006; pp 269-284.

62. Bolton, W.R.; Hinzman, L.; Yoshikawa, K. In *Stream flow studies in a watershed underlain by discontinuous permafrost*, Water Resources in Extreme Environments, American Water Resources Association, Anchorage, AK, 2000; Kane, D.L., Ed. Anchorage, AK, pp 31-36.

63. Jones, J.B.; Rinehart, A.J. The long-term response of stream flow to climatic warming in headwater streams of interior Alaska. *Canadian Journal of Forest Research* **2010**, *40*, 1210-1218.

64. Shenoy, A.; Johnstone, J.F.; Kasischke, E.S.; Kielland, K. Persistent effects of fire severity on early successional forests in interior Alaska. *Forest Ecology and Management* **2011**, *261*, 381-390.

Conclusions

Our findings from three studies across four soil landscapes in interior Alaska consistently showed an inverse relationship between surface organic layer thickness and thaw depth. The effects of fire on permafrost degradation were strongly controlled by the severity of burning, as measured by the thickness of the remaining surface organic layer. Our mapping results further suggest that spatial variation in burn severity in large part controlled the distribution of permafrost after fire. Burn severity, in turn, was also influenced by topography, vegetation, and their interaction; whereby poorly drained areas tended to support the accumulation of saturated peat, which is more resistant to deep burning. There were, however, significant deviations from this general pattern where severe burning occurred in poorly drained landscape positions. The sensitivity of permafrost to burn severity is of particular significance in light of the changing fire regime in this region, which has been characterized by increased fire severity, extent, and frequency [*Kasischke et al.*, 2010]. Our research suggests that these changes to the fire regime will be a strong positive feedback to permafrost degradation.

Even without a shift in the fire regime, we found that permafrost has become increasingly vulnerable to degradation from fire due to changes in climate. For example, our thermal models suggest that a moderate severity fire would have had only modest effects on permafrost given the historical climate from 1930 to 1970, but from 1970 to 2014 it would have caused deep and sustained permafrost loss. The increased susceptibility to deep thawing was due to both increased air temperatures and increased snow accumulation, as well as the interactions between the two. We also found that both short- and long-term shifts in weather can have lasting effects on permafrost dynamics. Once permafrost thaws deeply enough to develop a thick perennially unfrozen layer (talik), it becomes less likely that permafrost will be able to fully recover if climatic or environmental conditions were to become more favorable for permafrost. Climate models project a significant increase in air temperature [*Romero-Lankao et al.*, 2014], which is expected to cause widespread thawing of permafrost without considering the effects of

fire [*Jafarov et al.*, 2012]. Here, we showed how wildfire and climate interact to exacerbate this permafrost thawing.

We also found that the vulnerability of permafrost to deep thawing after fire varied throughout interior Alaska due to differences in regional climate and mineral soil texture. Permafrost in the Yukon Flats ecoregion was generally more resilient than in the Yukon-Tanana Uplands and Tanana Flats, in part because of its strongly continental climate, with greater freezing degree days and less snowfall. However, soil texture interacted with climate to influence the effects of fire on ground thermal and moisture regimes. In the Yukon Flats, silty soils were more resilient to thawing than sandy soils. This resilience was likely influenced by the high moisture content of the fine-textured active layer soils, which facilitated substantial ground heat loss in winter, and by the high latent heat content of the ice-rich permafrost. In contrast, the drier, coarse-textured soils thawed rapidly after fire. In the Yukon-Tanana Uplands and Tanana Flats lowlands, with fewer freezing degree days and more snowfall than the Yukon Flats, fine-textured, coarse-textured, and rocky soils all lacked near-surface permafrost after fire when surface organic layers were thin, despite high ice content of permafrost.

The thawing of permafrost could become a significant positive feedback to climate warming over time due to the atmospheric release of large stores of carbon currently immobilized in frozen soils [*Schuur et al.*, 2015]. The effects of permafrost thawing on ecosystems and hydrology in our studies varied widely, however, and were dependent on factors such as topography, soil texture, and permafrost ice content. In coarse-textured or rocky soils, permafrost thawing increased drainage and better aeration of surface soils. This change is likely to increase carbon dioxide emissions [*Schuur et al.*, 2015] and alter landscape hydrology [*Jones and Rinehart*, 2010]. In contrast, fine-textured soils associated with ice-rich permafrost in the Tanana Flats collapsed substantially upon thawing after fire. The resulting inundation of forests with water perpetuates a positive feedback to permafrost degradation. This fire-initiated collapse is increasing wetland expansion and the decline of forested ecosystems on this landscape. The long-term implications for climate feedbacks from changes in this landscape are less clear. Methane emissions are likely to increase with water impoundment and the associated low soil oxygen tension [*Olefeldt et al.*,

2013]. However, it is uncertain whether these emissions will be offset by future carbon storage in peat accumulation over longer time scales [*O'Donnell et al.*, 2012; *Turetsky et al.*, 2007].

My research revealed some of the complexities governing the role of fire in influencing permafrost degradation, highlighting the patterns and underlying mechanisms of its temporal and spatial variation. Climate has warmed significantly in this region and across the circumpolar north [*Shulski and Wendler*, 2007], causing permafrost to respond more strongly to fire than it has in the past. With projections for sustained climate warming, the sensitivity of permafrost to fire disturbance will continue to increase, with permafrost stability passing a threshold where ecological succession will no longer enable the recovery of permafrost after disturbance in the discontinuous permafrost zone of interior Alaska.

References

Jafarov, E. E., S. S. Marchenko, and V. E. Romanovsky (2012), Numerical modeling of permafrost dynamics in Alaska using a high spatial resolution dataset, *The Cryosphere*, *6*(3), 613-624.

Jones, J. B., and A. J. Rinehart (2010), The long-term response of stream flow to climatic warming in headwater streams of interior Alaska, *Canadian Journal of Forest Research*, *40*(7), 1210-1218.

Kasischke, E. S., et al. (2010), Alaska's changing fire regime — implications for the vulnerability of its boreal forests, *Canadian Journal of Forest Research*, *40*(7), 1313-1324.

O'Donnell, J. A., M. T. Jorgenson, J. W. Harden, A. D. McGuire, M. Z. Kanevskiy, and K. P. Wickland (2012), The effects of permafrost thaw on soil hydrologic, thermal, and carbon dynamics in an Alaskan peatland, *Ecosystems*, *15*(2), 213-229.

Olefeldt, D., M. R. Turetsky, P. M. Crill, and A. D. McGuire (2013), Environmental and physical controls on northern terrestrial methane emissions across permafrost zones, *Glob Chang Biol*, *19*(2), 589-603.

Romero-Lankao, P., J.B. Smith, D.J. Davidson, N.S. Diffenbaugh, P.L. Kinney, P. Kirshen, P. Kovacs, and L. Villers Ruiz (2014), North America, in *Climate Change 2014: Impacts, Adaptation, and Vulnerability. Part B: Regional Aspects. Contribution of Working Group II to the Fifth Assessment Report of the Intergovernmental Panel on Climate Change*, edited by V. R. Barros, C.B. Field, D.J. Dokken, M.D. Mastrandrea, K.J. Mach, T.E. Bilir, M. Chatterjee, K.L. Ebi, and R. C. Genova, Y.O. Estrada, B. Girma, E.S. Kissel, A.N. Levy, S. MacCracken, P.R. Mastrandrea, and L.L. White, pp. 1439-1498, Cambridge University Press, Cambridge, United Kingdom and New York, NY, USA.

Schuur, E. A., et al. (2015), Climate change and the permafrost carbon feedback, *Nature*, *520*(7546), 171-179.

Shulski, M., and G. Wendler (2007), *Climate of Alaska*, University of Alaska Press.

Turetsky, M. R., R. K. Wieder, D. H. Vitt, R. J. Evans, and K. D. Scott (2007), The disappearance of relict permafrost in boreal north America: Effects on peatland carbon storage and fluxes, *Global Change Biology*, *13*(9), 1922-1934.